

NBSIR 73-201

Composite-Overlay Reinforcement of Cutouts and Cracks in Metal Sheet

Richard A. Mitchell, Ruth M. Woolley, and Daniel J. Chwirut

Engineering Mechanics Section
Mechanics Division
Institute for Basic Standards
National Bureau of Standards
Washington, D. C. 20234

February 1973

Final Report

Prepared for
Langley Research Center
National Aeronautics and Space Administration
Hampton, Virginia 23365

NBSIR 73-201

COMPOSITE-OVERLAY REINFORCEMENT OF CUTOUTS AND CRACKS IN METAL SHEET

Richard A. Mitchell, Ruth M. Woolley, and Daniel J. Chwirut

Engineering Mechanics Section
Mechanics Division
Institute for Basic Standards
National Bureau of Standards
Washington, D. C. 20234

February 1973

Final Report

Prepared for
Langley Research Center
National Aeronautics and Space Administration
Hampton, Virginia 23365



U. S. DEPARTMENT OF COMMERCE, Frederick B. Dent, Secretary

NATIONAL BUREAU OF STANDARDS, Richard W. Roberts, Director

CONTENTS

	Page
1. INTRODUCTION	2
2. FINITE ELEMENT ANALYSES	5
2.1. Finite Element Formulation	5
2.2. Planform Analysis	12
a. Analysis of a Reinforced Cutout	14
b. Analysis of a Reinforced Cutout-with-Crack	17
c. Analysis of a Reinforced Crack	17
2.3. Longitudinal Cross-Section Analysis	18
2.4. Nonlinear-Shear Analysis	21
2.5. Progressive-Debond Analysis	23
3. DESCRIPTION OF LABORATORY TESTS	23
3.1. Specimen Materials	24
3.2. Specimen Configurations	25
a. Material Property Specimens	25
b. Unreinforced Sheet Specimens	25
c. Reinforced Cutout Specimens	26
d. Reinforced Cutout-with-Slit Specimens	26
e. Reinforced Transverse-Slit Specimens	26
f. Double-Lap Joint Specimens	26
3.3. Specimen Fabrication	27
3.4. Instrumentation	27
3.5. Test Procedures	28
a. Quasi-Static Tension Tests	28
b. Tension-Tension Fatigue Tests	28
4. TEST RESULTS AND CORRELATIONS WITH ANALYSES	29
4.1. Material Properties	29
4.2. Unreinforced Sheet	29
4.3. Reinforced Cutout	30
4.4. Reinforced Cutout-with-Slit	32
4.5. Reinforced Transverse Slit	34
4.6. Double-Lap Joints	34
4.7. Discussion of Results	37
5. CONCLUSION	38
6. REFERENCES	39

COMPOSITE-OVERLAY REINFORCEMENT OF COUTOUTS AND CRACKS IN METAL SHEET

Richard A. Mitchell, Ruth M. Woolley, and Daniel J. Chwirut

ABSTRACT

Finite element computer programs were developed for the planform analysis and the longitudinal cross-section analysis of metal sheet reinforced by adhesively bonded overlays of composite material. The analyses articulate the separate responses of the metal sheet, the composite overlays, and the adhesive layers. All materials are assumed to be orthotropic and linear elastic, with the provision that nonlinear interlaminar shear deformation can be approximated by a series of stepwise-linear solutions. The computer programs were developed specifically for the study of three general configurations: (1) a sheet with a reinforced cutout; (2) a sheet with a reinforced cutout with two symmetrical transverse cracks, within the sheet, radiating away from the cutout edge; and (3) a sheet with a reinforced transverse crack. The programs are also suitable for the study of bonded lap joints. The principal output of the computer programs is a set of contour plots of stress and strain fields throughout the sheet, the overlays, and the adhesive layers.

A series of laboratory tests was conducted to demonstrate the validity of the analyses. Strains measured on the surfaces of specimens representing the general configurations studied were, for the most part, in good agreement with strains predicted by the finite element analyses. Significant correlations between certain failure modes and the stresses computed by the finite element analyses were apparent. Similarities between the modes of failure under static and fatigue loading were also evident.

Key Words: Adhesively bonded joints; composite materials; composite-overlay reinforcement;

contour plotting; cracks, reinforcement of;
cutouts, reinforcement of; debond analysis,
progressive; finite element analysis; joints,
adhesively bonded; nonlinear analysis, shear;
reinforcement, composite overlay; reinforcement,
cutouts and cracks; shear analysis, nonlinear.

1. INTRODUCTION

An overlay of high-strength, high-stiffness composite material offers an efficient means of achieving local reinforcement of cutouts and cracks in metal sheet. This concept can be used in the design of new structures or it can be used to strengthen existing structures. Where a crack is anticipated, on the basis of stress analysis or service experience, a composite overlay can be used to reduce the stresses that might otherwise initiate a fatigue crack. Where a crack already exists, a composite overlay can be used to bridge across the crack and stop or retard its growth.

The primary objectives of the work reported here were to develop methods of analysis of composite-reinforced cutouts and cracks and to demonstrate the validity of the analyses by laboratory testing. Finite-element computer programs were developed (in FORTRAN V code) for the study of three general configurations: (1) a sheet with a reinforced cutout, (2) a sheet with a reinforced cutout with two symmetrical transverse cracks within the sheet radiating away from the cutout edge, and (3) a sheet with a reinforced transverse crack. The computer programs generate contour plots of the computed stress, strain, and stress-direction fields for the entire region including and adjacent to the reinforced area. This form of computer output enables one to visualize the interaction between the metal sheet and the reinforcement. The contour plots can also indicate the presence of stress conditions that might initiate or drive a crack or a debond.

Sixteen test specimens, representing the general configurations simulated by the finite element analyses, were instrumented with resistance strain gages and loaded to failure in quasi-static tension. Strains measured on the surfaces of these specimens were, for the most part, in good agreement with the finite element analyses. Thirteen similar specimens were tested to failure in low-cycle tension-tension fatigue. There were significant similarities in modes of failure of specimens of the same design, whether subjected to static or fatigue loading. There were also significant correlations between certain failure modes and the stresses computed by the finite element analyses. The experimental results suggest that the finite element analyses would be appropriate and useful for the design of reinforcement where either static or fatigue loading is involved.

This work was done at the National Bureau of Standards under the sponsorship and with the financial assistance of the National Aeronautics and Space Administration, Langley Research Center.

LIST OF SYMBOLS

- A_s area of the shear stiffness element in the x-y plane;
- [A] matrix relating nodal point displacements to generalized displacement coordinates;
- a, b dimensions of a finite element;
- [B] matrix relating components of strain to generalized displacement coordinates;
- C parameter defining the linear range of a nonlinear stress-strain curve;
- E_{11} , E_{22} Young's moduli in the longitudinal and transverse principal material directions of an orthotropic lamina, respectively;
- {F} column matrix of forces applied to a structure;
- {f} column matrix of forces acting at the nodal points of a triangular finite element;
- { f_s } column matrix of shear forces acting in the adhesive layer of a shear-stiffness element;
- G shear modulus;
- i, j, k index symbols for corners of triangular finite elements;
- K shape parameter of a nonlinear stress-strain curve;
- [K] matrix relating the forces applied to a structure to the resulting nodal-point displacements;
- [k] matrix relating nodal point forces to nodal point displacements of a triangular finite element;
- [k_s] matrix relating nodal point forces to nodal point displacements of a shear-stiffness element;

- n shape parameter of a nonlinear stress-strain curve;
- $[\sigma]$ stress-strain matrix for an orthotropic lamina, referred to the principal material axes;
- $[\tau]$ stress-strain matrix for an orthotropic lamina, referred to the axes x, y ;
- $T, -1$ superscripts indicating matrix transposition and inversion, respectively;
- t_s, t_a, t_o thickness of sheet, adhesive, and overlay, respectively;
- u nodal point displacement in the x direction;
- u_s x component of relative displacement of an overlay with respect to a sheet;
- v nodal point displacement in the y direction;
- v_s y component of relative displacement of an overlay with respect to a sheet;
- V volume of a triangular finite element;
- $\{w\}$ column matrix of nodal point displacements;
- $\{w_s\}$ column matrix of relative displacements of an overlay with respect to a sheet;
- (x, y, z) rectangular coordinates;
- α_n a generalized displacement coordinate;
- γ shear strain;
- ϵ normal strain;
- ν_{12}, ν_{21} major and minor Poisson's ratios, respectively;
- σ normal stress;
- τ shear stress;
- θ angle between the major material axis of a lamina and the x axis.

2. FINITE ELEMENT ANALYSES

Separate finite element computer programs were developed for the planform analysis and the longitudinal cross-section analysis of metal sheet reinforced by overlays of composite material. The analyses are formulated to articulate the separate responses of the metal sheet, the composite overlays, and the adhesive layers. Although the basic finite element formulation is linear, the computer programs permit nonlinear shear deformations and progressive debonding to be approximated by a series of stepwise-linear solutions.

The analyses were coded in FORTRAN V and run on a UNIVAC 1108 computer. Computed results were contour plotted using an SC 4020 plotter.

2.1. Finite Element Formulation

In a finite-element analysis the continuum structure is subdivided into a network of elements that are connected to adjacent elements only at common nodal points. Displacements within individual elements are assumed to be defined by generalized functions that assure displacement compatibility at common boundaries of adjacent elements. The stiffness matrix of each element, relating nodal point forces and displacements, is then computed in terms of the assumed displacement functions, dimensions, and material properties of the element. The stiffness matrix of the entire structure, relating applied external forces to nodal point displacements throughout the structure, is formed by superposing the element stiffness matrices.

Figure 1 shows a representative network of triangular finite elements as might be used in a planform analysis of a reinforced cutout. Symmetry is assumed about the horizontal (x) and vertical (y) axes of the cutout and, therefore, only one quadrant is analyzed. The sheet and the overlay are each divided into separate networks of triangular elements that are connected to adjacent elements of the same adherend only at common nodal points. Within the bonded-overlay region the triangular networks of the two adherends are congruent and the two networks are coupled together by an array of special shear-stiffness elements linking conjugate pairs of nodal points.

Figure 2 shows a representative network of triangular finite elements as might be used in a cross-section analysis of a reinforced transverse crack. Symmetry is assumed about the vertical (z) axis. Such a network can be used for the cross-section analysis of either singly reinforced or doubly reinforced sheet. For the case of a doubly reinforced sheet, symmetry about the horizontal (x) axis is imposed.

A general triangular finite element of the type used in both the planform and the cross-section analyses is shown in Fig.3. In this formulation the state of strain within a triangular element is assumed to be uniform. Therefore, the displacement of any point within the triangle can be expressed by

$$\begin{Bmatrix} u \\ v \end{Bmatrix} = \begin{bmatrix} 1 & x & y & 0 & 0 & 0 \\ 0 & 0 & 0 & 1 & x & y \end{bmatrix} \begin{Bmatrix} \alpha_1 \\ \alpha_2 \\ \alpha_3 \\ \alpha_4 \\ \alpha_5 \\ \alpha_6 \end{Bmatrix} \quad (1)$$

in which

u = displacement in the x direction,
 v = displacement in the y direction,
 α_n = a generalized coordinate.

A particular generalized coordinate represents either the x or y component of displacement of nodal point i or a rate of change of a displacement component with respect to x or y . The assumed displacement functions (eq.(1)) give linear variations in displacement along element boundaries and, therefore, complete displacement compatibility between adjacent elements. Stresses within adjacent elements are not, in general, in equilibrium along common boundaries, but the resultant forces acting at nodal points are required to be in equilibrium. Substitution of nodal point coordinates (defined in Fig. 3) into eq.(1) gives the following equation for nodal point displacements in terms of the generalized coordinates:

$$\begin{Bmatrix} u_i \\ u_j \\ u_k \\ v_i \\ v_j \\ v_k \end{Bmatrix} = \begin{bmatrix} 1 & 0 & 0 & 0 & 0 & 0 \\ 1 & a_j & b_j & 0 & 0 & 0 \\ 1 & a_k & b_k & 0 & 0 & 0 \\ 0 & 0 & 0 & 1 & 0 & 0 \\ 0 & 0 & 0 & 1 & a_j & b_j \\ 0 & 0 & 0 & 1 & a_k & b_k \end{bmatrix} \begin{Bmatrix} \alpha_1 \\ \alpha_2 \\ \alpha_3 \\ \alpha_4 \\ \alpha_5 \\ \alpha_6 \end{Bmatrix}, \quad (2)$$

or

$$\{w\} = [A] \{\alpha\}. \quad (3)$$

Element strains are obtained by applying the definitions of strain from elasticity theory to eq.(1) as follows:

$$\begin{pmatrix} \epsilon_x \\ \epsilon_y \\ \gamma_{xy} \end{pmatrix} = \begin{pmatrix} \frac{\delta u}{\delta x} \\ \frac{\delta v}{\delta y} \\ \frac{\delta u}{\delta y} + \frac{\delta v}{\delta x} \end{pmatrix} = \begin{bmatrix} 0 & 1 & 0 & 0 & 0 & 0 \\ 0 & 0 & 0 & 0 & 0 & 1 \\ 0 & 0 & 1 & 0 & 1 & 0 \end{bmatrix} \begin{pmatrix} \alpha_1 \\ \alpha_2 \\ \alpha_3 \\ \alpha_4 \\ \alpha_5 \\ \alpha_6 \end{pmatrix}, \quad (4)$$

or
$$\{\epsilon\} = [B] \{\alpha\} . \quad (5)$$

In this analysis, all stiffness computations for triangular finite elements are formulated to accommodate generally orthotropic materials as defined by four independent elastic constants in two-dimensional stress states. A composite overlay can consist of several lamina, each having an arbitrary orientation of the two orthogonal material axes that lie within the midplane of the lamina. The assumed stress-strain relationship for a particular orthotropic lamina in a state of plane stress, as presented in Ref.1, is

$$\begin{pmatrix} \sigma_1 \\ \sigma_2 \\ \tau_{12} \end{pmatrix} = \begin{bmatrix} Q_{11} & Q_{12} & 0 \\ Q_{12} & Q_{22} & 0 \\ 0 & 0 & Q_{66} \end{bmatrix} \begin{pmatrix} \epsilon_1 \\ \epsilon_2 \\ \gamma_{12} \end{pmatrix} \quad (6)$$

in which

$$Q_{11} = \frac{E_{11}}{1 - \nu_{12} \nu_{21}} ,$$

$$Q_{22} = \frac{E_{22}}{1 - \nu_{12} \nu_{21}} ,$$

$$Q_{12} = \frac{\nu_{12} E_{22}}{1 - \nu_{12} \nu_{21}} ,$$

$$Q_{66} = G_{12} .$$

E_{11} and E_{22} are, respectively, the Young's moduli in the longitudinal and transverse directions; ν_{12} and ν_{21} are, respectively, the major and minor Poissons' ratios; and G_{12} is the shear modulus. Only four of the five material constants are independent since

$$\nu_{21} E_{11} = \nu_{12} E_{22} .$$

The stress-strain relationship given by eq.(6) is referred to the material axes 1,2 of a lamina. As described in Ref. 1, eq.(6) can be transformed to give the following stress-strain relationship for the lamina referred to the axes x, y of the finite element analysis:

$$\begin{pmatrix} \sigma_x \\ \sigma_y \\ \tau_{xy} \end{pmatrix} = \begin{bmatrix} \bar{Q}_{11} & \bar{Q}_{12} & \bar{Q}_{16} \\ \bar{Q}_{12} & \bar{Q}_{22} & \bar{Q}_{26} \\ \bar{Q}_{16} & \bar{Q}_{26} & \bar{Q}_{66} \end{bmatrix} \begin{pmatrix} \epsilon_x \\ \epsilon_y \\ \gamma_{xy} \end{pmatrix}, \quad (7)$$

or
$$\{\sigma\} = [\bar{Q}] \{\epsilon\} \quad (8)$$

in which

$$\begin{aligned} \bar{Q}_{11} &= Q_{11} \cos^4\theta + 2(Q_{12} + 2Q_{66}) \sin^2\theta \cos^2\theta + Q_{22} \sin^4\theta \\ \bar{Q}_{22} &= Q_{11} \sin^4\theta + 2(Q_{12} + 2Q_{66}) \sin^2\theta \cos^2\theta + Q_{22} \cos^4\theta \\ \bar{Q}_{12} &= (Q_{11} + Q_{22} - 4Q_{66}) \sin^2\theta \cos^2\theta + Q_{12} (\sin^4\theta + \cos^4\theta) \\ \bar{Q}_{66} &= (Q_{11} + Q_{22} - 2Q_{12} - 2Q_{66}) \sin^2\theta \cos^2\theta + Q_{66} (\sin^4\theta + \cos^4\theta) \\ \bar{Q}_{16} &= (Q_{11} - Q_{12} - 2Q_{66}) \sin\theta \cos^3\theta + (Q_{12} - Q_{22} + 2Q_{66}) \sin^3\theta \cos\theta \\ \bar{Q}_{26} &= (Q_{11} - Q_{12} - 2Q_{66}) \sin^3\theta \cos\theta + (Q_{12} - Q_{22} + 2Q_{66}) \sin\theta \cos^3\theta \end{aligned}$$

and θ is the angle between the major material axis of the lamina and the x axis.

By equating internal to external virtual work, using eqs. (3), (5), and (8), the general equation for nodal point stiffness of a triangular finite element can be shown to be (see Refs.2 and 3)

$$[k] = [A^{-1}]^T [B]^T [\bar{Q}] [B] [A^{-1}] V \quad (9)$$

in which V is the volume of the element and the superscripts T and -1 indicate matrix transposition and inversion, respectively. The stiffness matrix $[k]$ relates the six components of force $\{f\}$ acting at the three nodal points of a triangular finite element to the six components of nodal point displacement $\{w\}$ by the expression

$$\{f\} = [k]\{w\} . \quad (10)$$

A different formulation is required for computation of the special shear-stiffness elements that couple conjugate pairs of nodal points in the two adherends. Figure 4(a) and 4(b) show, respectively, schematic plan and cross-section views of a region of an overlay-reinforced sheet. In Fig. 4(b) the x axis is a line of symmetry in the doubly reinforced case; it is a free boundary in the singly reinforced case. In the shear-stiffness element formulation the interlaminar shear stress is assumed to vary as shown in Fig. 4(c). That is, the shear stress is assumed to have a uniform maximum value at the adhesive layer (c to d) and to decrease uniformly to zero at a free surface (a or f) or at a plane of symmetry (a). The area of a shear-stiffness element in the x - y plane is equal to one-third of the sum of the bonded triangular areas meeting at an overlay nodal point. For example, the shear-stiffness element areas for nodal points (1) and (2) in Fig. 4(a) are equal to the areas within the dashed rectangles. The specific shapes of the shear-stiffness elements, in plan, are not defined in the analysis.

The nodal point stiffness matrix for a shear-stiffness element $[k_s]$ relates the two components of shear force $\{f_s\}$ acting in the adhesive layer to the two components of relative displacement of the overlay with respect to the sheet $\{w_s\}$ by the expression

$$\begin{Bmatrix} f_{sx} \\ f_{sy} \end{Bmatrix} = \begin{bmatrix} k_{sx} & 0 \\ 0 & k_{sy} \end{bmatrix} \begin{Bmatrix} u_s \\ v_s \end{Bmatrix} , \quad (11)$$

or

$$\{f_s\} = [k_s] \{w_s\} \quad (12)$$

in which u_s and v_s are, respectively, the x and y components of the difference in displacement of the midplanes of the overlay and the sheet. It is assumed that the shear moduli are uniform within the sheet, within the adhesive, and within the overlay, and that each shear-stiffness element is deformed in pure shear. With these assumptions,

the relative displacement within a shear-stiffness element can be approximated by an integral of the form (see Fig. 4(d))

$$\left(u_s\right)_{me} = \int_m^c \frac{\tau_{xz}}{G_s} dz + \int_c^d \frac{\tau_{xz}}{G_a} dz + \int_d^e \frac{\tau_{xz}}{G_o} dz \quad (13)$$

in which

$$\begin{aligned} m &\equiv a \text{ in the case of a doubly reinforced sheet,} \\ m &\equiv b \text{ in the case of a singly reinforced sheet,} \\ \left(u_s\right)_{me} &= \text{difference between x components of displacement at} \\ &\quad \text{points e and m (point a or b in Fig. 4(b)),} \end{aligned}$$

and G_s , G_a , and G_o are, respectively, the shear moduli of the sheet, the adhesive, and the overlay. In the doubly-reinforced case, integration of eq.(13) between points a and e and substitution into eq.(11) gives the shear-stiffness coefficient

$$k_{sx} = \frac{A_s}{\frac{1}{2} \frac{t_s}{G_s} + \frac{t_a}{G_a} + \frac{3}{8} \frac{t_o}{G_o}} \quad (14)$$

in which

$$\begin{aligned} A_s &= \text{the area of the shear stiffness element in the x-y plane,} \\ t_s &= \text{one-half the thickness of the doubly-reinforced sheet,} \\ t_a &= \text{the thickness of the adhesive,} \\ t_o &= \text{the thickness of the overlay.} \end{aligned}$$

In the singly-reinforced case, integration of eq.(13) between points b and e (Fig.4(b)) and substitution into eq.(11) gives the shear-stiffness coefficient

$$\bar{k}_{sx} = \frac{A_s}{\frac{3}{8} \frac{t_s}{G_s} + \frac{t_a}{G_a} + \frac{3}{8} \frac{t_o}{G_o}} \quad (15)$$

in which t_s is the total thickness of the singly-reinforced sheet, and the other symbols are defined as above.

The stiffness matrices of the various finite elements, $[k]$ in eq.(9) and $[k_s]$ in eq.(12), are superposed to form the stiffness matrix of the entire structure. This is done by adding the stiffness matrix elements that relate displacements to resulting forces for common or adjacent nodal points of adjacent elements. The resulting stiffness matrix of the entire structure $[K]$ relates the external forces applied to the structure $\{F\}$ to the resulting nodal point displacements $\{w\}$ according to the equation

$$\{F\} = [K] \{w\} . \quad (16)$$

This equation can be solved for nodal point displacements $\{w\}$ throughout the structure. In the work reported here, eq.(16) was solved by Gauss-Seidel iteration with overrelaxation and group relaxation as described by Wilson [4].

After the nodal point displacements have been computed, the strains and stresses within the elements can be computed by the use of eqs.(3), (5), (8), and (12). The strains within the triangular finite elements are given by

$$\{\epsilon\} = [B] [A^{-1}] \{w\} , \quad (17)$$

and the corresponding element stresses are given by eq.(8). The adhesive shear stresses $\{\tau_s\}$ are obtained by dividing the adhesive shear forces $\{f_s\}$ by the shear area A_s (see eq.(14)); that is

$$\begin{Bmatrix} \tau_{sx} \\ \tau_{sy} \end{Bmatrix} = \frac{1}{A_s} \begin{bmatrix} k_{sx} & 0 \\ 0 & k_{sy} \end{bmatrix} \begin{Bmatrix} u_s \\ v_s \end{Bmatrix} . \quad (18)$$

The adhesive shear stress components τ_{sx} and τ_{sy} can be added vectorially to give the resultant adhesive shear stress τ_s at each nodal point within the bonded area.

An approximate value for a stress or strain component at the location of a nodal point can be determined by a process of averaging

the stress or strain values already computed for the triangular elements surrounding the nodal point. In the work reported here, weighted average values of nodal point stresses were computed by the following formulas recommended by Wilson [4]:

$$\left(\sigma_x\right)_p = \frac{\sum_{n=1}^N \left(\frac{a_j + a_k}{a_j + a_k + b_j + b_k} \right)^{(n)} \sigma_x^{(n)}}{\sum_{n=1}^N \left(\frac{a_j + a_k}{a_j + a_k + b_j + b_k} \right)^{(n)}} \quad (19)$$

$$\left(\sigma_y\right)_p = \frac{\sum_{n=1}^N \left(\frac{b_j + b_k}{a_j + a_k + b_j + b_k} \right)^{(n)} \sigma_y^{(n)}}{\sum_{n=1}^N \left(\frac{b_j + b_k}{a_j + a_k + b_j + b_k} \right)^{(n)}} \quad (20)$$

$$\left(\tau_{xy}\right)_p = \frac{1}{N} \sum_{n=1}^N \tau_{xy}^{(n)} \quad (21)$$

in which the element dimensions are as defined in Fig.3, and N is the number of surrounding elements that are averaged. Some stress components are discontinuous at an interface between two materials of different stiffness. Therefore, for nodal points located at an interface between the adhesive material and either the sheet or the overlay, separate weighted averages were computed for each material. Nodal point strains were computed by a similar process of averaging element strains. These nodal point stresses and strains are the quantities that were contour plotted. The locations of the contour lines were linearly interpolated between pairs of adjacent nodal points.

2.2. Planform Analysis

A single finite element computer program was developed for the planform analysis of all three of the general configurations

studied. The program computes the in-plane stresses and strains in both the sheet and the overlay and the shear stress in the adhesive. The computer program generates the triangular element networks from input data in the form of gross dimensions, and it controls an electron beam plotter which produces contour plots of the computed stress and strain fields. A plot of the triangular network (FINITE ELEMENT MESH) and contour plots of the following stress and strain fields are produced:

ADHESIVE SHEAR STRESS - The resultant τ_s of the two adhesive shear stress components, τ_{sx} and τ_{sy} , given by eq.(18).

ADHESIVE SHEAR ANGLE - The angle between the direction of the adhesive shear stress resultant τ_s and the x axis.

COMPOSITE X-STRESS - The x component of normal stress (σ_x) in the overlay.

METAL X-STRESS - The x component of normal stress (σ_x) in the sheet.

COMPOSITE Y-STRESS - The y component of normal stress (σ_y) in the overlay.

METAL Y-STRESS - The y component of normal stress (σ_y) in the sheet.

COMPOSITE XY-STRESS - The xy component of shear stress (τ_{xy}) in the overlay.

METAL XY-STRESS - The xy component of shear stress (τ_{xy}) in the sheet.

COMPOSITE MAX-STRESS - The maximum principal stress in the overlay.

METAL MAX-STRESS - The maximum principal stress in the sheet.

COMPOSITE MIN-STRESS - The minimum principal stress in the overlay.

METAL MIN-STRESS - The minimum principal stress in the sheet.

SURFACE X-MICROSTRAIN - The x component of normal strain (ϵ_x) on the exposed surface of the overlay and the surrounding sheet.

SURFACE Y-MICROSTRAIN - The y component of normal strain (ϵ_y) on the exposed surface of the overlay and the surrounding sheet.

SURFACE XY-MICROSTRAIN - The xy component of shear strain (γ_{xy}) on the exposed surface of the overlay and the surrounding sheet.

The following three specific examples serve to describe the planform analysis for the three general configurations.

a. Analysis of a Reinforced Cutout

Figure 5 is a computer-generated plot of the finite element network and the input data for an analysis of a boron/epoxy-reinforced cutout in an aluminum-alloy sheet. The x axis is horizontal and the y axis is vertical. In the table of input data (Fig. 5), all length dimensions are given in inches, stresses and elastic moduli in pounds-force per square inch, and angles in degrees. The following definitions of the terms used in the table of data serve to describe, in part, the scope and character of the analysis:

PLATE - Length, width, and half-thickness of the metal sheet in the first quadrant.

COMPOSITE - Length, width, and maximum thickness of a single composite overlay in the first quadrant.

ADHESIVE - Adhesive thickness. (In this particular plot the number 0.0020 is incorrect. It should be equal to the adhesive depth (ADH DEPTH) of 0.003 given elsewhere in the table.)

CUSHION - Cushion thickness. A cushion is a rectangular layer of unreinforced polymer that, in some cases, reduces the peak adhesive shear stresses at the edge of an overlay. In the analysis reported here the cushion is assumed to have the same material constants as the adhesive. Cross sections of two cushions are shown in Fig. 6 and a cross section of one is shown in Fig. 2.

HOLE CUSHION X - The x coordinate of the right edge of a rectangular cushion surrounding a cutout.

HOLE CUSHION Y - The y coordinate of the upper edge of a rectangular cushion surrounding a cutout.

X CUSHIONS - The x coordinates of the vertical edges of two rectangular cushions. Both cushions extend the full width of the overlay. The first is adjacent to the y axis; the second is adjacent to the vertical edge of the overlay.

Y CUSHION - The y coordinate of the horizontal edge of a cushion adjacent to the horizontal edge of the overlay. If there is no cushion, the coordinate of the overlay edge is given.

X TAPER - The x coordinate of the beginning of a step taper in the x direction. In the analysis the actual step taper is approximated by a uniform taper as indicated by the dashed line in Fig. 6. To compute the stiffness matrix $[k]$ of a triangular planform element in a tapered region,

it is assumed that the element has uniform thickness equal to its tapered thickness at the centroid of the triangle.

Y TAPER - The y coordinate of the beginning of a step taper in the y direction. If there is no taper, the coordinate of the overlay edge is given.

X WIDTH OF HOLE - The maximum x dimension of the cutout in the first quadrant. The computer program permits the analysis of the general class of rectangular cutouts with n-degree-elliptical corner fillets.

Y WIDTH OF HOLE - The maximum y dimension of the cutout in the first quadrant.

X AXIS OF ELLIPSE - The half-length of the x axis of an elliptical cutout, or the x dimension of an elliptical fillet of a rectangular cutout.

Y AXIS OF ELLIPSE - The half-length of the y axis of an elliptical cutout, or the y dimension of an elliptical fillet of a rectangular cutout.

DEGREE OF ELLIPSE - The degree n of an ellipse defined by an equation of the form

$$\left(\frac{x}{a}\right)^n + \left(\frac{y}{b}\right)^n = 1, \quad n \geq 2.$$

CRACK LENGTH - The length of a through crack in the sheet radiating away from the cutout along the y axis. The overlay bridges over the crack. The crack is simulated by providing a free boundary condition for each cracked nodal point, with the exception that shear stiffness coupling with the overlay, eq.(12), is maintained.

NO. DEBOND AREAS - The number of rectangular regions of debonded overlay. The analysis permits up to two rectangular regions throughout which the shear-stiffness elements are disconnected. This is accomplished by setting $k_s = 0$ in the debonded regions. If there are debonded regions, the coordinates of their boundaries are listed here.

DATE - A date that is read in as data.

X BOUNDARY X-STRESS - The x component of normal stress distributed along the vertical x boundary of the sheet. A uniformly distributed stress is

approximated by statically equivalent forces applied at the boundary nodal points.

X BOUNDARY Y-STRESS - The y component of shear stress distributed uniformly along the vertical x boundary of the sheet.

Y BOUNDARY X-STRESS - The x component of shear stress distributed uniformly along the horizontal y boundary of the sheet.

Y BOUNDARY Y-STRESS - The y component of normal stress distributed uniformly along the horizontal y boundary of the sheet.

NONLINEAR K-C-N - The constants K, C, and n of a nonlinear shear stress-strain relationship of the form

$$\gamma_{xz} = \frac{\tau_{xz}}{G_{xz}} + K(\tau_{xz} - C)^n .$$

The three constants are given for the adhesive (ADH) and the overlay (COMP). The analysis permits nonlinear x-z shear response of both the adhesive and the overlay to be approximated by a series of stepwise-linear solutions.

METAL - The orthotropic properties of the sheet (E11, E22, V12, G12), the half-thickness of the sheet (DEPTH), and the angle in the x-y plane between the major material axis of the sheet and the x axis (ANGLE).

ADH - The orthotropic properties, the total thickness, and the material axis orientation of the adhesive layer.

COMP - The orthotropic properties, the maximum thicknesses, and the material axis orientations of one or more stacked layers making up a single overlay. A layer consists of one or more lamina having the same orthotropic properties and material axis orientation. In the analysis, the orthotropic properties for each layer, with respect to the material axes, are first transformed by eq.(8) to give the properties $[Q]$ with respect to the axes x,y. The effective (weighted average) orthotropic properties are then computed for each finite element according to the thicknesses of the separate layers at the centroid of the element.

Figures 7 through 13 are a sample of the fifteen different contour plots produced for the case defined in Fig.5. Figure 7, a plot of the resultant adhesive shear stress, indicates that there are peak adhesive shear stresses near the edge of the cutout and near the corner of the

overlay. Figure 8, a plot of shear stress within the overlay, indicates a longitudinal ridge of high shear stress intersecting the cutout. Figures 9 and 10, plots of the maximum principal stresses in the overlay and sheet, respectively, indicate high tensile stresses at the edge of the cutout. Figures 11 through 13 are plots of strain components in the overlay and in the surrounding sheet.

b. Analysis of a Reinforced Cutout-with-Crack

Figures 14 through 17 are plots of the finite element network and three stress fields for a case that is identical to the one defined in Fig.5, except for a through crack in the sheet radiating away from the cutout along the y axis (CRACK LENGTH 0.210). The x axis is horizontal and the y axis is vertical. The crack is simulated by providing a free boundary condition for the first two sheet nodal points on the y axis and adjacent to the cutout, with the exception that shear-stiffness coupling with the overlay, eq.(12), is maintained for these two points. The third nodal point on the y axis is made to coincide with the end of the crack; therefore, the finite element networks shown in Figs.5 and 14 differ slightly.

Figure 15 is a plot of the resultant adhesive shear stress and Figs.16 and 17 are plots of the maximum principal stress in the overlay and in the sheet, respectively. The stress contours for this case (Figs.15, 16, and 17) approximate those for the corresponding stress fields for the uncracked case (Figs.7, 9, and 10) except for the region adjacent to the crack. A comparison of Figs.7 and 15 indicates that, according to the analysis, the crack causes a significant increase in the peak adhesive shear stress. A comparison of Figs.9 and 16 indicates that the crack causes a significant increase in the maximum principal stress within the part of the overlay that directly bridges over the crack. The greatest value of maximum principal stress within the sheet adjacent to the crack, according to this analysis (Fig.17), is less than the peak value at the edge of the uncracked cutout (Fig.10). The finite element network used here to represent the cracked sheet (Fig.14), however, is far too coarse to indicate the actual peak stresses near the end of the sharp crack.

c. Analysis of a Reinforced Crack

Figure 18 is a computer-generated plot of the finite element network and the input data for the analysis of an aluminum sheet with a transverse crack that is reinforced by an overlay of boron/epoxy. The x axis is horizontal and the y axis is vertical. The format of the data table is the same as for the other planform analyses (Fig.5). The definitions of the terms used in the data table (Fig.18) that are

actually applicable to the cracked sheet analysis are the same as given above for the cutout analysis (Fig.5). The CRACK LENGTH given in Fig.18 is the half-length of the crack. Data terms given in Fig.18 that are actually not applicable to the cracked sheet analysis are given numerical values that are consistent with the concept of a zero size cutout.

For the case defined in Fig.18, Fig.19 is a plot of the resultant adhesive shear stress and Figs.20 and 21 are plots of the maximum principal stresses in the overlay and in the sheet, respectively. The stress contours are roughly parallel to the direction of the transverse crack for a large part of the overlay region. This suggests that a finite element analysis simulating the response within a longitudinal cross-section (an x-z plane) would be useful in the study of reinforced transverse cracks in metal sheet.

2.3. Longitudinal Cross-Section Analysis

A single finite element computer program was developed to simulate the response within a longitudinal cross-section of a sheet with a reinforced transverse crack. The program computes displacements, stresses, and strains (in the x-z plane) within the sheet, the overlay, and the adhesive layer. The triangular analysis network is generated by the program from input data in the form of gross dimensions. The program controls an electron beam plotter which produces a plot of the analysis network (FINITE ELEMENT MESH) and contour plots of the following stress fields:

X-STRESS - The x component of normal stress (σ_x).

Z-STRESS - The z component of normal stress (σ_z).

XZ-STRESS - The xz component of shear stress (τ_{xz}).

MAX-STRESS - The maximum principal stress.

MIN-STRESS - The minimum principal stress.

MAX-SHEAR - The maximum shear stress.

MAX-STRESS ANGLE - The angle between the direction of the maximum principal stress and the x axis.

Figure 22 is a computer-generated plot of the finite element network and the input data for an analysis of an aluminum-alloy sheet with a transverse crack that is doubly reinforced with an overlay of boron/epoxy. The x axis is horizontal and the z axis is vertical. The

z axis scale is magnified to twenty times the x axis scale. The left (z axis) boundary of the plot was lost in a photographic process; it should be continuous and straight as in Fig. 2. The crack extends along the z axis for the full thickness of the sheet. In this doubly reinforced case symmetry is imposed about both the x and z axes. In a singly reinforced case symmetry is imposed about the z axis and the x axis is a free boundary. Although the cross-section program was developed for the study of a sheet with a reinforced transverse crack, the analysis can accurately be interpreted as simulating the response of a bonded joint in which the overlay is either a lapped adherend or a splice plate.

The general definitions of the terms used in the table of input data (Fig.22) are listed below. In the table of data, all length dimensions are given in inches, stresses and elastic moduli in pounds-force per square inch, and angles in degrees.

PLATE - Length and thickness of the metal sheet in the first quadrant.

COMPOSITE - Length and maximum thickness of a single composite overlay in the first quadrant.

ADHESIVE - Adhesive thickness.

DATE - A date that is read in as data.

CUSHION - Cushion thickness (Fig.6).

CUSHION 1 - The x coordinate of the right end of a cushion located adjacent to the z axis.

CUSHION 2 - The x coordinate of the left end of a cushion located adjacent to the right edge of the overlay.

X TAPER - The x coordinate of the beginning of a step taper in the x direction. The actual step taper is approximated by a uniform taper as indicated by the dashed line in Fig.6.

NO. DEBOND AREAS - The number of areas of debonding at the interface between the sheet and the adhesive. Debonding is simulated by disconnecting the finite elements having common boundaries along a debonded interface. If there are debonded areas, the x coordinates of their ends are listed here.

X STRESS - The normal stress distributed along the vertical x boundary at the right end of the sheet. A uniform distributed stress is approximated by statically equivalent forces applied at the boundary nodal points.

NONLINEAR K-C-N - The constants K, C, and n of a nonlinear shear stress-strain relationship of the form

$$\gamma_{xz} = \frac{\tau_{xz}}{G_{xz}} + K(\tau_{xz} - C)^n.$$

The three constants are given for the adhesive (ADH) and the overlay (COMP).

METAL - The orthotropic properties of the sheet (E11, E22, V12, G12), the thickness of the sheet in the first quadrant (DEPTH), and the angle in the x-y plane between the major material axis of the sheet and the x axis (ANGLE).

ADH - The orthotropic properties, the total thickness, and the material axis orientation of the adhesive layer.

COMP - The orthotropic properties with respect to the material axes, the maximum thicknesses, and the material axis orientations of one or more stacked layers making up a single overlay. A layer consists of one or more lamina having the same orthotropic properties and material axis orientation. In the analysis, the orthotropic properties given here are first transformed by eq.(8) to give the properties $[\bar{Q}]$ with respect to the axes x,z. Then the effective (weighted average) orthotropic properties are computed for each triangular finite element according to the cross sectional areas of the separate layers within the triangular element. For example, the effective orthotropic properties for the element defined by the dashed triangle ijk in Fig.6 would be weighted according to the sub-areas of different ply-angle located within the triangle.

Figure 23 is a contour plot of the maximum principal stress for the case defined in Fig.22. This plot illustrates the nature of the discontinuities in a stress field at the interface between different materials.

For the case defined in Fig.22, Fig.24 gives a plot of three shear functions that can be related to the shear-stiffness computations, eqs.(11) through (14), of the planform analysis. An effective shear stiffness k'_{sx} can be computed from the results of the cross-section analysis by the formula

$$k'_{sx} = \frac{\tau_{xz} A_s}{u_s} \quad (22)$$

in which

τ_{xz} = the computed adhesive shear stress at the interface between the adhesive and the sheet,
 A_s = the area over which the shear stress is acting,
 u_s = the x component of the difference in displacement of the midplanes of the overlay and the sheet, that is, the relative x displacement.

The stiffness ratio plotted in Fig.24 is the ratio of the shear stiffness k'_{sx} computed by eq.(22) to the shear stiffness k_{sx} computed by eq.(14). Between $x = 1$ and $x = 3$, Fig.24, the values of both τ_{xz} and u_s are too near zero to permit meaningful numerical computation of k'_{sx} . The fact that k_{sx} roughly approximates k'_{sx} suggests that the assumptions on which eq.(14) was based are reasonably consistent with the cross-section analysis.

2.4. Nonlinear-Shear Analysis

Both the planform analysis and the cross-section analysis permit nonlinear interlaminar shear deformation to be approximated by a converging series of stepwise-linear finite element solutions. It is assumed that the nonlinear shear properties of each material are defined by analytical stress-strain relationships [5] of the type represented schematically in Fig.25. That is,

$$\gamma = \frac{\tau}{G_{12}}, \quad \tau \leq C \quad (23)$$

$$\gamma = \frac{\tau}{G_{12}} + K(\tau - C)^n, \quad \tau > C \quad (24)$$

in which C defines the linear range and the parameters K and n define the slope of the curve in the nonlinear range. The other orthotropic constants (E_{11} , E_{22} , and ν_{12}) are assumed to be unaffected by the nonlinear shear deformation.

In the planform computer program, nonlinear shear deformation is permitted only in the interlaminar shear-stiffness elements (see eq.(12) and Fig.4). Only linear elastic deformation is permitted in the triangular elements (eq.(10) and Fig.3). The following stepwise-linear procedure is used:

1. Obtain an initial finite element solution using the linear elastic material constants throughout the network of triangular and shear-stiffness elements.

2. For each shear-stiffness element, compute the resultant adhesive shear stress τ_s by the use of eq.(18), and select single representative values of the interlaminar shear stresses within the sheet and the overlay. In this analysis, the selected effective shear stresses are the values midway between the limits of integration in eq.(13) for the stress distribution shown in Fig.4(c).
3. For each shear-stiffness element, compute the shear strains within the adhesive, the sheet, and the overlay by substituting into eq.(23) or (24) the shear stresses from step 2.
4. Compute trial effective shear moduli \bar{G}_s , \bar{G}_a , and \bar{G}_o as the ratios of stresses from step 2 to strains from step 3.
5. Recompute the shear stiffness coefficients by substituting into eq.(14) or (15) the shear moduli from step 4.
6. Obtain a finite element solution using the shear-stiffness coefficients from step 5.
7. Repeat steps 2 through 6 until the process converges satisfactorily. Figure 25 shows, schematically, a progression of three iterative cycles for one material of a shear-stiffness element.

In the cross-section computer program, nonlinear shear deformation is permitted throughout the sheet, the adhesive, and the overlay. The following stepwise-linear procedure is used:

1. Obtain an initial finite element solution using the elastic material constants throughout the network of triangular elements.
2. For each element compute the shear stress component by the use of eq.(8).
3. For each element compute the shear strain by substituting into eq.(23) or (24) the shear stress component from step 2.
4. Compute trial effective shear moduli \bar{G}_{12} as the ratios of the stresses from step 2 to the strains from step 3.
5. Recompute the nodal point stiffnesses using the effective shear moduli from step 4.
6. Obtain a finite element solution using the shear stiffness from step 5.

7. Repeat steps 2 through 6 until the process converges satisfactorily.

2.5. Progressive-Debond Analysis

In the planform analysis, progressive adhesive debond can be approximated by a series of finite element solutions. This analysis is based on the premise that the adhesive bond will fail at any point where the resultant adhesive shear stress τ_s reaches a critical value. The following procedure is used in the computer program:

1. Obtain an initial finite element solution for an arbitrary set of uniformly distributed boundary stresses.
2. For each shear-stiffness element, compute the resultant adhesive shear stress τ_s by the use of eq.(18).
3. Determine which shear-stiffness element has the greatest resultant adhesive shear stress. Scale the uniformly distributed boundary stresses up or down to make the greatest value of adhesive shear stress equal the critical value required to cause debond.
4. Remove the critically stressed shear-stiffness element from the finite element network, thus debonding the conjugate pair of nodal points in the sheet and overlay.
5. Obtain a new finite element solution for the network as reduced in step 4 and subjected to the uniformly distributed boundary stresses as scaled in step 3.
6. Repeat steps 2 through 5 as many cycles as desired.

3. DESCRIPTION OF LABORATORY TESTS

A total of 34 specimens were designed, fabricated, instrumented, and tested. These consisted of the following:

1. Four 0.5 in (1.3 cm) wide boron/epoxy coupon tensile specimens for determination of the elastic constants E_{11} , E_{22} , and ν_{12} .
2. One 3.0 in (7.6 cm) diameter boron/epoxy thin-tube torsion specimen for determination of the elastic constant G_{12} .

3. Three 6.0 in (15.2 cm) wide aluminum sheet specimens with no composite reinforcement; one with a circular cutout, one with a circular cutout and sawed slits radiating away from each side of the cutout, and one with a transverse symmetrical sawed slit. The sawed slits were intended to simulate cracks.
4. Six 6.0 in (15.2 cm) wide aluminum sheet specimens with circular cutouts reinforced with overlays of boron/epoxy.
5. Five 6.0 in (15.2 cm) wide aluminum sheet specimens with circular cutouts and slits reinforced with overlays of boron/epoxy.
6. Six 6.0 in (15.2 cm) wide aluminum sheet specimens with transverse slits reinforced with overlays of boron/epoxy.
7. Nine 1.0 in (2.5 cm) wide double lap joint specimens consisting of two aluminum sheets spliced together by overlays of boron/epoxy.

Ten of the 6.0 in (15.2 cm) wide specimens were tested in static tension and ten were tested in low-cycle tension-tension fatigue. Six of the 1.0 in (2.5 cm) wide specimens were tested in static tension and three were tested in low-cycle tension-tension fatigue. The 6.0 in (15.2 cm) wide and 1.0 in (2.5 cm) wide specimens were designed on the basis of computer analyses. The specimens were not optimized with respect to structural efficiency, however, since the prime consideration was that they give definitive data for the evaluation of the computer analyses.

3.1. Specimen Materials

The composite material used in the test specimens was 3M* SP-292 unidirectionally reinforced boron/epoxy. This was purchased in 3.0 in (7.6 cm) wide continuous prepreg tape form with nominally 212 filaments per inch (83 filaments per cm) of tape width. The boron filaments are nominally 0.004 in (0.1 mm) in diameter and preimpregnated with PR-279 epoxy resin. Each ply of boron/epoxy had a glass fiber scrim backing 0.001 in (0.03mm) thick. The cushion material used in some specimens (see Fig.6) was unreinforced PR-279 epoxy resin.

*The identification of the suppliers of materials used in these tests is for information purposes only and is not intended to indicate endorsement by the National Bureau of Standards, nor does it imply that the material was necessarily the best available.

The metal sheet used in three of the 1.0 in (2.5 cm) wide test specimens was cut from a single sheet of 0.126 in (0.320 cm) thick 2024-T4 bare aluminum alloy. The metal sheet used in all other specimens was cut from a single sheet of 0.124 in (0.315 cm) thick 7075-T6 bare aluminum alloy.

The adhesive used to bond the composite overlays to the metal sheet was Armstrong C-4 epoxy and activator W mixed in a 1:1 ratio.

3.2. Specimen Configurations

a. Material Property Specimens

The elastic constants E_{11} , E_{22} , and ν_{12} for the boron/epoxy material were determined by static tensile tests of 8-ply thick by 0.5 in (1.3 cm) wide by 12 in (30 cm) long coupon specimens. Glass-reinforced-plastic tabs, 3.0 in (7.6 cm) in length, were bonded to each end of the specimens. Two specimens used for the determination of E_{11} and ν_{12} had the boron filaments oriented in the longitudinal direction. The average thickness per ply for these two longitudinal specimens was 0.0056 in (0.142 mm). Two specimens used for the determination of E_{22} had the boron filaments oriented in the transverse direction.

The shear modulus G_{12} for the boron/epoxy material was determined by a torsion test of a 4-ply thick by 3.0 in (7.6 cm) diameter by 10 in (25 cm) long hollow cylindrical tube specimen. The boron filaments were oriented in the longitudinal direction.

The elastic constants E and ν for the aluminum-alloy materials were determined by averaging strain measurements made on ten of the 1.0 in (2.5 cm) wide and 6.0 in (15.2 cm) wide specimens. These strains were measured in a region of approximately uniform stress, between the composite-overlay region and an end tab or grip.

The elastic constant E for the epoxy adhesive material was determined by a compression test of a 0.5 in (1.3 cm) diameter by 1.5 in (3.8 cm) long solid cylindrical specimen (Ref.6). A value of 0.35 was assumed for the elastic constant ν on the basis of the manufacturer's literature.

b. Unreinforced Sheet Specimens

Details of the three 6.0 in (15.2 cm) wide unreinforced specimens are given in Fig.26. The first two digits of the specimen designations CUU1, CCU1, or CRU1 (Fig.26) indicate, respectively, the specimen

configuration Cutout, Cutout-with-Crack, or CRacked. The third digit indicates that the specimen is Unreinforced. The fourth digit is a serial number for specimens of the same design.

c. Reinforced Cutout Specimens

The details of the aluminum sheet of the six 6.0 in (15.2 cm) wide reinforced cutout specimens are the same as those for the unreinforced cutout specimen (CUU1) given in Fig.26(a). The 1.50 in (3.81 cm) diameter cutouts were reinforced on both surfaces of the specimen with composite overlays of one of the designs detailed in Fig.27. Three specimens (CUA1, CUA2, and CUA3) were reinforced with overlays of Design A ($\alpha = 45^\circ$) and three specimens (CUB1, CUB2, and CUB3) were reinforced with overlays of Design B ($\alpha = 30^\circ$).

d. Reinforced Cutout-with-Slit Specimens

The details of the aluminum sheet of the five 6.0 in (15.2 cm) wide reinforced cutout-with-slit specimens are the same as those for the unreinforced cutout-with-slit specimen (CCU1) given in Fig.26(b). The 1.50 in (3.81 cm) diameter cutouts with 0.20 in (0.51 cm) long transverse radial slits were reinforced on each side by composite overlays of one of the designs detailed in Fig.27, the same as the overlays that were used to reinforce the cutout specimens. Two specimens (CCA1 and CCA2) were reinforced with overlays of Design A ($\alpha = 45^\circ$) and three specimens (CCB1, CCB2, and CCB3) were reinforced with overlays of Design B ($\alpha = 30^\circ$).

e. Reinforced Transverse-Slit Specimens

The details of the aluminum sheet of the six 6.0 in (15.2 cm) wide reinforced transverse-slit specimens are the same as those for the unreinforced transverse-slit specimen (CRU1) given in Fig.26(c). The 2.4 in (6.1 cm) long transverse slits were reinforced on each side by composite overlays of one of the designs detailed in Figs.28 and 29. Three specimens (CRA1, CRA2, and CRA3) were reinforced with overlays as detailed in Fig.28 and three specimens (CRB1, CRB2, and CRB3) were reinforced with overlays as detailed in Fig.29.

f. Double-Lap Joint Specimens

The nine 1.0 in (2.5 cm) wide double-lap joint specimens consisted of two 12 in (30 cm) long aluminum-alloy sheets, spliced together, end to end, with 6-ply by 1.0 in (2.5 cm) wide by 12.0 in (30.5 cm) long unidirectional 0° boron/epoxy overlays bonded to each surface. The four different overlay configurations detailed schematically in Fig.30 were

represented in the nine specimens. Three specimens (PA1, PB1, PB2) were spliced with plain, fully bonded, uniform-thickness overlays (Fig.30(a)). Three specimens (DA1, DB1, DB2) were spliced with plain, uniform-thickness overlays that were adhesively bonded over only two-thirds of their contact surfaces (Fig.30(b)). Two specimens (CB1, CB2) were spliced with fully bonded, uniform-thickness overlays with 1-ply thick cushions at the center and at each end (Fig.30(c)). One specimen (TA1) was spliced with a fully bonded step-tapered overlay (Fig.30(d)). The aluminum-alloy sheet of three specimens (PA1, DA1, TA1) was 2024-T4; for the other six specimens it was 7075-T6.

- 3.3. Specimen Fabrication

Each boron/epoxy overlay or coupon tensile specimen was laid up and fully cured as a unit before being adhesively bonded to another material. The boron/epoxy was cured in a heated platen press using pressures and temperatures recommended by the manufacturer of the composite prepreg tape.

The aluminum-alloy surface was degreased with acetone and/or methyl ethyl ketone and chemically neutralized with an acidic conditioner and alkaline neutralizer before bonding of the boron/epoxy overlay.

The overlays were bonded to the aluminum-alloy sheet using the epoxy adhesive and a nominal confining pressure, and the specimen was allowed to cure at room temperature for at least seven days before testing.

The boron/epoxy thin-tube torsion specimen was laid up on a plastic-covered wooden mandrel. A heat-shrinkable fluorocarbon plastic tube was then shrunk over the laminate. The specimen was cured using the temperature-time cycle recommended by the manufacturer of the boron/epoxy tape. This fabrication process is described in greater detail in Ref.7.

3.4. Instrumentation

The four boron/epoxy coupon tensile specimens were each instrumented with four resistance strain gages, two longitudinal and two transverse, mounted back to back to permit bending corrections. The boron/epoxy torsion specimen was instrumented with fifteen resistance strain gages grouped in three-gage 45° rosette configurations.

The 6.0 in (15.2 cm) wide specimens were each instrumented with from four to forty-seven resistance strain gages, and the 1.0 in (2.5 cm) wide specimens were each instrumented with from four to twenty-one gages.

For most tests, strains were recorded by a multi-channel data acquisition system. Figure 31 shows a test setup using this system. For some tests involving relatively few strain gages, a single-channel strain indicator and a switching box were used.

3.5. Test Procedures

a. Quasi-Static Tension Tests

The four boron/epoxy coupon specimens were statically loaded to failure in tension using a hydraulic universal testing machine. The boron/epoxy torsion specimen was loaded only within the elastic range using a torsion testing machine.

Ten 6.0 in (15.2 cm) wide specimens were statically loaded to failure in tension using an electrohydraulic testing machine in a setup similar to the one shown in Fig.31. Steel tab plates were bolted to each end of a specimen, and the load was applied to the tab plates through 1.0 in (2.5 cm) diameter steel pins.

Six 1.0 in (2.5 cm) wide double-lap joint specimens were statically loaded to failure in tension using a hydraulic testing machine. The load was applied directly to each end of a specimen by wedge grips.

In all static tests loads were applied slowly in increments and surface strains were measured at each increment. The duration of loading in a material property test was no more than several minutes. The duration of loading in the other static tests, however, was typically thirty minutes or more.

b. Tension-Tension Fatigue Tests

Ten 6.0 in (15.2 cm) wide specimens were tested to failure in tension-tension fatigue using an electrohydraulic testing machine in a setup similar to the one shown in Fig.31. Three 1.0 in (2.5 cm) wide specimens were similarly tested in an electrohydraulic testing machine of smaller capacity.

In all fatigue tests the minimum cyclic load was one-tenth the maximum load ($R = 0.1$). Fatigue loading frequencies of from 1 to 4 Hz were used. Maximum cyclic loads were chosen that were expected to cause failure in less than 100,000 cycles.

Fatigue cycling was interrupted several times during each test and a single cycle of quasi-static load was applied. At maximum cyclic load (static) the specimen was visually examined for any indication of damage and strains were recorded from the resistance gages attached to the specimen.

4. TEST RESULTS AND CORRELATIONS WITH ANALYSES

4.1. Material Properties

The elastic constants determined by tensile tests of the four boron/epoxy coupon specimens were:

$$E_{11} = 28.6 \times 10^6 \text{ lbf/in}^2 = 197 \times 10^9 \text{ N/m}^2$$

$$E_{22} = 2.10 \times 10^6 \text{ lbf/in}^2 = 14.5 \times 10^9 \text{ N/m}^2$$

$$\nu_{12} = 0.168$$

The average tensile strength of the two specimens with longitudinal fiber orientation was 195000 lbf/in² (1340 x 10⁶N/m²). The average tensile strength of the two specimens with transverse fiber orientation was 5400 lbf/in² (37 x 10⁶N/m²).

The shear modulus determined by a torsion test of the boron/epoxy tube specimen was:

$$G_{12} = 0.759 \times 10^6 \text{ lbf/in}^2 = 5.22 \times 10^9 \text{ N/m}^2$$

The elastic constants determined by averaging strain measurements made on the surfaces of seven specimens made with 7075-T6 aluminum alloy were:

$$E = 9.92 \times 10^6 \text{ lbf/in}^2 = 68.4 \times 10^9 \text{ N/m}^2$$

$$\nu = 0.318$$

The value of Young's modulus determined by averaging strain measurements made on the surfaces of three specimens made with 2024-T4 aluminum alloy was:

$$E = 10.40 \times 10^6 \text{ lbf/in}^2 = 71.7 \times 10^9 \text{ N/m}^2$$

It was assumed that Poisson's ratio for the 2024-T4 alloy was the same as that determined for the 7075-T6 alloy.

The value of Young's modulus determined by a compression test of a cylindrical specimen of the epoxy adhesive material was:

$$E = 0.27 \times 10^6 \text{ lbf/in}^2 = 1.9 \times 10^9 \text{ N/m}^2$$

The value of Poisson's ratio for the adhesive was assumed to be 0.35.

4.2. Unreinforced Sheet

Figure 32 shows the three unreinforced aluminum sheet specimens after they were tested to failure in static tension.

The cutout specimen (CUU1) failed at a surprisingly high load of 46000 lbf (205000 N). This was a ductile failure with visible elongation of the cutout and necking of the specimen in both the thickness and width directions. A lower bound on the maximum tensile stress at the failure surface can be computed by dividing the failure load by the net cross sectional area. This computation gives a value of 82500 lbf/in² (569 x 10⁶ N/m²) which is slightly higher than the handbook value of ultimate tensile strength for this material (Ref.8). This suggests that the tensile stresses were distributed rather uniformly across the net cross section just before failure.

The cutout-with-slit specimen (CCU1) failed at a load of 19900 lbf (88500 N) and the transverse slit specimen (CRU1) failed at a load of 18750 lbf (83400 N).

Strains measured on the surface of the three unreinforced specimens can be compared directly with strains predicted by the planform finite element analysis. Figure 33 indicates the locations and orientations of strain gages on the specimens, the measured microstrains (in parentheses), and the microstrains predicted by the analysis, for an applied tensile load of 4000 lbf (17800 N). The multiple numbers (in parentheses) indicate microstrain measurements from strain gages symmetrically located in different quadrants of a specimen. The analytical strains were linearly interpolated from the contour plots of strain components. For comparison with strains measured by gages oriented at an angle, the analytical strains were computed from the x and y components of normal strain and the xy component of shear strain.

4.3. Reinforced Cutout

Figures 34 and 35 show the six reinforced cutout specimens after they were tested to failure in static tension or tension-tension fatigue. During the static tensile test of specimen CUA1 there was a shear failure of the tab bolts at one end at a load of 38250 lbf (170100 N). The sudden release of load caused failure of one overlay without failure of the aluminum sheet (Fig.34).

The maximum tensile loads (static or fatigue) and the cycles to failure (fatigue) for all seven cutout specimens (including the unreinforced cutout) are given in Table 1. The table also gives certain stress components, computed by the planform finite element analysis, that have been scaled to correspond to the applied maximum tensile load for the particular specimen. The x and y coordinates of the point at which a stress is acting are given below the stress. Some of these stress components may be related to the failure modes evident in Figs.34 and 35. Notice, for example, the very high values of tensile stress in the composite at the edge of the cutout for specimens CUA2 and CUB1 and the corresponding tensile failure modes evident in the photographs.

Table 1 - Tests of Cutout Specimens (a)

Specimen No.	CUU1	CUA1	CUA2	CUA3	CUB1	CUB2	CUB3
Maximum load, lbf	46000	38250 ^(b)	47000	33750	46400	29250	22500
Cycles to failure	static	static	static	2773	static	3306	9151
Mean tensile stress applied (max), lbf/in ²	61800	51400	63200	45400	62400	39300	30200
σ_x (max) in sheet at y axis, lbf/in ²	202700 (0, .75)	92400 (0, .75)	113500 (0, .75)	81500 (0, .75)	108600 (0, .75)	68500 (0, .75)	52700 (0, .75)
σ_x (max) in overlay at y axis, lbf/in ²	-	232200 (0, .75)	285400 (0, .75)	204900 (0, .75)	304900 (0, .75)	192200 (0, .75)	147900 (0, .75)
σ_x (max) in overlay near edge of overlay, lbf/in ²	-	134800 (2.5, 1.25)	165600 (2.5, 1.25)	118900 (2.5, 1.25)	171100 (2.5, 1.5)	107900 (2.5, 1.5)	81000 (2.5, 1.5)
σ_y (max tension) in overlay, lbf/in ²	-	9980 (.25, .71)	12260 (.25, .71)	8800 (.25, .71)	10420 (.13, .74)	6570 (.13, .74)	5050 (.13, .74)
τ_{xy} (max) in overlay, lbf/in ²	-	19030 (.31, .68)	23380 (.31, .68)	16790 (.31, .68)	20200 (.31, .68)	12740 (.31, .68)	9800 (.31, .68)
τ_s (max) in adhesive near edge of cutout lbf/in ²	-	3150 (.31, .68)	3870 (.31, .68)	2780 (.31, .68)	4540 (.37, .65)	2860 (.37, .65)	2200 (.37, .65)
τ_s (max) in adhesive near edge of overlay, lbf/in ²	-	3740 (2.5, 1.5)	4600 (2.5, 1.5)	3300 (2.5, 1.5)	5000 (2.07, 1.5)	3150 (2.07, 1.5)	2430 (2.07, 1.5)

(a) Stresses are scaled from the finite element analyses. The x and y coordinates of the point at which a stress is acting are given below the stress.

(b) Shear failure of tab bolts.

Longitudinal splitting and debonding of the boron/epoxy overlays is evident in all six reinforced cutout specimens (Figs.34 and 35). In the three fatigue specimens the splitting and debonding was visible long before fatigue failure. In specimen CUB2, for example, after only 500 fatigue cycles the splitting and debonding had progressed to the extent that there was little effective reinforcement from the overlay on one side of the specimen. The contour plots of xy shear stress in the composite indicate longitudinal ridges of high stress in the locations of these splitting failure surfaces. See, for example, Fig.8 which is from the analysis of specimen CUB1.

Strains measured on the surfaces of specimens CUA1 and CUB1 were compared with strains computed by the finite element analysis for an applied load of 11250 lbf (50040 N). Figures 36 and 37 indicate the locations and orientations of strain gages on the specimens, the measured microstrains (in parentheses), and the microstrains predicted by the analysis.

4.4. Reinforced Cutout-with-Slit

Figures 38 and 39 show the five reinforced cutout-with-slit specimens after they were tested to failure in static tension or tension-tension fatigue. The maximum tensile loads (static or fatigue) and the cycles to failure (fatigue) for all six cutout-with-slit specimens (including the unreinforced cutout-with-slit) are given in Table 2. The table also gives certain stress components, computed by the planform finite element analysis, that have been scaled to correspond to the applied maximum load for the particular specimen. The x and y coordinate of the point at which a stress is acting are given below the stress. Some of these stress components may be related to the failure modes evident in Figs.38 and 39. The relatively low failure load for specimen CCB1 may be related to the presence of an air pocket, roughly 0.8 in^2 (5 cm^2) in area, in the adhesive layer near one end of an overlay.

A combination of tensile failure, splitting, and debonding is evident in the three fatigue specimens (Figs.38 and 39). Splitting and debonding were observed during fatigue testing in only one specimen (CCB3). That occurred in a corner of one overlay midway through the fatigue test and then apparently remained stable until failure of the specimen.

In all three fatigue specimens, the extent of crack growth before failure is clearly visible on the fracture surface of the aluminum-alloy sheet. The lengths of crack growth in the three specimens were 0.10, 0.24, 0.30, 0.30, 0.47, and 0.53 in (2.5, 6.1, 7.6, 7.6, 12.0, 13.5 mm). There was no tensile failure evident in the boron/epoxy overlay near the 0.10 in (2.5 mm) crack extension. There was tensile failure in the overlays near the five longer crack extensions, however.

Table 2 - Tests of Cutout-with-Slit Specimens (a)

Specimen No.	CCU1	CCA1	CCA2	CCB1	CCB2	CCB3
Maximum load, lbf	19900	29250	22500	24000	22500	16875
Cycles to failure	static	static	2740	static	5582	7697
Mean tensile stress applied (max), lbf/in ²	26700	39300	30200	32300	30200	22700
σ_x (max) in sheet at y axis, lbf/in ²	108300 (0, .96)	55500 (0, .96)	42700 (0, .96)	43500 (0, .96)	40800 (0, .96)	30600 (0, .96)
σ_x (max) in overlay at y axis, lbf/in ²	-	223400 (0, .75)	171800 (0, .75)	194600 (0, .75)	182400 (0, .75)	136800 (0, .75)
σ_x (max) in overlay near edge of overlay, lbf/in ²	-	103800 (2.5, 1.25)	79800 (2.5, 1.25)	89000 (2.5, 1.25)	83400 (2.5, 1.25)	62600 (2.5, 1.25)
σ_y (max tension) in overlay, lbf/in ²	-	11200 (0, .96)	8620 (0, .96)	7400 (0, .96)	6940 (0, .96)	5200 (0, .96)
τ_{xy} (max) in overlay, lbf/in ²	-	13400 (.31, .68)	10310 (.31, .68)	9560 (.31, .68)	8960 (.31, .68)	6720 (.31, .68)
τ_s (max) in adhesive near edge of cutout, lbf/in ²	-	13340 (.06, .75)	10260 (.06, .75)	10460 (.06, .75)	9810 (.06, .75)	7360 (.06, .75)
τ_s (max) in adhesive near edge of overlay, lbf/in ²	-	2880 (2.5, 1.5)	2220 (2.5, 1.5)	2600 (2.1, 1.5)	2440 (2.1, 1.5)	1830 (2.1, 1.5)

(a) Stresses are scaled from the finite element analyses. The x and y coordinates of the point at which a stress is acting are given below the stress.

Strains measured on the surfaces of specimens CCA1 and CCB1 were compared with strains computed by the finite element analysis for an applied load of 11250 lbf (50040 N). Figures 40 and 41 indicate the locations and orientations of strain gages on the specimens, the measured microstrains (in parentheses), and the microstrains predicted by the analysis.

4.5. Reinforced Transverse Slit

Figures 42 and 43 show the six reinforced transverse-slit specimens after they were tested to failure in static tension or tension-tension fatigue. The maximum tensile loads (static or fatigue) and the cycles to failure (fatigue) for all seven transverse crack specimens (including the unreinforced transverse crack) are given in Table 3. The table also gives certain stress components, computed by the planform finite element analysis, that have been scaled to correspond to the applied maximum load for the particular specimen. The x and y coordinates of the point at which a stress is acting are given below the stress. Some of the stress components may be related to the failure modes evident in Figs.42 and 43.

The relatively low failure load and the mode of failure for specimen CRB1 was caused by the inadvertent inclusion of a sheet of plastic release material between two plies of one overlay. The outer four plies popped off the specimen and the remaining two plies failed in tension.

In all four fatigue specimens, the extent of crack growth before failure is clearly visible on the fracture surface of the aluminum-alloy sheet. The lengths of fatigue crack growth in the four specimens ranged from 0.02 to 0.28 in (0.5 to 7.1 mm). There was no apparent correlation between length of fatigue crack growth and either strength or mode of failure for these specimens.

Strains measured on the surfaces of specimens CRA1 and CRB1 were compared with strains computed by the finite element analysis for an applied load of 11250 lbf (50040 N). Figures 44 and 45 indicate the locations and orientations of strain gages on the specimens, the measured microstrains (in parentheses), and the microstrains predicted by the analysis.

4.6. Double-Lap Joints

Figures 46 through 49 show the nine double-lap joint specimens after they were tested to failure in static tension or tension-tension fatigue. The maximum tensile loads (static or fatigue) and the cycles to failure (fatigue) for all nine double-lap joint specimens are given in Table 4. The table also gives certain stress components, computed by

Table 3 - Tests of Transverse Slit Specimens (a)

Specimen No.	CRU1	CRA3	CRA1	CRA2 ^(b)	CRB1	CRB2	CRB3
Maximum load, lbf	18750	34850	22500	(1) 11250 (2) 16875	30000 (c)	22500	16875
Cycles to failure	static	static	5191	(1) 100000 (2) 19342	static	5777	5935
Mean tensile stress applied (max), lbf/in ²	25200	46800	30200	22700	40300	30200	22700
σ_x (max) in sheet at y axis, lbf/in ²	86400 (0, 1.2)	35500 (0, 1.2)	22900 (0, 1.2)	17200 (0, 1.2)	28700 (0, 1.2)	21500 (0, 1.2)	16100 (0, 1.2)
σ_x (max) in overlay at y axis, lbf/in ²	-	118900 (0, .76)	76800 (0, .76)	57600 (0, .76)	70500 (0, .6)	52900 (0, .6)	39700 (0, .6)
σ_x (max) in overlay near edge of overlay, lbf/in ²	-	133600 (2, 1.2)	86300 (2, 1.2)	64700 (2, 1.2)	108300 (2, 1.2)	81200 (2, 1.2)	60900 (2, 1.2)
σ_y (max tension) in overlay, lbf/in ²	-	411 (0, 0)	265 (0, 0)	199 (0, 0)	7500 (1.47, 1.2)	5620 (1.47, 1.2)	4220 (1.47, 1.2)
τ_{xy} (max) in overlay, lbf/in ²	-	722 (2, 1.5)	466 (2, 1.5)	350 (2, 1.5)	8140 (1.47, 1.2)	6110 (1.47, 1.2)	4580 (1.47, 1.2)
τ_s (max) in adhesive near y axis, lbf/in ²	-	7150 (0, .6)	4610 (0, .6)	3460 (0, .6)	5290 (0, .6)	3960 (0, .6)	2970 (0, .6)
τ_s (max) in adhesive near edge of overlay, lbf/in ²	-	2800 (1.47, 1.5)	1810 (1.47, 1.5)	1350 (1.47, 1.5)	2410 (2, 1.2)	1810 (2, 1.2)	1350 (2, 1.2)

(a) Stresses are scaled from the finite element analyses. The x and y coordinates of the point at which a stress is acting are given below the stress.

(b) Loaded 100000 cycles to 11250 lbf, then loaded 19342 cycles to 16875 lbf.

(c) Sheet of release material inadvertently included in one overlay.

Table 4 - Tests of Double-Lap Joints (a)

Specimen No.	PAL	PB2	PB1	DA1	DB2	DB1	CB2	CB1	TA1
Overlay	Plain	Plain	Plain	Partial bond	Partial bond	Partial bond	Cushion	Cushion	Taper
Aluminum alloy	2024-T4	7075-T6	7075-T6	2024-T4	7075-T6	7075-T6	7075-T6	7075-T6	2024-T4
Maximum Load, lbf	6400	6000	4000	6300	8250	3000	6690	4000	6740
Cycles to failure	Static	Static	14000	Static	Static	35567	Static	10934	Static
Mean tensile stress applied (max), lbf/in ²	51200	48600	32400	50000	66900	24300	54200	32400	53700
σ_x (max) in overlay at joint, lbf/in ²	100900 (0, .066)	102300 (0, .062)	68200 (0, .062)	95700 (0, .083)	125700 (0, .082)	45700 (0, .082)	127300 (0, .071)	76100 (0, .071)	107600 (0, .066)
σ_x (max) in overlay away from joint, lbf/in ²	-	-	-	107900 (.93, .066)	139600 (1, .065)	50700 (1, .065)	-	-	143300 (6, .066)
σ_z (max) in adhesive, lbf/in ²	4460 (6, .063)	5670 (6, .062)	3780 (6, .062)	2430 (5, .063)	4180 (5, .062)	1520 (5, .062)	3470 (6, .062)	2080 (6, .062)	240 (.19, .063)
τ_{xz} in adhesive at inside end of bond, lbf/in ²	11180 (0, .063)	10560 (0, .062)	7040 (0, .062)	7790 (1, .063)	10650 (1, .062)	3870 (1, .062)	8180 (0, .062)	4890 (0, .062)	11810 (0, .063)
τ_{xz} in adhesive at outside end of bond, lbf/in ²	15200 (6, .063)	15410 (6, .062)	10270 (6, .062)	11340 (5, .063)	16610 (5, .062)	6040 (5, .062)	10270 (6, .062)	6140 (6, .062)	1990 (6, .063)

(a) Stresses are scaled from the finite element analyses. The x and z coordinates of the point at which a stress is acting are given below the stress.

the longitudinal cross-section finite element analysis, that have been scaled to correspond to the applied maximum load for the particular specimen. The x and z coordinates of the point at which a stress is acting are given below the stress.

The tensile failure evident in one tapered boron/epoxy overlay of specimen TA1 (Fig.49) was probably a secondary failure that occurred after debonding of the other overlay. The two specimens with single-ply cushions (both static and fatigue, Fig.48) failed in a combination of debond and delamination. The delaminations occurred between the first and second inner plies and apparently were precipitated by the inner cushions. The other six double-lap joint specimens (both static and fatigue, Figs. 46 and 47) failed by debonding of the overlays in two or three quadrants.

The progression of debonding was clearly visible during each of the three fatigue tests. It began at the end of an overlay and grew toward the center of the specimen. In specimen PB1, for example, debonding over a length of about 1 in (3 cm) was observed after 4000 fatigue cycles; just before failure at 14000 cycles there was visible debonding over a length of about 4 in (10 cm) in two quadrants.

Longitudinal strains measured on the surface of specimens PB2, DA1, CB2, and TA1 were compared with strains computed by the longitudinal cross-section analysis for an applied load of 2500 lbf (11120 N). Figures 50 through 53 are plots of the longitudinal surface strain distributions as predicted by the analysis (continuous curve) and as measured (data points).

4.7. Discussion of Results

Strains measured on the surfaces of the test specimens are, for the most part, in good agreement with strains computed by the finite element analyses. Agreement is best in the reinforced transverse-slit specimen (CR1) which had relatively thin 4-ply overlays. There is apparent systematic disagreement at two locations in both the cutout and cutout-with-slit specimens. On the x axis, adjacent to the cutout, the measured strains on five specimens (CUU1, CUA1, CUB1, CCA1, CCB1) are, on the average, only 58 percent of the corresponding computed strains. On the y axis, adjacent to the cutout, the measured strains on the same five specimens are, on the average, 82 percent of the corresponding computed strains.

Examination of the specimens after testing indicates significant similarities in modes of failure of specimens of the same design, whether subjected to static or fatigue loading (Figs.34, 35, 38, 39, 42, 43, 46, 47 and 48). These similarities are more clearly evident in the

transverse-slit specimens and the lap-joint specimens than in the cutout and the cutout-with-slit specimens. Examination of the debonded surfaces suggests that there was considerable variation in bond quality from specimen to specimen and within a single specimen.

5. CONCLUSION

Finite element computer programs have been developed to analyze the reinforcement of cutouts and cracks in metal sheet by adhesively bonded overlays of composite materials. The programs are also suitable for the analysis of adhesively bonded lap joints. The analyses articulate the separate responses of the bonded adherends and the adhesive.

The outputs from the computer programs include contour plots of stress and strain fields throughout each of the constituents of a bonded system. This form of output enables one to visualize the interactions between the different elements of the total system. The contour plots can also indicate the presence of a stress condition that might initiate or drive a crack or a debond.

The computer programs can accommodate the analysis of a broad class of reinforced-cutout, reinforced-crack, and lap-joint configurations. Such special features as cushions, tapers, and debonded regions can be explicitly studied. The computer programs generate the finite element networks from input data in the form of gross dimensions. These characteristics of the programs make them efficient for use in design studies.

A series of laboratory tests was conducted to demonstrate the validity of the analyses. Strains measured on the surfaces of a wide variety of test specimens were, for the most part, in good agreement with strains predicted by the analyses. Significant correlations between some failure modes and the stresses computed by the analyses were apparent. Some similarities in modes of failure of similar specimens, whether subjected to static or fatigue loading, were evident.

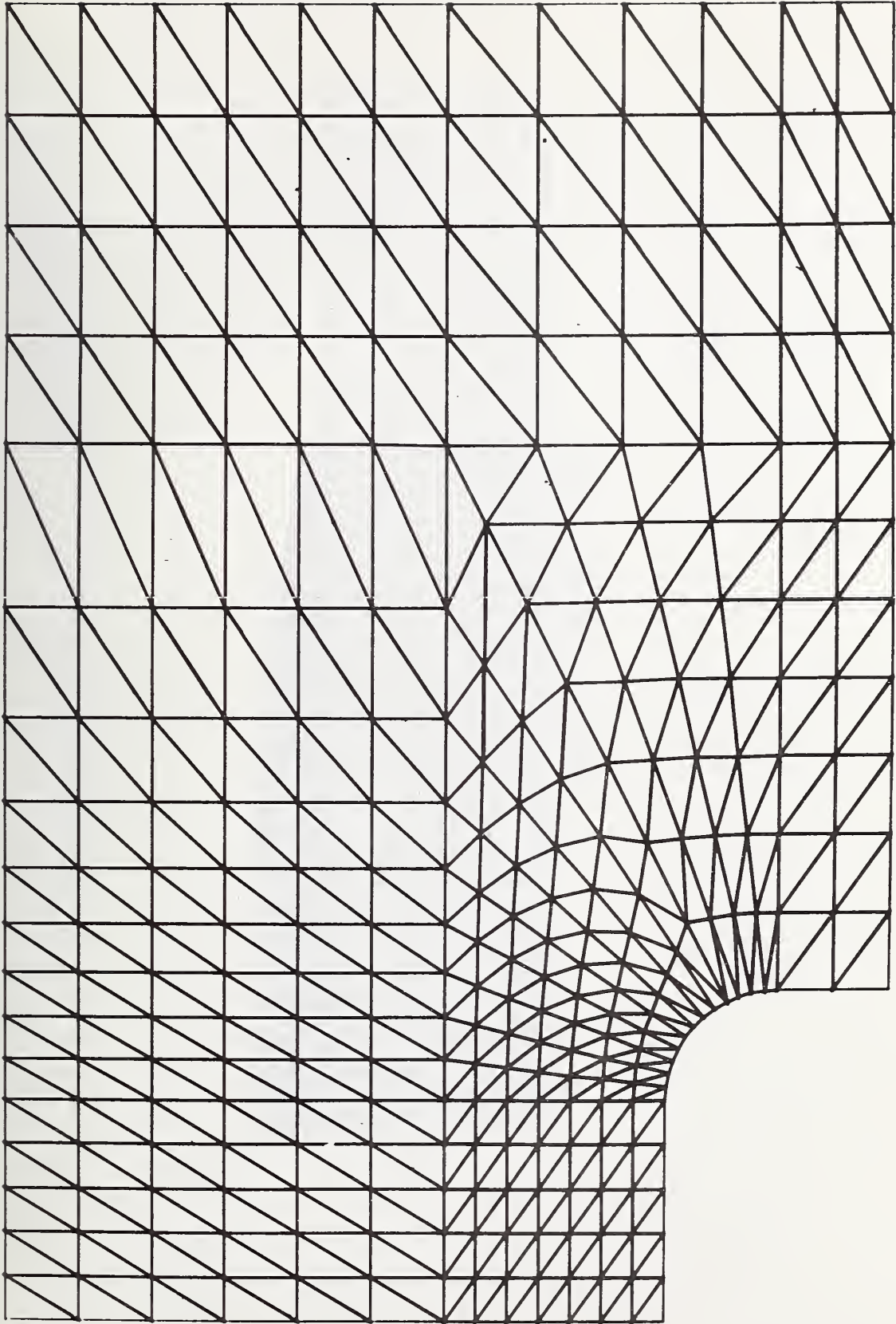
* * *

The following valuable contributions to this work are gratefully acknowledged:

Technical review and consultation	- Leonard Mordfin
Computer programming	- Saul M. Baker
Specimen fabrication	- Robert L. Breeden
Instrumentation	- Robert E. Snyder.

6. REFERENCES

- 1 Ashton, J.E., Halpin, J.C., and Petit, P.H., Primer on Composite Materials: Analysis (Technomic, 1969).
- 2 Clough, R.W., The finite element method in structural mechanics, chapter 7 of Stress Analysis, Eds. Zienkiewicz, O.C. and Holister, G.S. (Wiley, 1965).
- 3 Zienkiewicz, O.C., The Finite Element Method in Engineering Science (McGraw-Hill, 1971).
- 4 Wilson, E.L., Finite Element Analysis of Two-Dimensional Structures, Structures and Materials Research Report No. 63-2, U. of Calif. Berkeley (June 1963).
- 5 Osgood, W.R., Stress-Strain Formulas, J. Aeronautical Sci. 13, No.1, 45-48 (Jan. 1946).
- 6 Halsey, N., Mitchell, R.A., and Mordfin, L., Evaluation of GRP Rod and Rope Materials and Associated End Fittings, NBSIR 73-129 (Dec. 1972).
- 7 Marlowe, D.E., Torsional Instabilities in Composite and Composite-Reinforced Aluminum-Alloy Thin-Walled Cylinders, NBS Technical Note 728 (June 1972).
- 8 Metallic Materials and Elements for Aerospace Vehicle Structures, MIL-HDBK-5A (Aug. 1972).



FINITE ELEMENT MESH .

Figure 1 - Finite element network for a planform analysis of a reinforced cutout.



FINITE ELEMENT MESH

Figure 2 - Finite element network for a longitudinal cross-section analysis of a reinforced transverse crack.

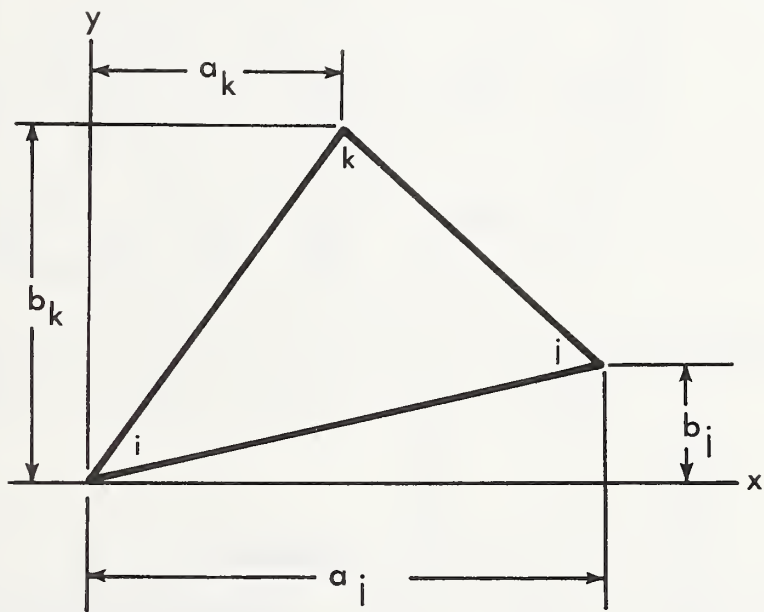


Figure 3 - General triangular finite element.

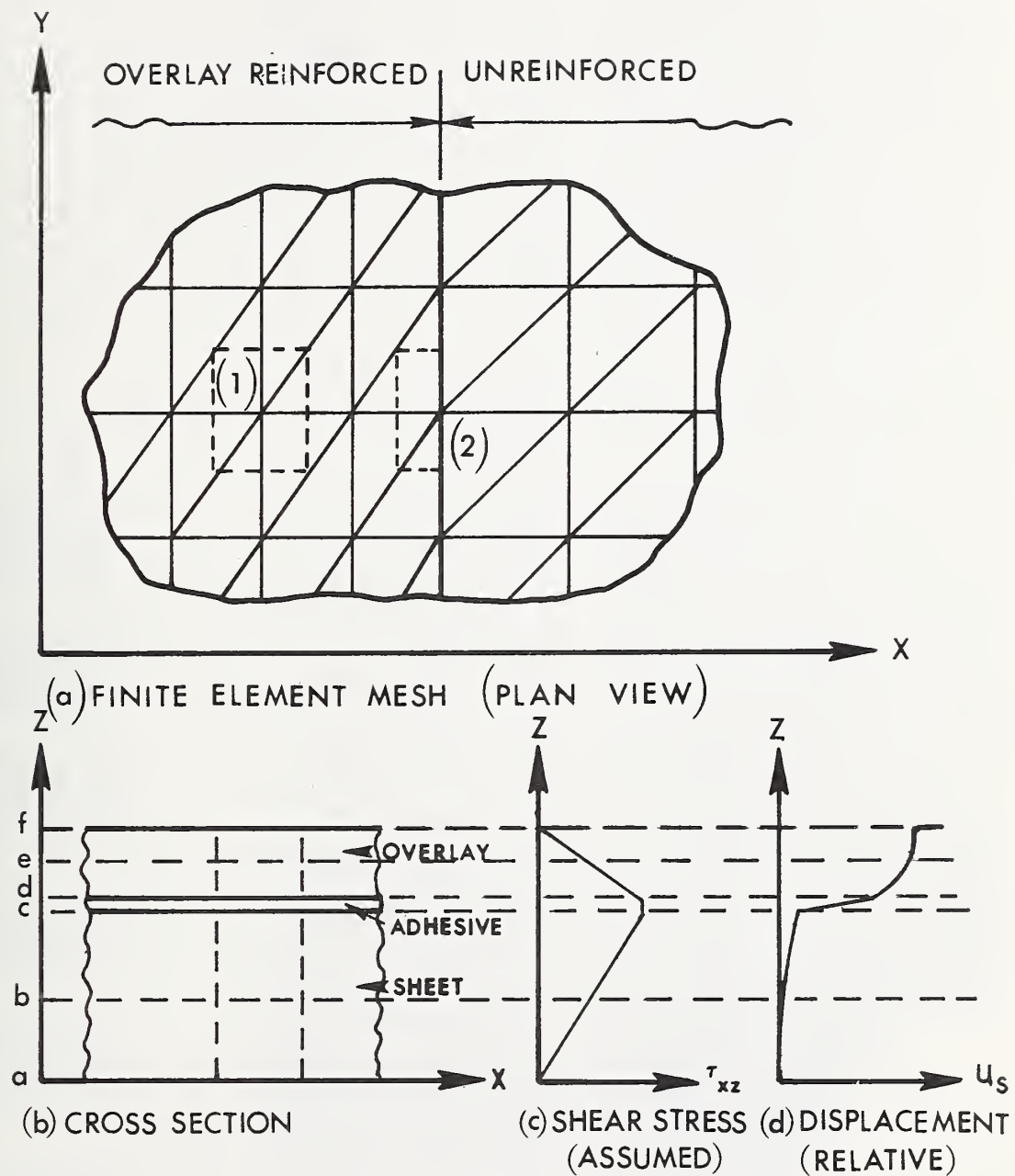


Figure 4 - Schematic basis for shear-stiffness element.



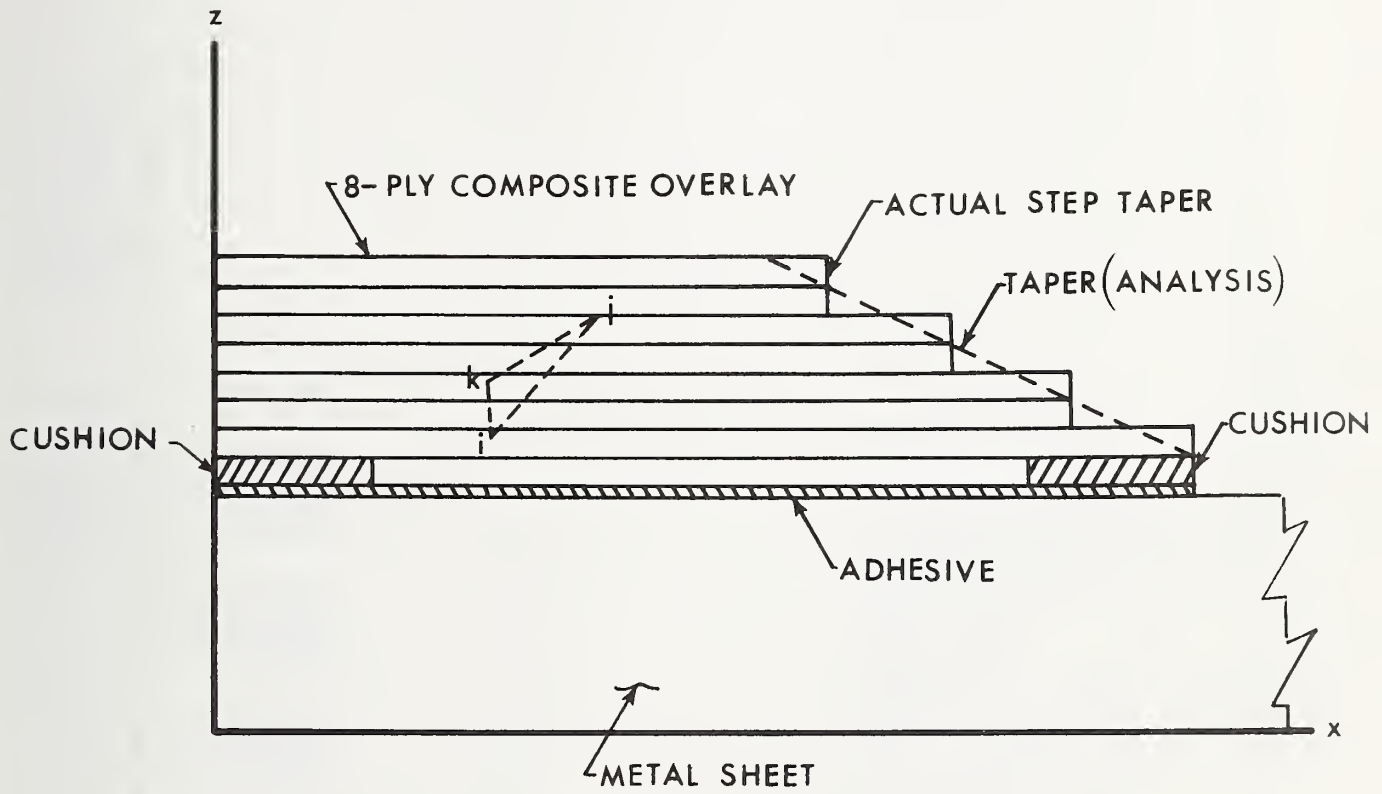
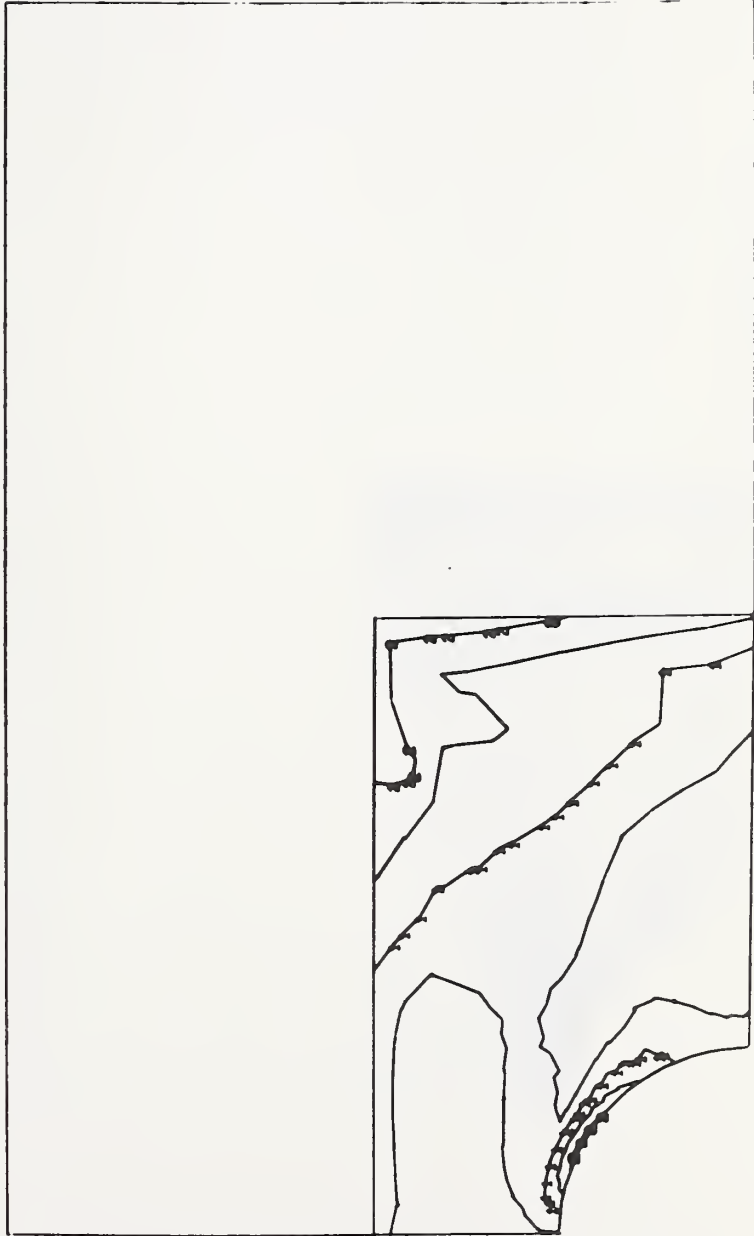


Figure 6 - Schematic cross-section of an overlay-reinforced sheet.



CUSHION .0056
X WIDTH OF HOLE .750
Y WIDTH OF HOLE .750
DEGREE OF ELLIPSE 2.000
DATE AUGUST 17, 1972
Y BOUNDARY Y-STRESS 0.

PLATE 5.00 X 3.00 X .0620 COMPOSITE -2.50 X 1.50 X .0445 ADHESIVE .0020
HOLE CUSHION X .000 X CUSHIONS .000 2.000 X TAPER 1.100
HOLE CUSHION Y .000 Y CUSHION 1.500 Y TAPER 1.500
CRACK LENGTH .000 X AXIS OF ELLIPSE .750 Y AXIS OF ELLIPSE .750
NO. DEBOND AREAS 0 X BOUNDARY X-STRESS 0. Y BOUNDARY X-STRESS 0.
NONLINEAR K-C-N ADH .0000 - 0. - .00 CONF .0000 - 0. - .00
E11 E22 E33 G12 G13 G14 G15 G16 G17 G18 G19 G20 G21 G22 G23 G24 G25 G26 G27 G28 G29 G30
METAL .9920000+07 .9920000+07 .3160000+00 .3763277+07 .6200000-01 .0
ADH .2700000+06 .2700000+06 .3500000+00 .1000000+06 .3000000-02 .0
CONF .2680000+08 .2100000+07 .1660000+00 .7590000+06 .1112500-01 .0
CONF .2680000+08 .2100000+07 .1660000+00 .7590000+06 .5980000-02 30.0
CONF .2680000+08 .2100000+07 .1660000+00 .7590000+06 .5963000-02 -30.0
CONF .2680000+08 .2100000+07 .1660000+00 .7590000+06 .2225000-01 .0



ADHESIVE SHEAR STRESS
CONTOUR INTERVAL 500 LABEL INTERVAL 1000

Figure 7 - Contour plot of the resultant adhesive shear stress for the case defined in Fig. 5.





PLATE 5.00 X 3.00 X .0620 COMPOSITE 2.50 X 1.50 X .0445 ADHESIVE .0020
 HOLE CUSHION X .000 X CUSHIONS .000 X TAPER 1.100
 HOLE CUSHION Y .000 Y CUSHION 1.500 Y TAPER 1.500
 CRACK LENGTH .000 X AXIS OF ELLIPSE .750 Y AXIS OF ELLIPSE .750
 NO. DEBOND AREAS 0
 X BOUNDARY X-STRESS 30000. X BOUNDARY Y-STRESS 0. Y BOUNDARY X-STRESS 0.
 NONLINEAR K-C-N E11 E22 V12 G12 DEFTH ANGLE
 .99200000+07 .99200000+07 .31600000+00 .37632777+07 .62000000-01 .0
 .27000000+06 .27000000+06 .35000000+00 .10000000+06 .30000000-02 .0
 .29600000+08 .21000000+07 .16600000+00 .79800000+06 .11112500-01 .0
 .29600000+08 .21000000+07 .16600000+00 .79800000+06 .59620000-02 30.0
 .29600000+08 .21000000+07 .16600000+00 .79800000+06 .59630000-02 -30.0
 .29600000+08 .21000000+07 .16600000+00 .79800000+06 .22230000-01 .0

CUSHION .0056
 X WIDTH OF HOLE .750
 Y WIDTH OF HOLE .750
 DEGREE OF ELLIPSE 2.000
 DATE AUGUST 17, 1972
 Y BOUNDARY Y-STRESS 0.

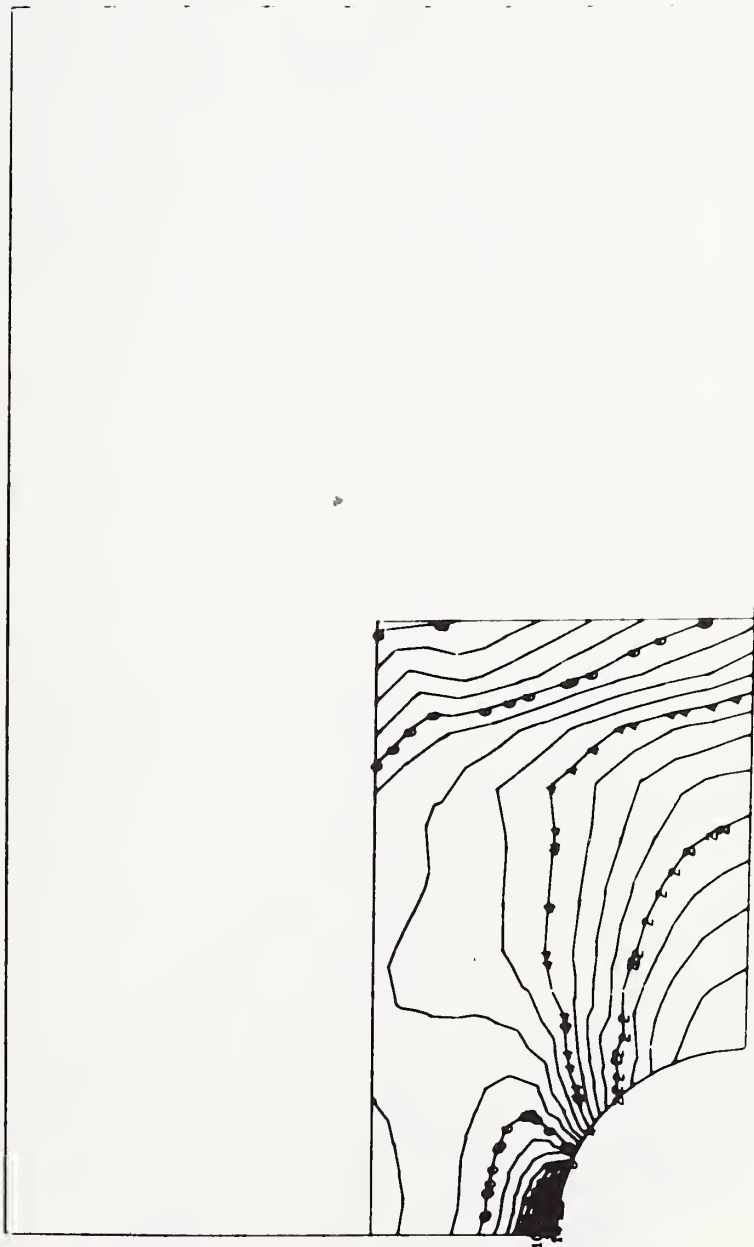


Figure 9 - Contour plot of maximum principal stress in the overlay for the case defined in Fig. 5.



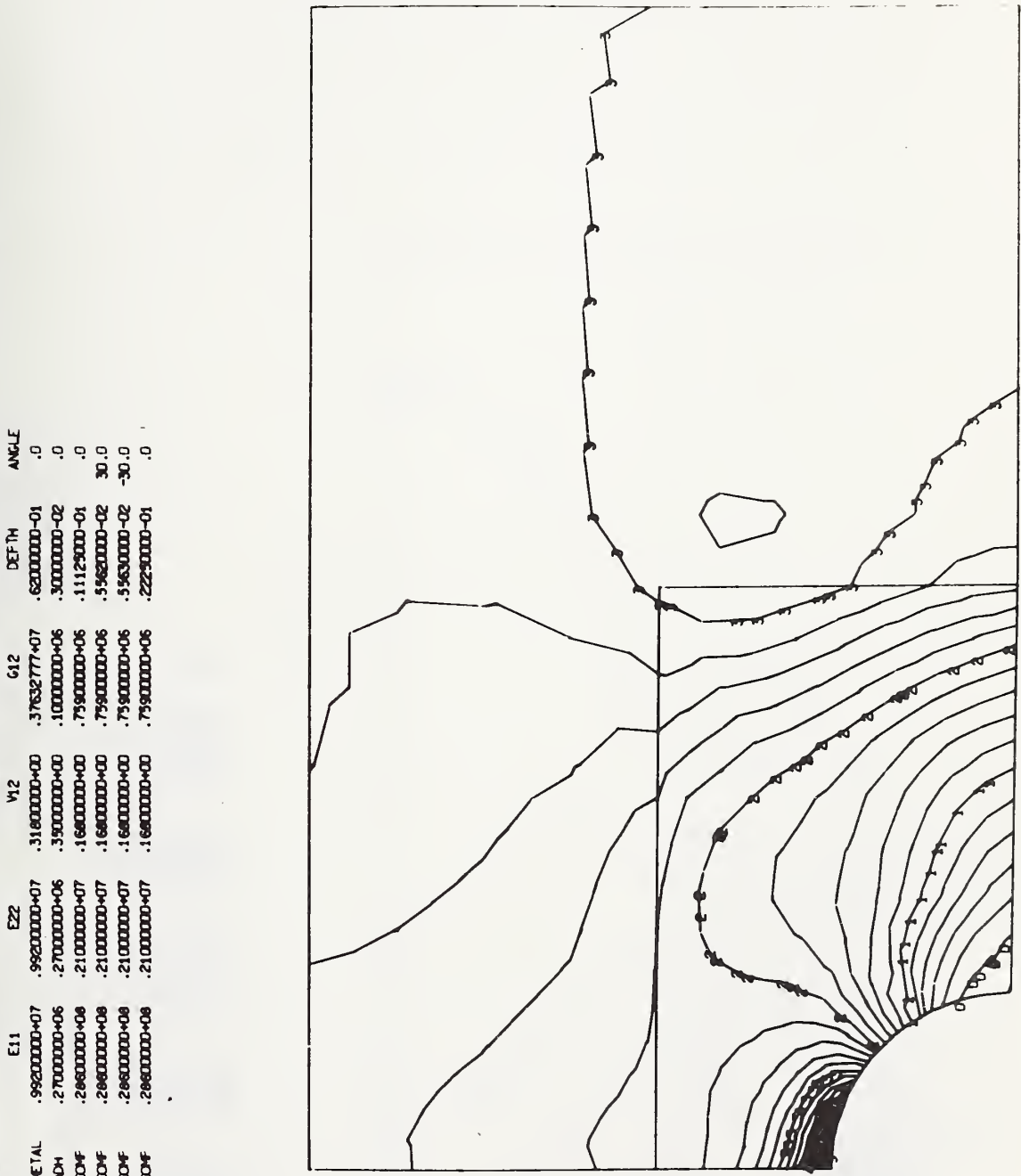
CUSHION .0056
X WIDTH OF HOLE .750
Y WIDTH OF HOLE .750
DEGREE OF ELLIPSE 2.000
DATE AUGUST 17, 1972
Y BOUNDARY Y-STRESS 0.

COMPOSITE 2.50 X 1.50 X .5445 ADHESIVE .0020
X CUSHIONS .000 2.000 X TAPER 1.100
Y CUSHION 1.500 Y TAPER 1.500
X AXIS OF ELLIPSE .750 Y AXIS OF ELLIPSE .750
Y BOUNDARY X-STRESS 0.

ADH .0000 - 0.1-. .00 CONF .0000 - 0.1-. .00
E11 E12
METAL .99200000+07 .31800000+00 .37632777+07 .62000000-01 .0
ADH .27000000+06 .39000000+00 .10000000+06 .30000000-02 .0
CONF .26800000+08 .21000000+07 .16800000+06 .11129000-01 .0
CONF .26800000+08 .21000000+07 .16800000+06 .59820000-02 30.0
CONF .26800000+08 .21000000+07 .16800000+06 .55630000-02 -30.0
CONF .26800000+08 .21000000+07 .16800000+06 .22290000-01 .0

FLATE 5.00 X 3.00 X .0620
HOLE CUSHION X .000
HOLE CUSHION Y .000
CRACK LENGTH .000
NO. DEBOND AREAS 0
X BOUNDARY X-STRESS 30000.
NONLINEAR X-C-N

Y BOUNDARY X-STRESS 0.
Y BOUNDARY Y-STRESS 0.



METAL MAX-STRESS
CONTOUR INTERVAL 2000 LABEL INTERVAL 10000

Figure 10 - Contour plot of maximum principal stress in the sheet for the case defined in Fig. 5. 08

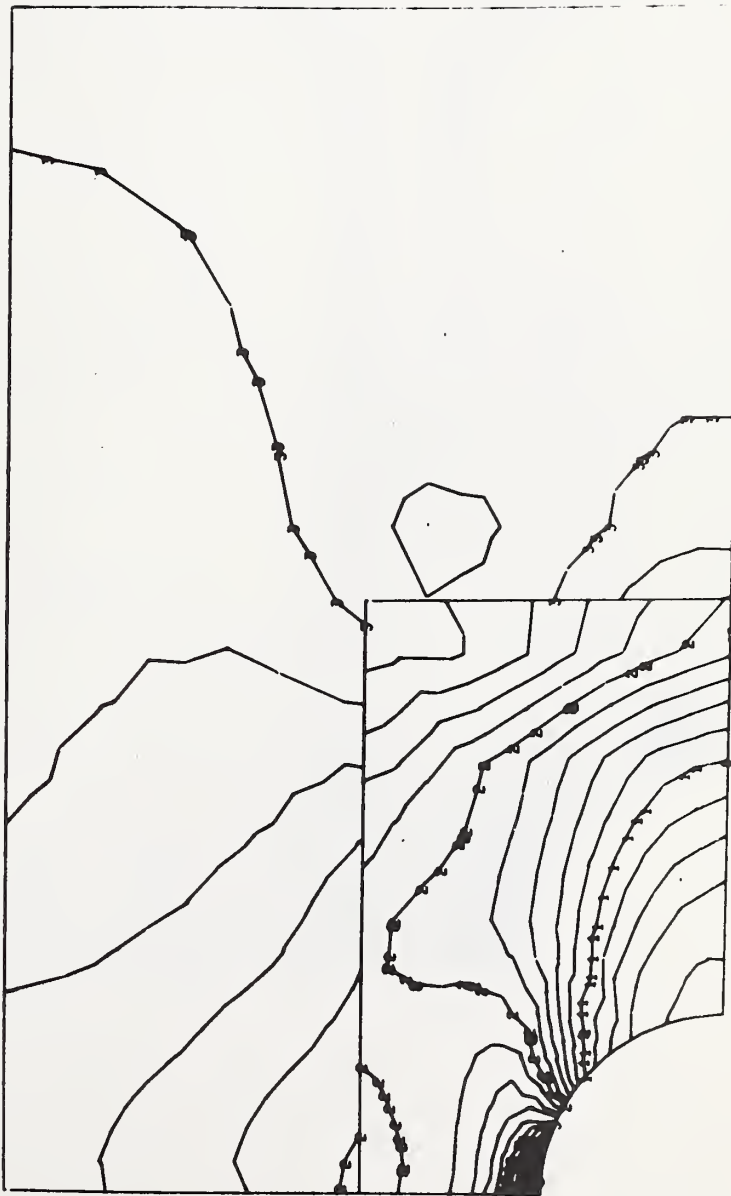


U1100/SC4020
0026 0026

CUSHION .0056
X WIDTH OF HOLE .750
Y WIDTH OF HOLE .750
DEGREE OF ELLIPSE 2.000
DATE AUGUST 17, 1972
Y BOUNDARY Y-STRESS 0.

PLATE 5.00 X 3.00 X .0620
HOLE CUSHION X .000
HOLE CUSHION Y .000
CRACK LENGTH .000
NO. DEBOND AREAS 0
X BOUNDARY X-STRESS 3000.
NONLINEAR K-C-N

COMPOSITE 2.50 X 1.50 X .0445	ADHESIVE .0020	X TAPER 1.100	Y TAPER 1.500	X AXIS OF ELLIPSE .750	Y AXIS OF ELLIPSE .750	X BOUNDARY X-STRESS 0.	Y BOUNDARY X-STRESS 0.
X CUSHIONS .000	2.000	X TAPER 1.100	Y TAPER 1.500	X AXIS OF ELLIPSE .750	Y AXIS OF ELLIPSE .750	X BOUNDARY X-STRESS 0.	Y BOUNDARY X-STRESS 0.
ADH .0000	0.0000	CONF .0000	0.0000	0.0000	0.0000	0.0000	0.0000
E11	E22	V12	G12	DEFIN	ANGLE		
.99000000-07	.99000000-07	.31000000-00	.37632777-07	.62000000-01	.0		
.27000000-06	.27000000-06	.39000000-00	.10000000-06	.30000000-02	.0		
.20000000-08	.21000000-07	.16000000-00	.79000000-08	.11125000-01	.0		
.20000000-08	.21000000-07	.16000000-00	.79000000-08	.59000000-02	30.0		
.20000000-08	.21000000-07	.16000000-00	.79000000-08	.59000000-02	-30.0		
.20000000-08	.21000000-07	.16000000-00	.79000000-08	.22250000-01	.0		



SURFACE X-MICROSTRAIN
CONTOUR INTERVAL 200 LABEL INTERVAL 1000

Figure 11 - Contour plot of the x component of normal strain in the overlay and in the surrounding sheet for the case defined in Fig. 5.



PLATE 5.00 X 3.00 X .0620
 HOLE CUSHION X .000
 HOLE CUSHION Y .000
 CRACK LENGTH .000
 NO. DEBOND AREAS 0
 X BOUNDARY X-STRESS 30000.
 NONLINEAR K-C-N

COMPOSITE 2.50 X 1.50 X .0445 ADHESIVE .0020
 X CUSHIONS .000 2.000 X TAPER 1.100
 Y CUSHION 1.500 Y TAPER 1.500
 X AXIS OF ELLIPSE .750 Y AXIS OF ELLIPSE .750
 X BOUNDARY Y-STRESS 0. Y BOUNDARY X-STRESS 0.
 ADH .0000 - 0.- .00 CONF .0000 - 0.- .00
 E11 E22 G12 DEFTH ANGLE

.99200000+07 .31800000+00 .37632777+07 .62000000-01 .0
 .27000000+06 .35000000+00 .10000000+06 .30000000-02 .0
 .28600000+08 .16800000+00 .75900000+06 .11125000-01 .0
 .28600000+08 .16800000+00 .75900000+06 .55620000-02 30.0
 .28600000+08 .16800000+00 .75900000+06 .55630000-02 -30.0
 .28600000+08 .16800000+00 .75900000+06 .22230000-01 .0

CUSHION .0056
 X WIDTH OF HOLE .750
 Y WIDTH OF HOLE .750
 DEGREE OF ELLIPSE 2.000
 DATE AUGUST 17, 1972
 Y BOUNDARY Y-STRESS 0.



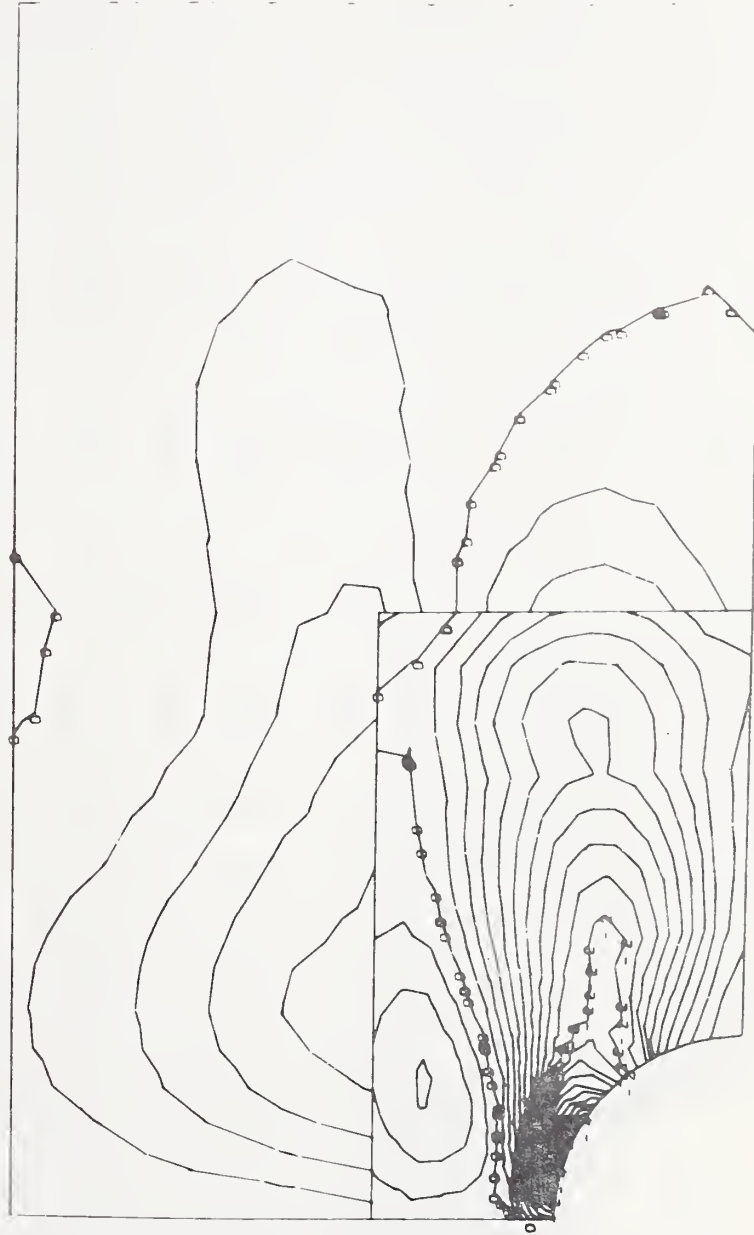
SURFACE Y-MICROSTRAIN
 CONTOUR INTERVAL 100 LABEL INTERVAL .1000

Figure 12 - Contour plot of the y component of normal strain in the overlay and in the surrounding sheet for the case defined in Fig. 5.



CUSHION .0056
X WIDTH OF HOLE .75
Y WIDTH OF HOLE .75
DEGREE OF ELLIPSE 2.000
DATE AUGUST 17, 1972
Y BOUNDARY Y-STRESS

PLATE 5.00 X 3.00 X .0625	UPR-SLITE 2.50 X 1.50 X .0445	ADHESIVE .0020	
HOLE CUSHION X .000	X CUSHIONS .000	X TAPER 1.100	
HOLE CUSHION Y .000	Y CUSHION 1.500	Y TAPER 1.500	
CRACK LENGTH .000	X AXIS OF ELLIPSE .750	Y AXIS OF ELLIPSE .750	
NO. DEBOND AREAS 0			
X BOUNDARY X-STRESS 30000.	X BOUNDARY Y-STRESS 0.	Y BOUNDARY X-STRESS 0.	
NONLINEAR K-C-N	ADH .0000	COFF .0000	G12 DEF TH ANGLE
	E11	V12	
METAL .99200000+07	.99200000+07	.31600000+00	.37632777+07
ADH .27000000+06	.27000000+06	.35000000+00	.62000000-01
COFF .28600000+08	.21000000+07	.16600000+00	.30000000-02
COFF .28600000+08	.21000000+07	.16600000+00	.11125000-01
COFF .28600000+08	.21000000+07	.16600000+00	.55620000-02
COFF .28600000+08	.21000000+07	.16600000+00	.75900000+06
COFF .28600000+08	.21000000+07	.16600000+00	.75900000+06
COFF .28600000+08	.21000000+07	.16600000+00	.75900000+06
COFF .28600000+08	.21000000+07	.16600000+00	.22290000-01
COFF .28600000+08	.21000000+07	.16600000+00	.0

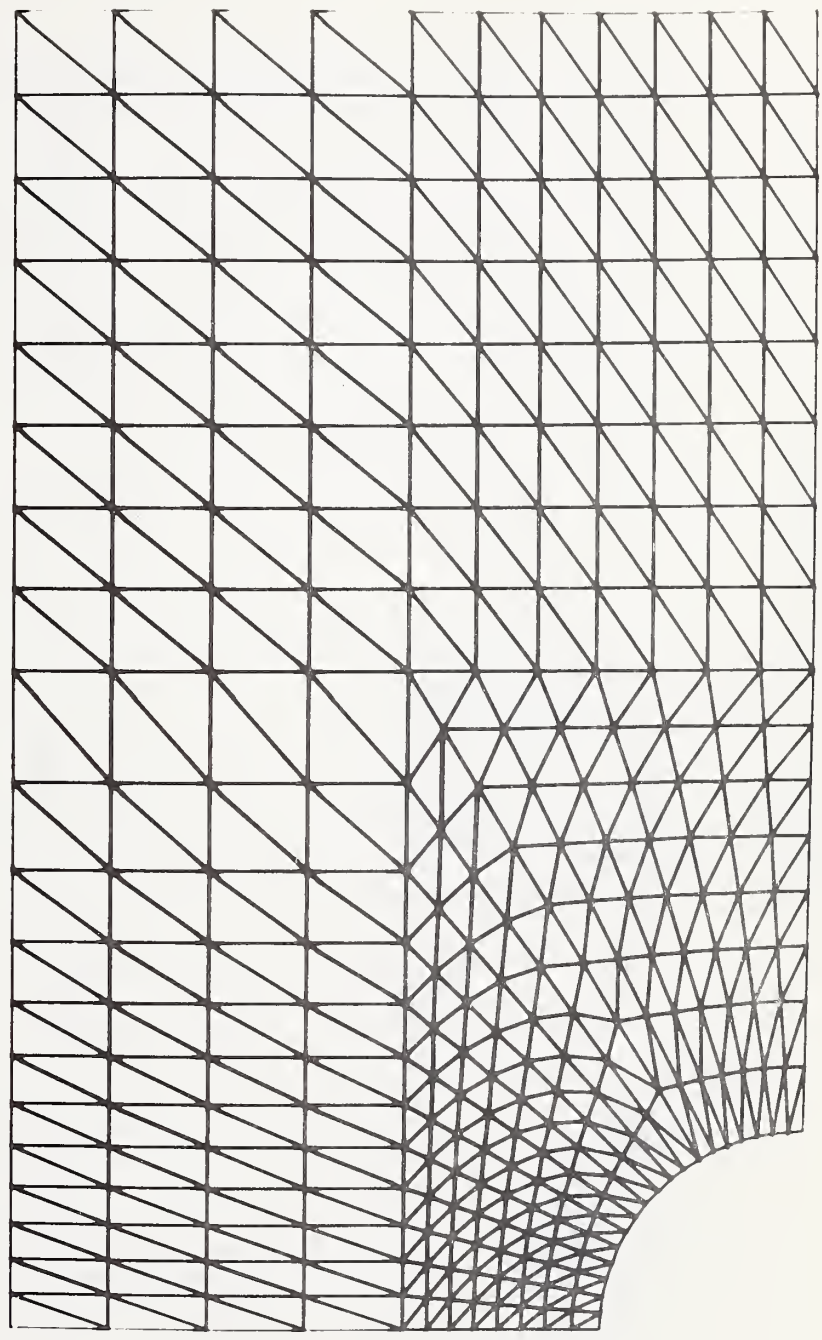


SURFACE XY-MICROSTRAIN
CONTOUR INTERVAL 200 LABEL INTERVAL 2000

Figure 13 - Contour plot of the xy component of shear strain in the overlay and in the surrounding sheet for the case defined in Fig. 5.



PLATE 5.00 X 3.00 X .0620 COMPOSITE 2.50 X 1.50 X .0445 ADHESIVE .0020
 HOLE CUSHION X .000 X CUSHIONS .000 2.000 X TAPER 1.100
 HOLE CUSHION Y .000 Y CUSHION 1.500 Y TAPER 1.500
 CRACK LENGTH .210 X AXIS OF ELLIPSE .750 Y AXIS OF ELLIPSE .750
 NO. DEBOND AREAS 0 X BOUNDARY X-STRESS 30000. X BOUNDARY Y-STRESS 0. Y BOUNDARY X-STRESS 0.
 NONLINEAR K-C-N ADH .0000 - 0.1 - .00 COMF .0000 - 0.1 - .00 DEFTH ANGLE
 E11 V12 612
 METAL .99200000+07 .99200000+07 .31600000+00 .37632777+07 .62000000-01 .0
 ADH .27000000+06 .27000000+06 .35000000+00 .10000000+06 .30000000-02 .0
 COMF .28600000+08 .21000000+07 .16800000+00 .75900000+06 .11125000-01 .0
 COMF .28600000+08 .21000000+07 .16800000+00 .75900000+06 .59620000-02 30.0
 COMF .28600000+08 .21000000+07 .16800000+00 .75900000+06 .59630000-02 -30.0
 COMF .28600000+08 .21000000+07 .16800000+00 .75900000+06 .22250000-01 .0



FINITE ELEMENT MESH

Figure 14 - Finite element network and input data for the analysis of a composite-reinforced cutout-with-crack.





CUSHION .0036
 X WIDTH OF HOLE .750
 Y WIDTH OF HOLE .750
 DEGREE OF ELLIPSE 2.000
 DATE AUGUST 25, 1972
 Y BOUNDARY Y-STRESS 0.

ADHESIVE .0020
 X TAPER 1.100
 Y TAPER 1.500
 Y AXIS OF ELLIPSE .750
 Y BOUNDARY X-STRESS 0.
 DEFTH .00
 ANGLE .0

COMPOSITE 2.50 X 1.50 X .0445
 X CUSHIONS .000 2.000
 Y CUSHION 1.500
 X AXIS OF ELLIPSE .750
 COMF .0000 - 0. - .00
 G12
 G12
 DEFTH

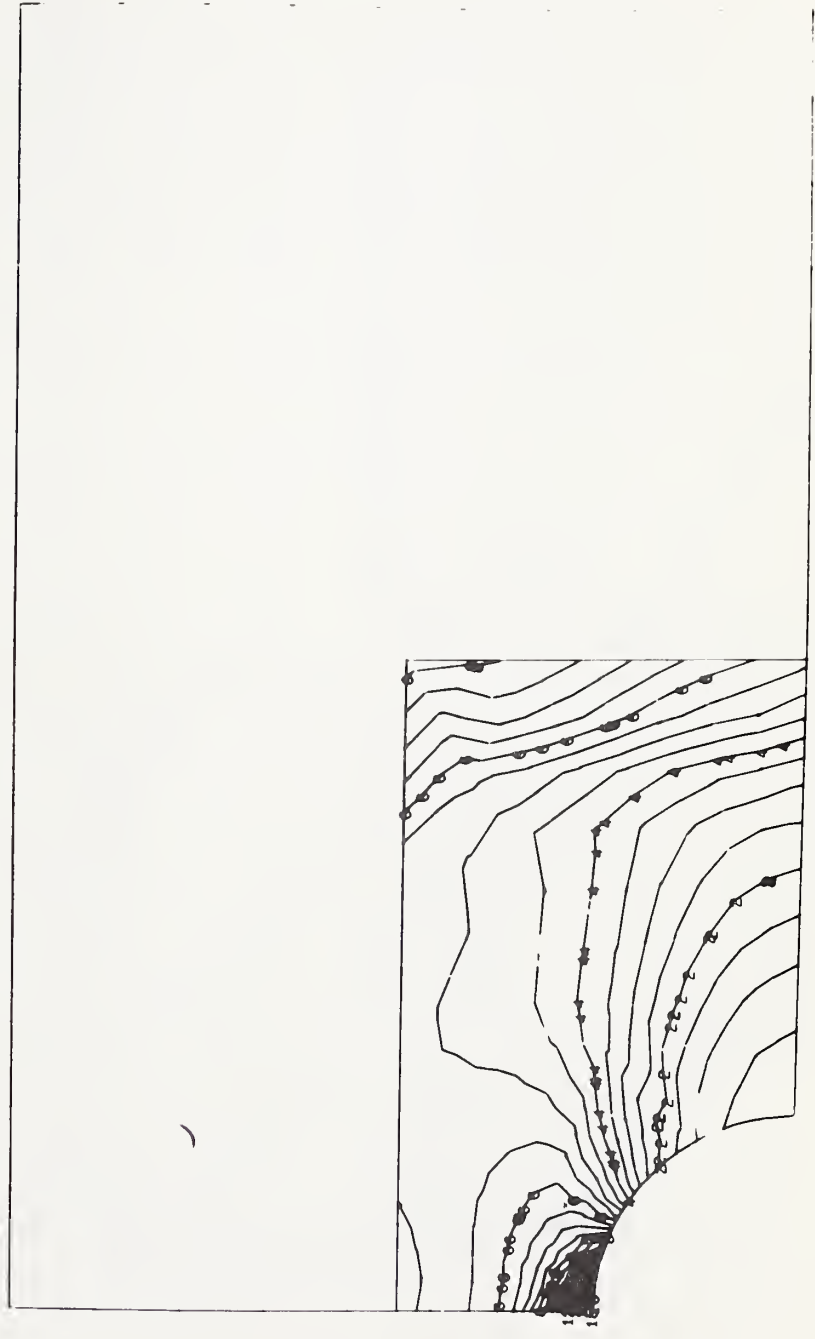
PLATE 5.00 X 3.00 X .0620
 HOLE CUSHION X .000
 HOLE CUSHION Y .000
 CRACK LENGTH .210
 NO. DEBOND AREAS 0
 X BOUNDARY X-STRESS 30000.
 NONLINEAR K-C-N
 E11
 E22
 V12
 X BOUNDARY Y-STRESS 0.
 COMF .0000 - 0. - .00
 G12
 G12
 DEFTH

METAL .99200000+07.
 ADH .27000000+06.
 COMF .28600000+08.
 COMF .28600000+08.
 COMF .21000000+07.
 COMF .21000000+07.

.31800000+00
 .35000000+00
 .16800000+07
 .16800000+07
 .16800000+07
 .16800000+07

.37632777+07
 .10000000+06
 .75900000+06
 .75900000+06
 .75900000+06
 .75900000+06

.62000000-01
 .30000000-02
 .11125000-01
 .55620000-02
 .55630000-02
 .22250000-01



COMPOSITE MAX-STRESS
 CONTOUR INTERVAL 5000
 LABEL INTERVAL 20000

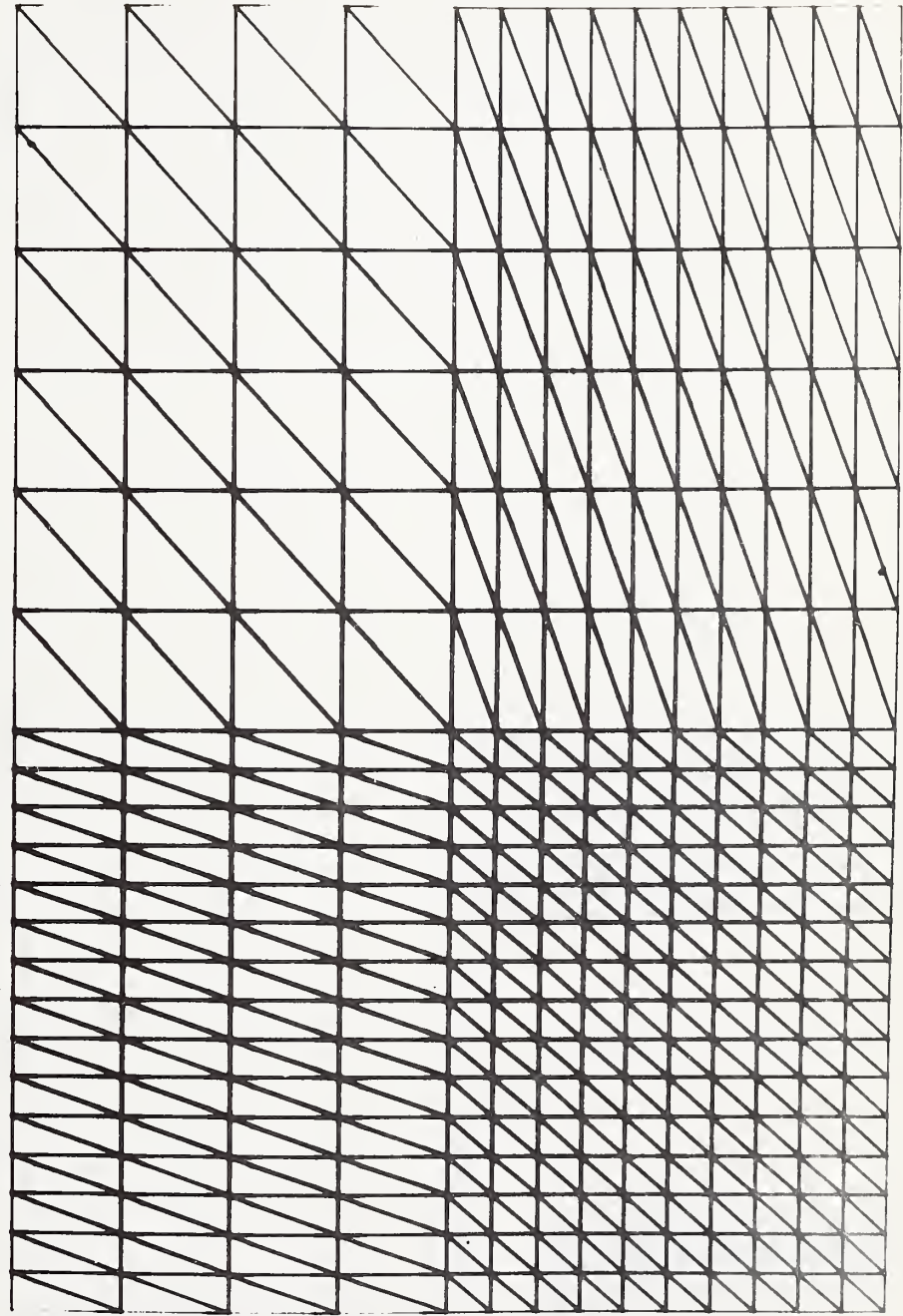
Figure 16 - Contour plot of maximum principal stress in the overlay for the case defined in Fig. 14.





PLATE 4.50 X 3.00 X .0825
 HOLE CUSHION X .000
 HOLE CUSHION Y .000
 CRACK LENGTH 1.190
 NO. DEBOND AREAS 0
 X BOUNDARY X-STRESS 30000.
 NONLINEAR K-C-N
 COMPOSITE 2.00 X 1.50 X .0334 ADHESIVE .0030
 X CUSHIONS .000 1.500 X TAPER .750
 Y CUSHION 1.500 Y TAPER 1.500
 X AXIS OF ELLIPSE .000 Y AXIS OF ELLIPSE .000
 X BOUNDARY Y-STRESS 0. Y BOUNDARY X-STRESS 0.
 ADH .0000 - 0.- .00 CONF .0000 - 0.- .00
 E11 V12 G12 DEPTH ANGLE
 .98200000+07 .31000000+00 .37632777+07 .62000000-01 .0
 .27000000+06 .35000000+00 .10000000+06 .30000000-02 .0
 .20000000+08 .10000000+00 .79000000+06 .11120000-01 .0
 .20000000+08 .10000000+00 .79000000+06 .59000000-02 45.0
 .20000000+08 .10000000+00 .79000000+06 .59000000-02 -45.0
 .20000000+08 .10000000+00 .79000000+06 .11120000-01 .0

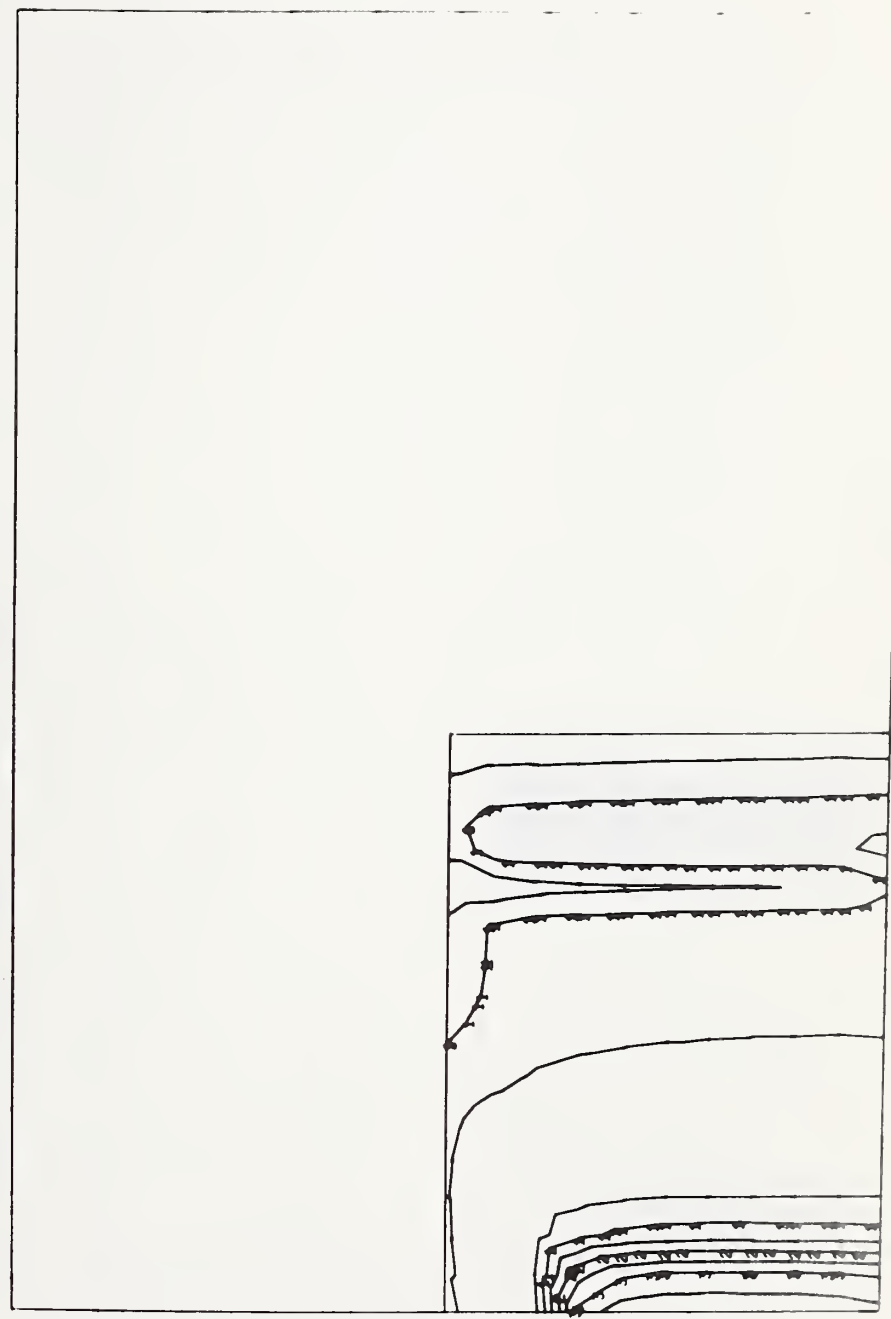
CUSHION .0056
 X WIDTH OF HOLE .000
 Y WIDTH OF HOLE .000
 DEGREE OF ELLIPSE .000
 DATE AUGUST 31, 1972
 Y BOUNDARY Y-STRESS 0.



FINITE ELEMENT MESH

Figure 18 - Finite element network and input data for the analysis of a composite-reinforced transverse crack.

FLATE 4.90 X 3.00 X .0620 COMPOSITE 2.00 X 1.90 X .0334 ADHESIVE .0030 CUSHION .0036
 HOLE CUSHION X .000 X CUSHIONS .000 1.90 X TAPER .750 X WIDTH OF HOLE .000
 HOLE CUSHION Y .000 Y CUSHION 1.900 Y TAPER 1.900 Y WIDTH OF HOLE .000
 CRACK LENGTH 1.190 X AXIS OF ELLIPSE .000 Y AXIS OF ELLIPSE .000 DEGREE OF ELLIPSE .000
 NO. DEBOND AREAS 0 X BOUNDARY X-STRESS 30000. X BOUNDARY Y-STRESS 0. Y BOUNDARY X-STRESS 0. DATE AUGUST 31, 1972
 NONLINEAR K-C-N E11 ADH .0000 - 0.- .00 CONF .0000 - 0.- .00 Y BOUNDARY Y-STRESS 0.
 E22 V12 G12 DEPTH ANGLE
 METAL .99200000+07 .99200000+07 .31600000+00 .37632777+07 .62000000-01 .0
 ADH .27000000+06 .27000000+06 .39000000+00 .10000000+06 .30000000-02 .0
 CO#F .28600000+08 .21000000+07 .16800000+00 .79900000+06 .11120000-01 .0
 CO#F .28600000+08 .21000000+07 .16800000+00 .79900000+06 .55600000-02 45.0
 CO#F .28600000+08 .21000000+07 .16800000+00 .79900000+06 .55600000-02 -45.0
 CO#F .28600000+08 .21000000+07 .16800000+00 .79900000+06 .11120000-01 .0



ADHESIVE SHEAR STRESS
 CONTOUR INTERVAL 500 LABEL INTERVAL 1000

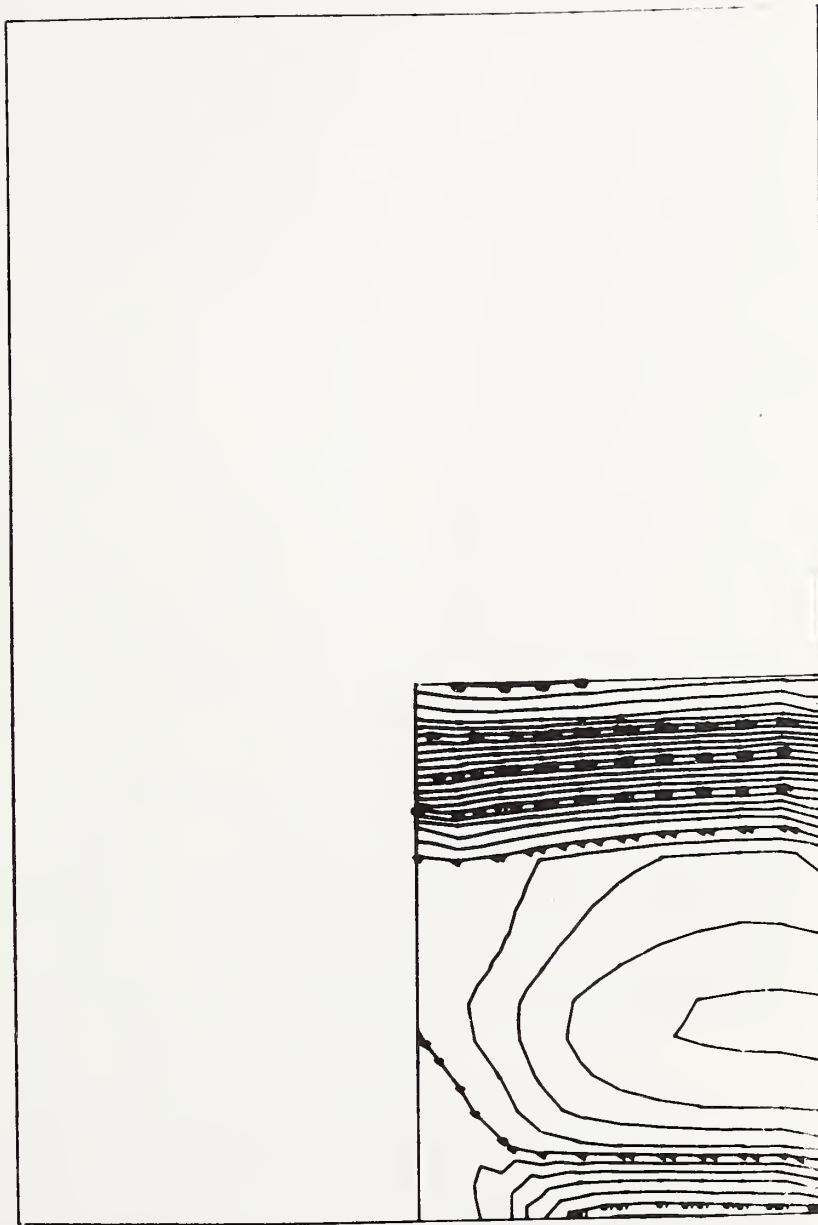
Figure 19 - Contour plot of the resultant adhesive shear stress for the case defined in Fig. 18.

CUSHION .0056
X WIDTH OF HOLE .000
Y WIDTH OF HOLE .000
DEGREE OF ELLIPSE .000
DATE AUGUST 31, 1972
Y BOUNDARY Y-STRESS 0.

COMPOSITE 2.00 X 1.50 X .0334 ADHESIVE .0030
X CUSHIONS .000 X TAPER .750
Y CUSHION 1.500 Y TAPER 1.500
X AXIS OF ELLIPSE .000 Y AXIS OF ELLIPSE .000
X BOUNDARY Y-STRESS 0. Y BOUNDARY X-STRESS 0.

PLATE 4.50 X 3.00 X .0620
HOLE CUSHION X .000
HOLE CUSHION Y .000
CRACK LENGTH 1.190
NO. DEBOIC AREAS 0
X BOUNDARY X-STRESS 30000.
NONLINEAR K-C-N

	E11	E22	V12	CONF	612	DEPTH	ANGLE
METAL	.99200000+07	.99200000+07	.31600000+00	.37632777+07	.62000000-01	.0	.0
ADH	.27000000+06	.27000000+06	.35000000+00	.10000000+06	.30000000-02	.0	.0
CONF	.20000000+08	.21000000+07	.16000000+00	.75900000+06	.11120000-01	.0	.0
CONF	.20000000+08	.21000000+07	.16000000+00	.75900000+06	.55000000-02	45.0	45.0
CONF	.20000000+08	.21000000+07	.16000000+00	.75900000+06	.55000000-02	-45.0	-45.0
CONF	.20000000+08	.21000000+07	.16000000+00	.75900000+06	.11120000-01	.0	.0

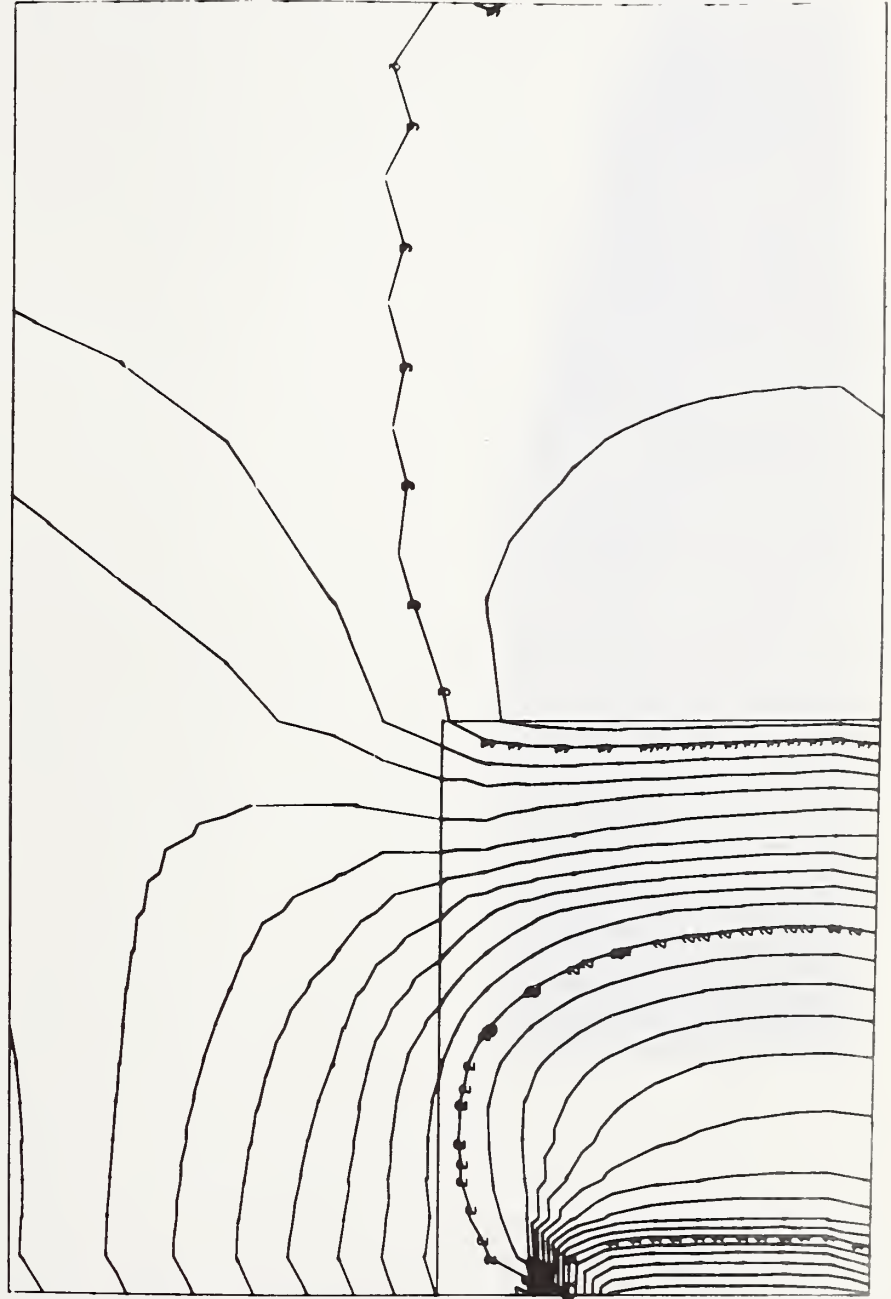


COMPOSITE MAX-STRESS
CONTOUR INTERVAL 2000 LABEL INTERVAL 10000

Figure 20 - Contour plot of maximum principal stress in the overlay for the case defined in Fig. 18.



FLATE 4.50 X 3.00 X .0620 COMPOSITE 2.00 X 1.50 X .0334 ADHESIVE .0030
 HOLE CUSHION X .000 X CUSHIONS .000 1.500 X TAPER .750 X WIDTH OF HOLE .000
 HOLE CUSHION Y .000 Y CUSHION 1.500 Y TAPER 1.500 Y WIDTH OF HOLE .000
 CRACK LENGTH 1.190 X AXIS OF ELLIPSE .000 Y AXIS OF ELLIPSE .000
 NO. DEBOND AREAS 0
 X BOUNDARY X-STRESS 30000. X BOUNDARY Y-STRESS 0. Y BOUNDARY X-STRESS 0.
 NONLINEAR K-C-N ADH .0000 - 0. - .00 CONF .0000 - 0. - .00
 METAL E11 E22 V12 G12 DEPTH ANGLE
 .99200000+07 .99200000+07 .31800000+00 .37632777+07 .62000000-01 .0
 .27000000+06 .27000000+06 .39000000+00 .10000000+06 .30000000-02 .0
 .28600000+08 .21000000+07 .16800000+00 .79900000+06 .11120000-01 .0
 .28600000+08 .21000000+07 .16800000+00 .79900000+06 .55600000-02 45.0
 .28600000+08 .21000000+07 .16800000+00 .79900000+06 .55600000-02 -45.0
 .28600000+08 .21000000+07 .16800000+00 .79900000+06 .11120000-01 .0



METAL MAX-STRESS
 CONTOUR INTERVAL 1000 LABEL INTERVAL 10000

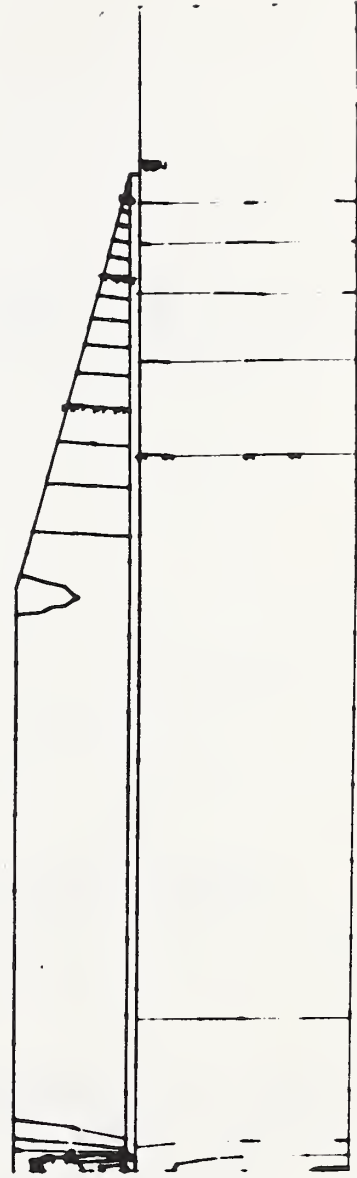
Figure 21 - Contour plot of maximum principal stress in the sheet for the case defined in Fig. 18.





DATE SEPTEMBER 29, 1972
X TAPER 3.5000
X STRESS 19801.

PLATE 7.00 X .0600	COMPOSITE 6.00 X .0336	ADHESIVE .0030
CUMULON .0000	CUMULON .0000	CUMULON 6.0000
NO. DIBOND AREAS 0		
NONLINEAR K-C-N	ADM .0000 , 0.10 .00	COF .0000 , 0.10 .00
	SIZE	SIZE
	E11	E12
METAL .10-00000-08	.10-00000-08	.30-00000-00
ADM .2700000-04	.2700000-04	.1000000-06
COF .2800000-08	.2100000-07	.7000000-06
		DEPTH
		ANGLE
		.0
		.0
		.3350-000-01



MAX-STRESS
CONTOUR INTERVAL 8000 LABEL INTERVAL 10000

Figure 23 - Contour plot of maximum principal stress for the case defined in Fig. 22.



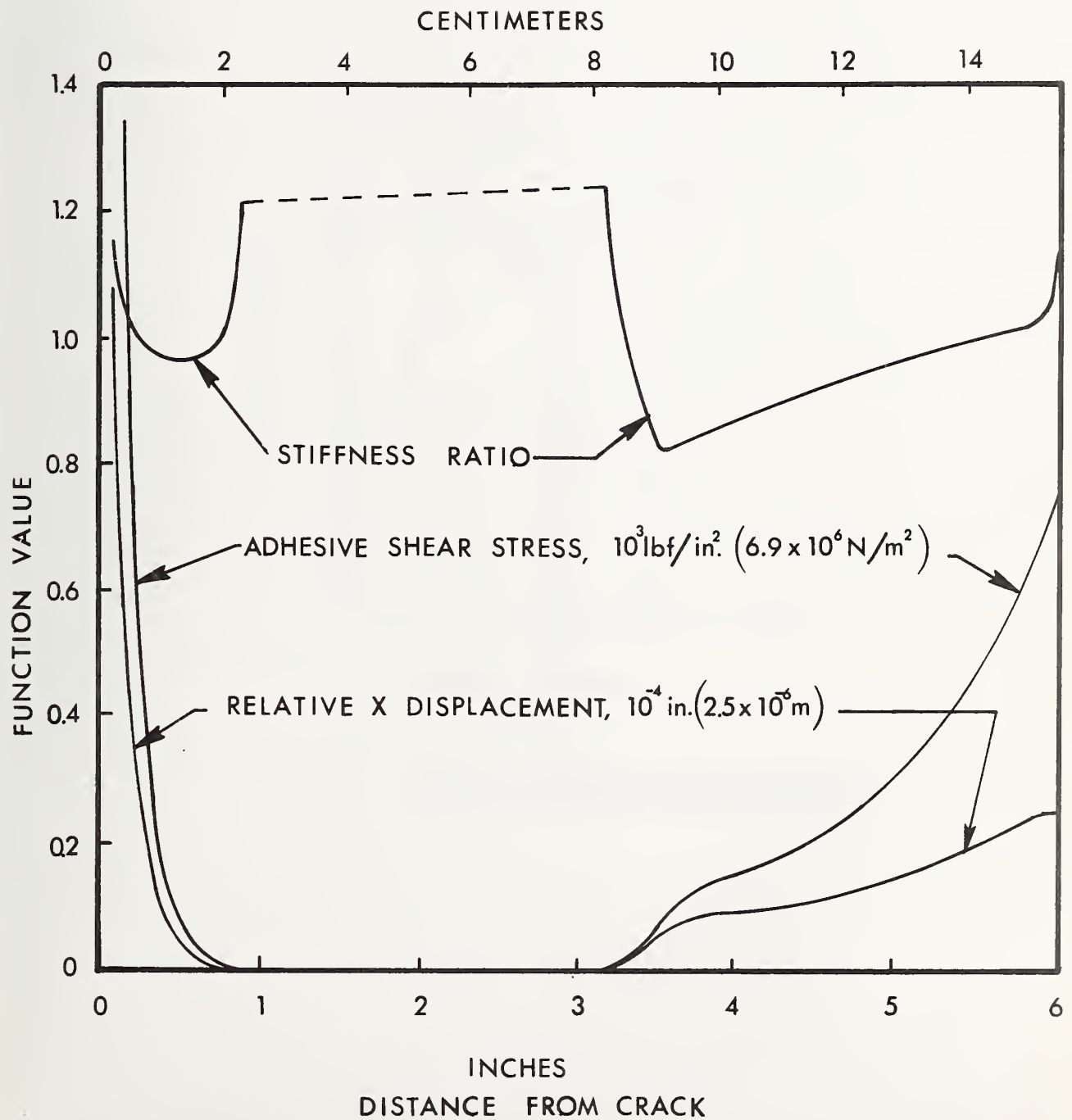


Figure 24 - Plots of three shear functions for the case defined in Fig. 22.



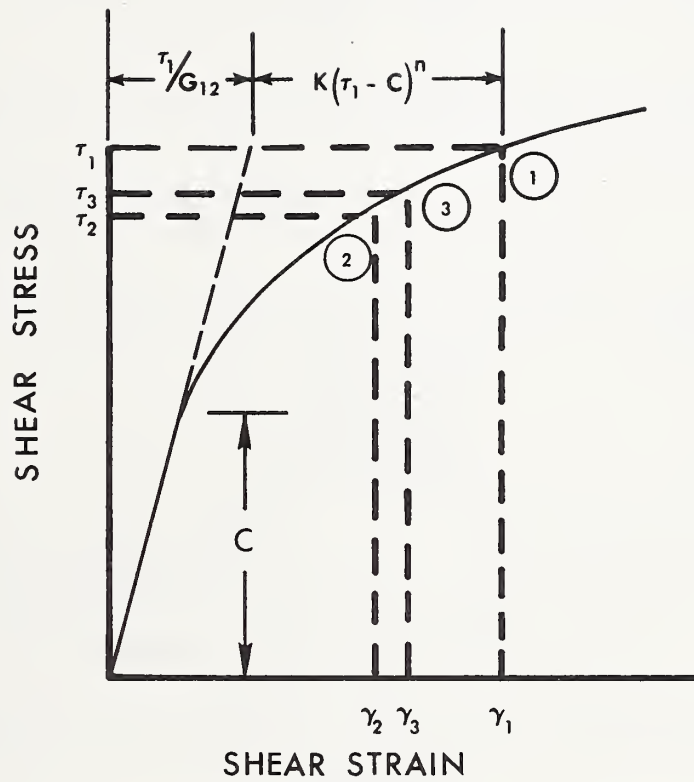
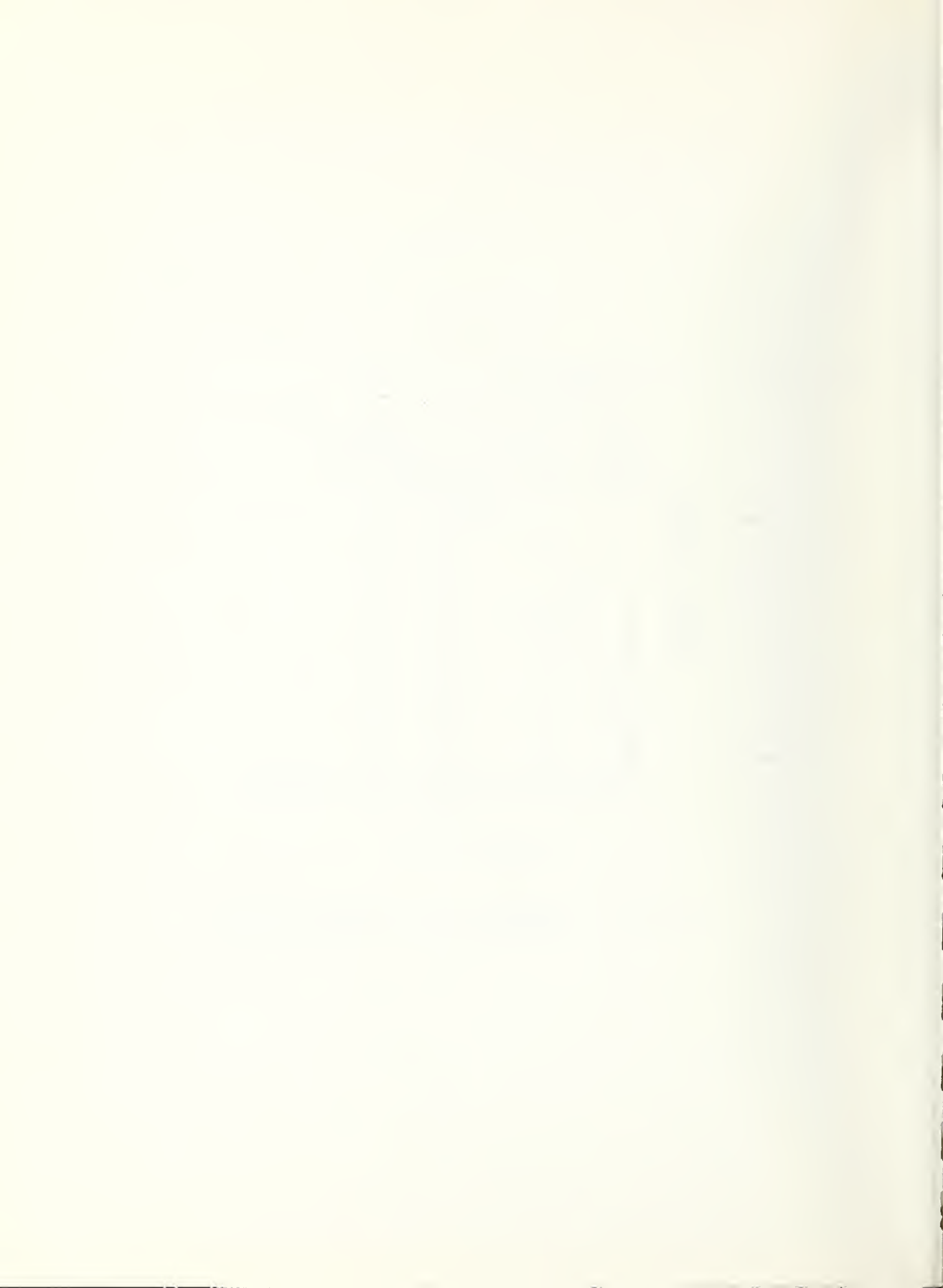
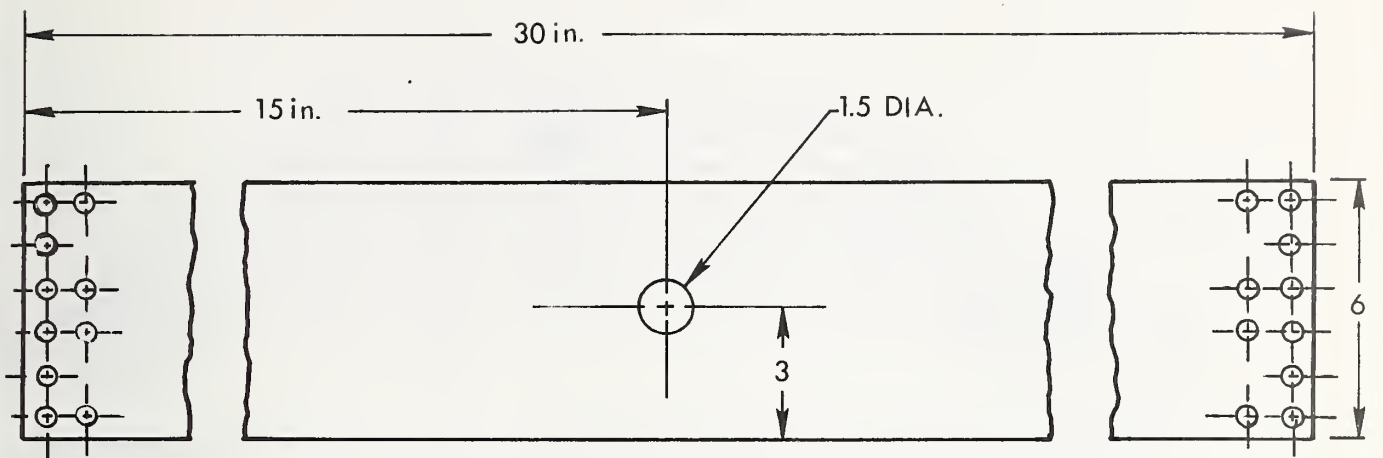
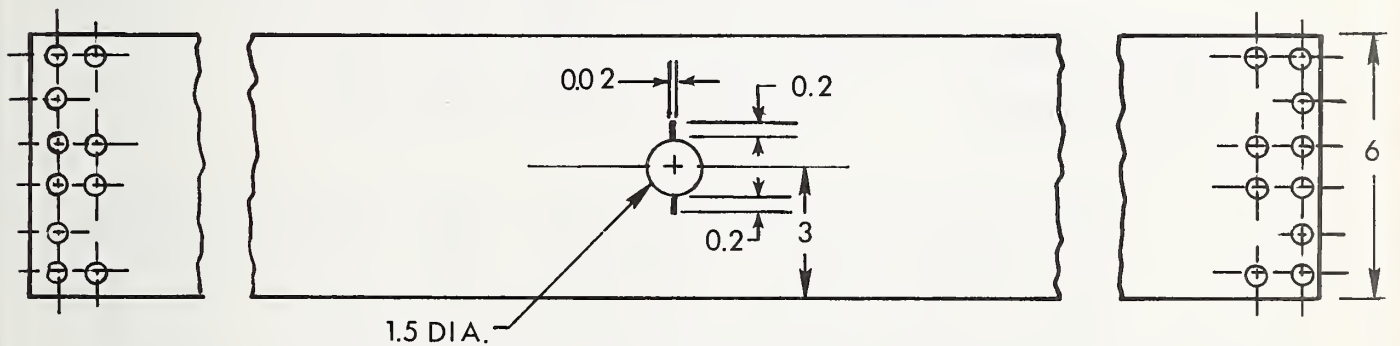


Figure 25 - Schematic stress-strain curve for a nonlinear shear-stiffness material.

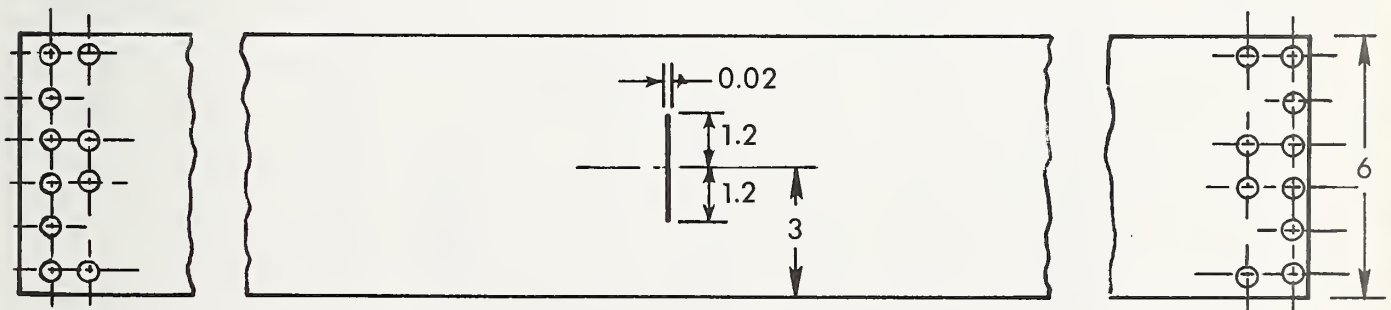




(a) CUTOUT (CUU1)



(b) CUTOUT - WITH-SLIT (CCU1)



(c) TRANSVERSE SLIT (CRU1)

Figure 26 - Details of the unreinforced sheet specimens. Sheet material is 0.124 in (0.315 cm) thick 7075-T6 aluminum alloy. Dimensions shown are in inches (1 in = 2.54 cm).



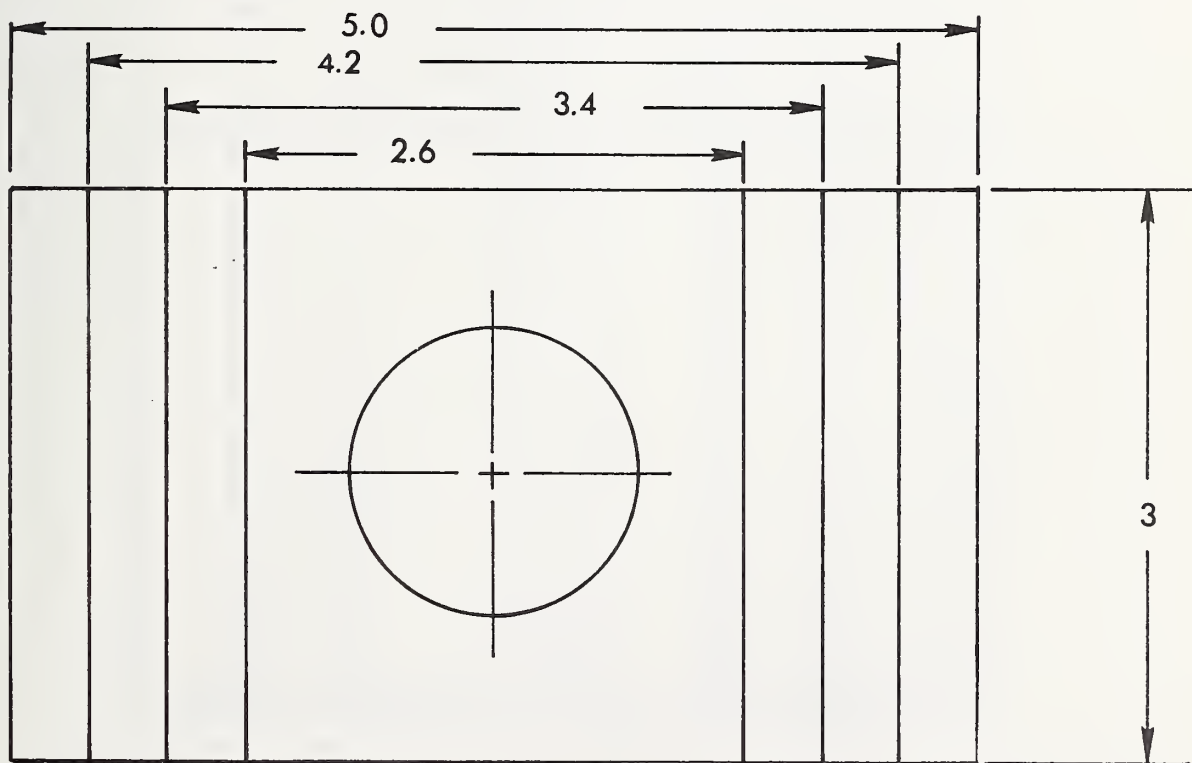
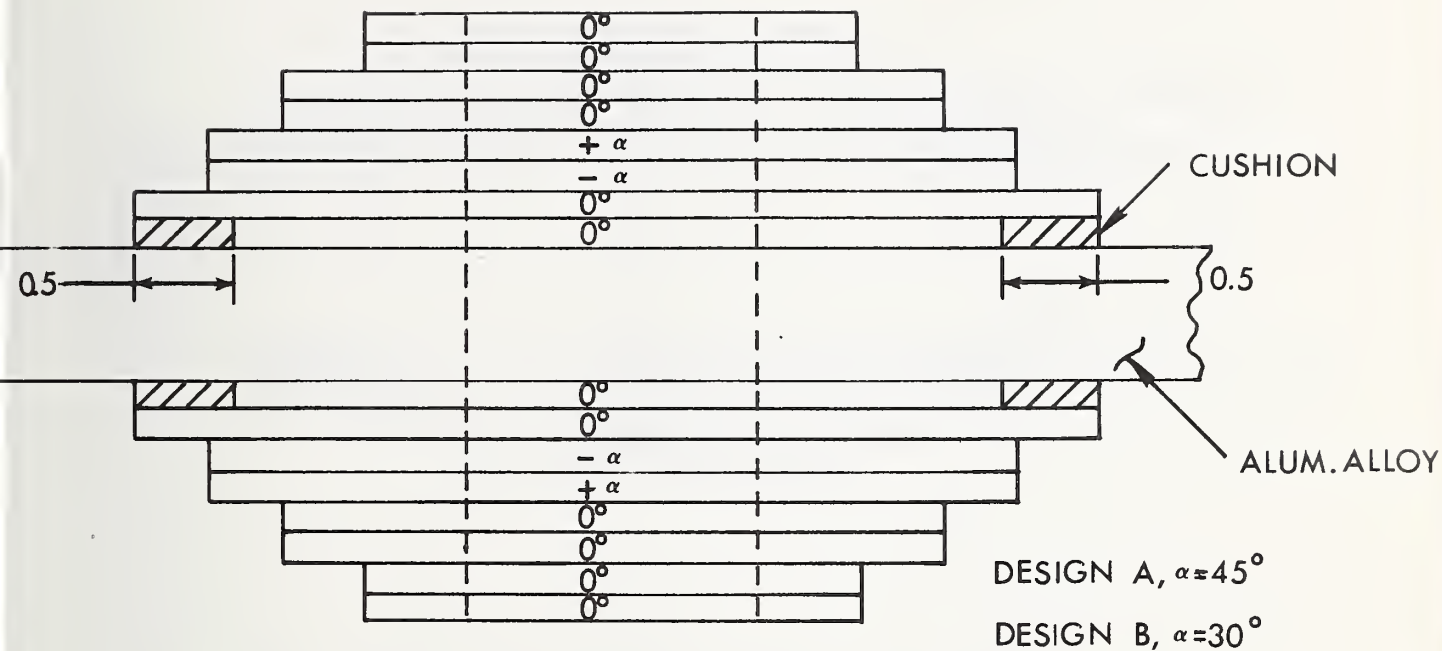
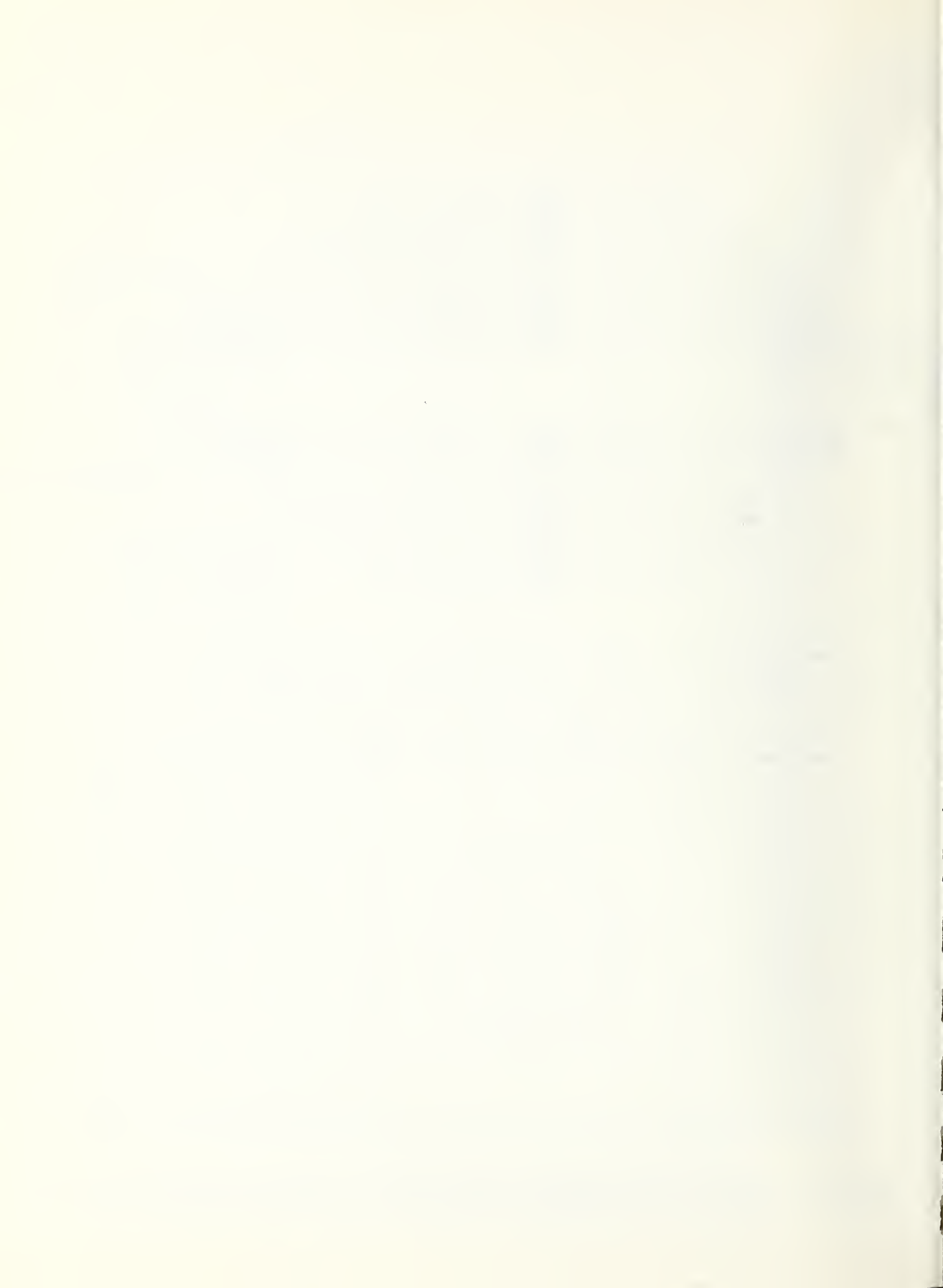


Figure 27 - Details of the composite overlays used to reinforce the cutout and cutout-with-slit specimens. Dimensions shown are in inches (1 in = 2.54 cm).



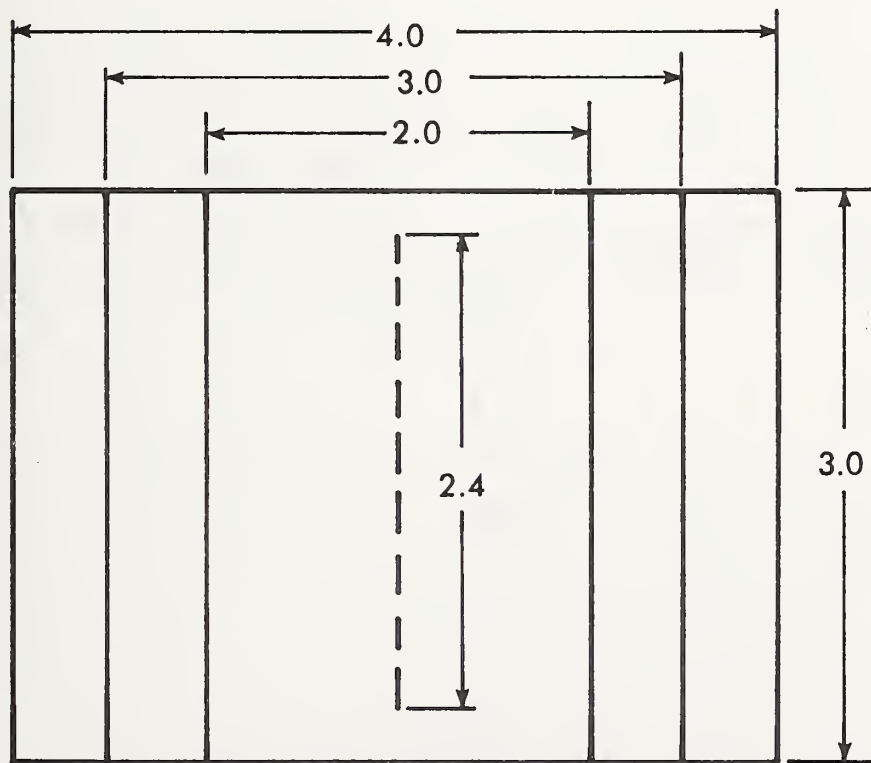
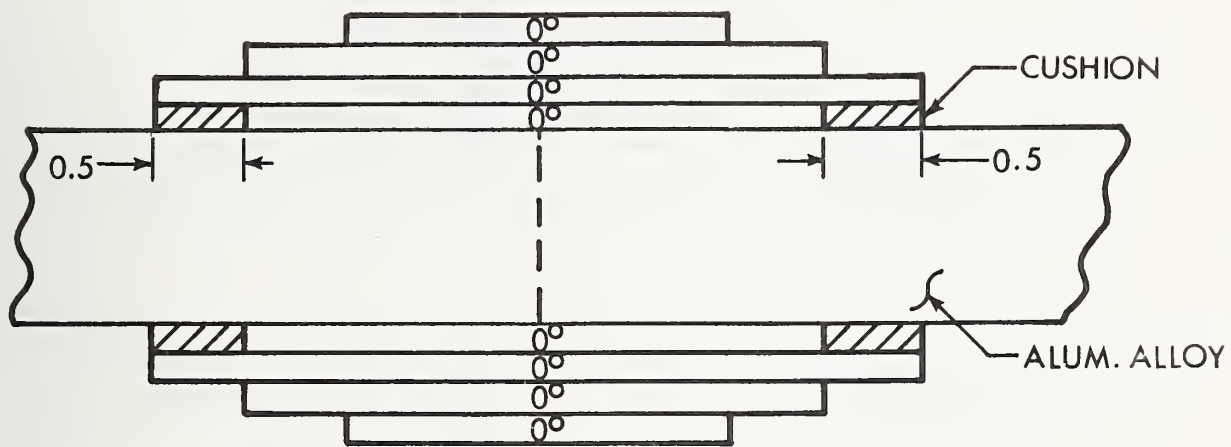
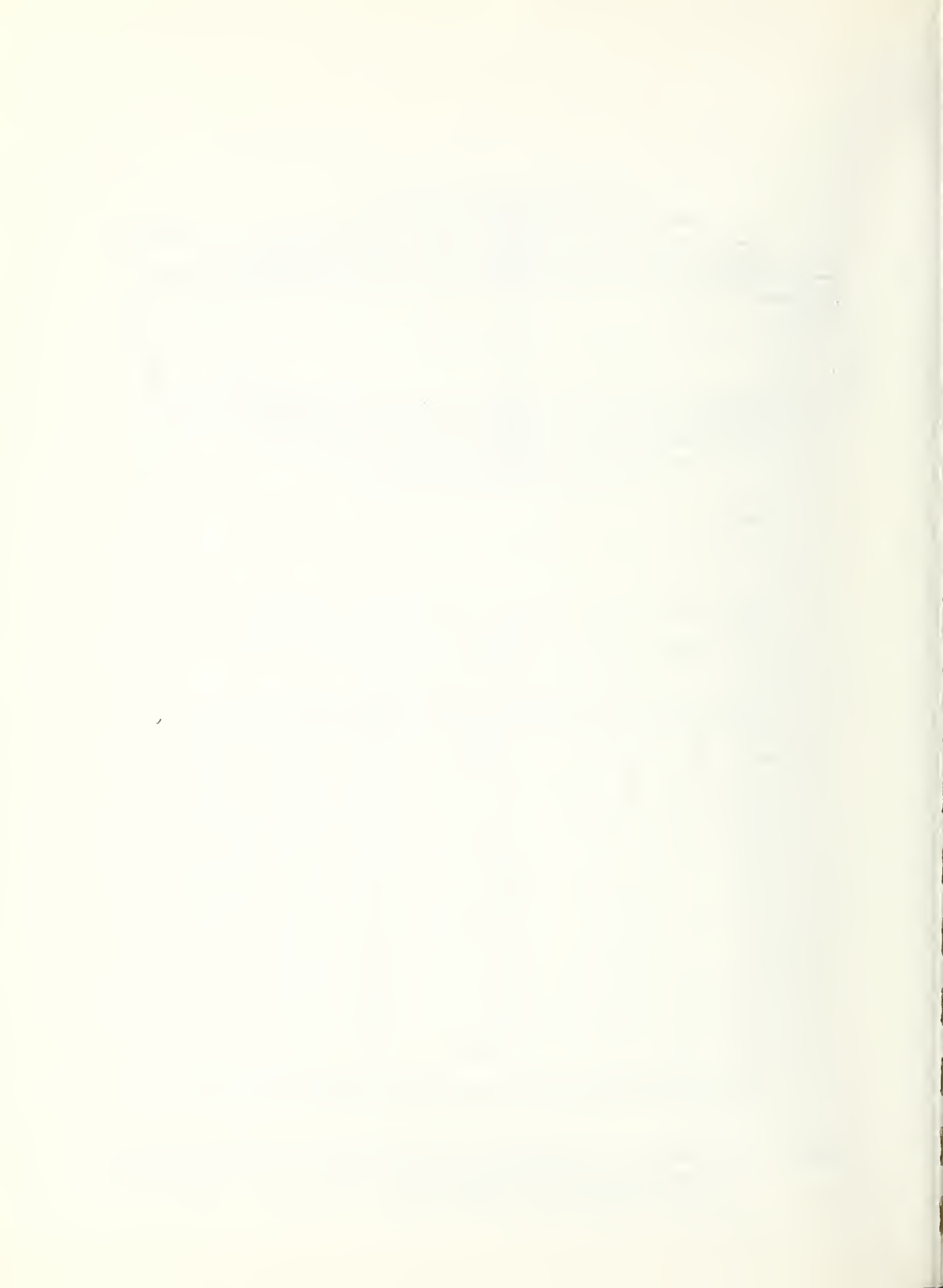


Figure 28 - Details of the composite overlays used to reinforce three of the transverse-slit specimens (CRA1, CRA2, CRA3). Dimensions shown are in inches (1 in = 2.54 cm).



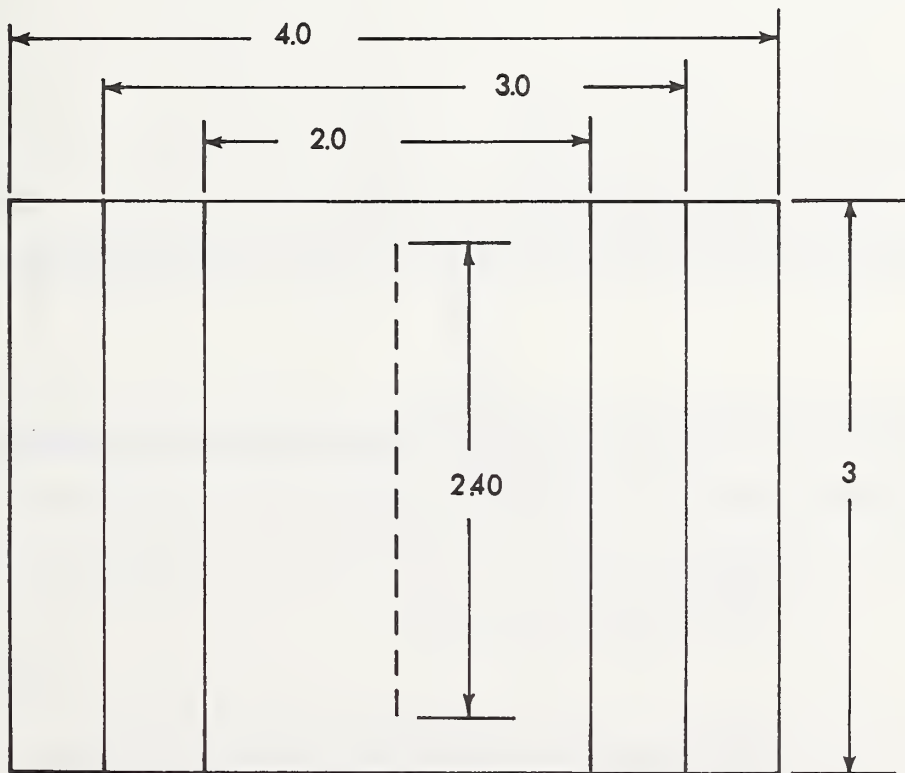
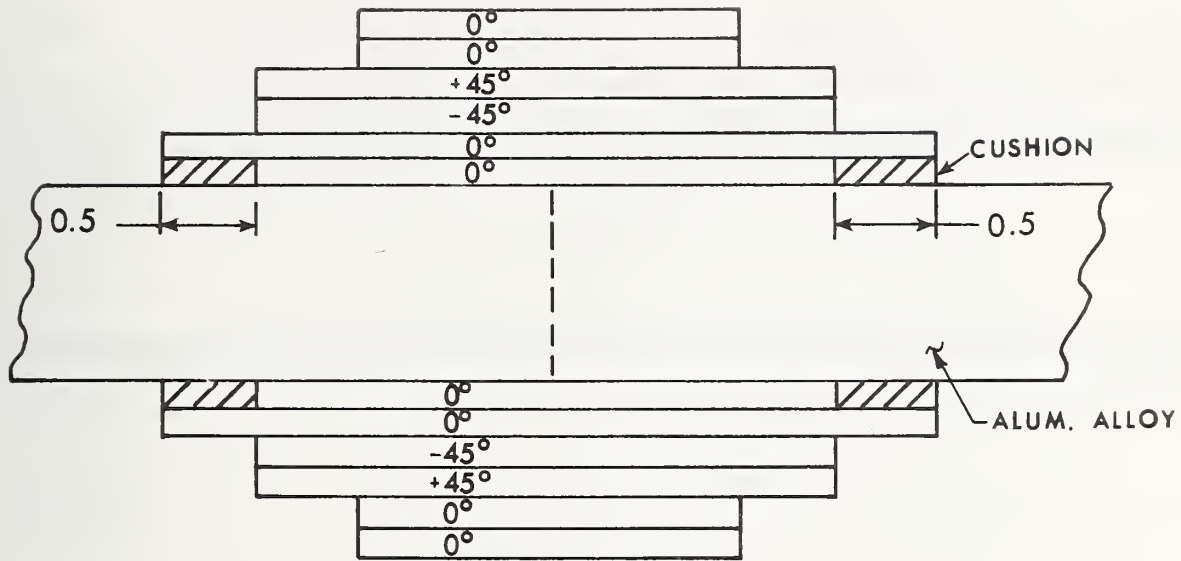
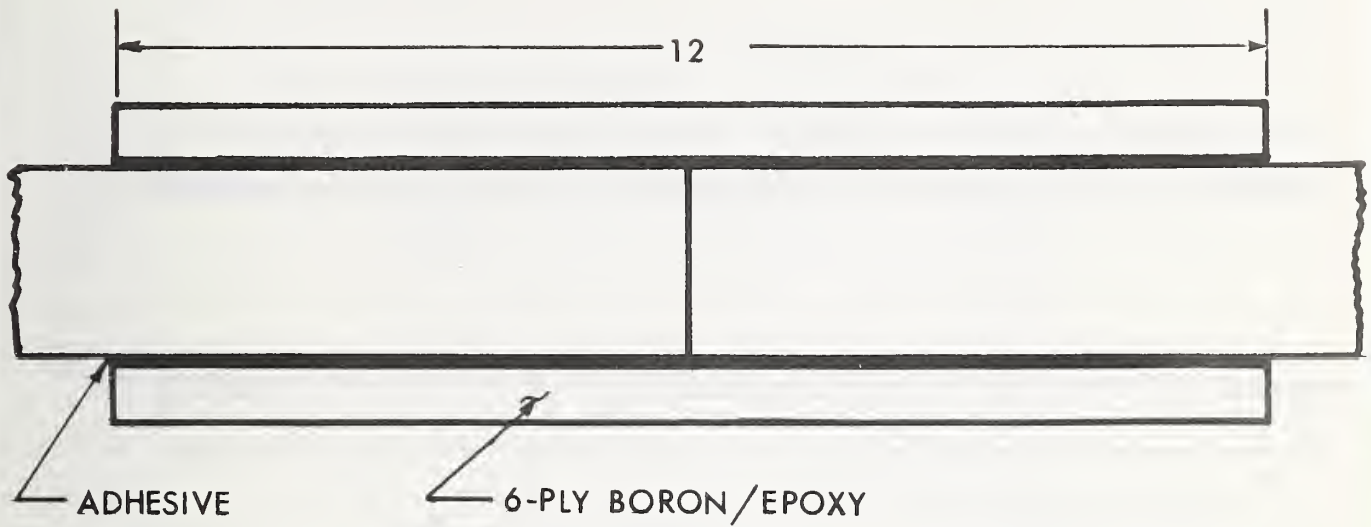
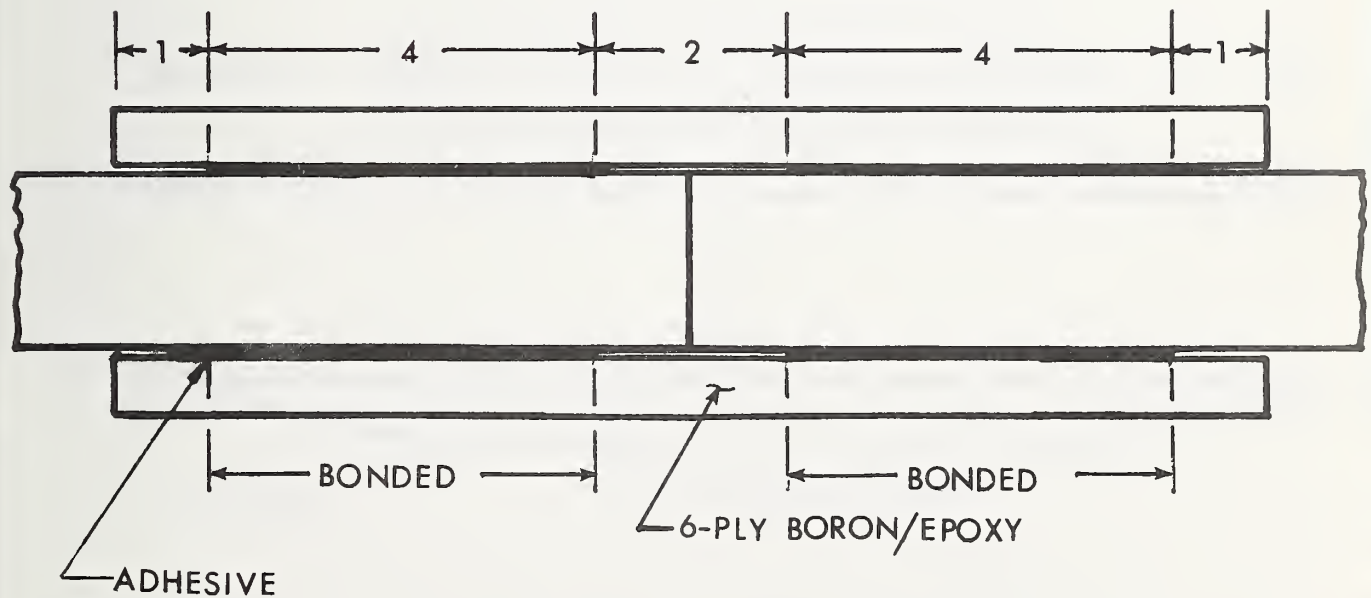


Figure 29 - Details of the composite overlays used to reinforce three of the transverse-slit specimens (CRB1, CRB2, CRB3). Dimensions shown are in inches (1 in = 2.54 cm).



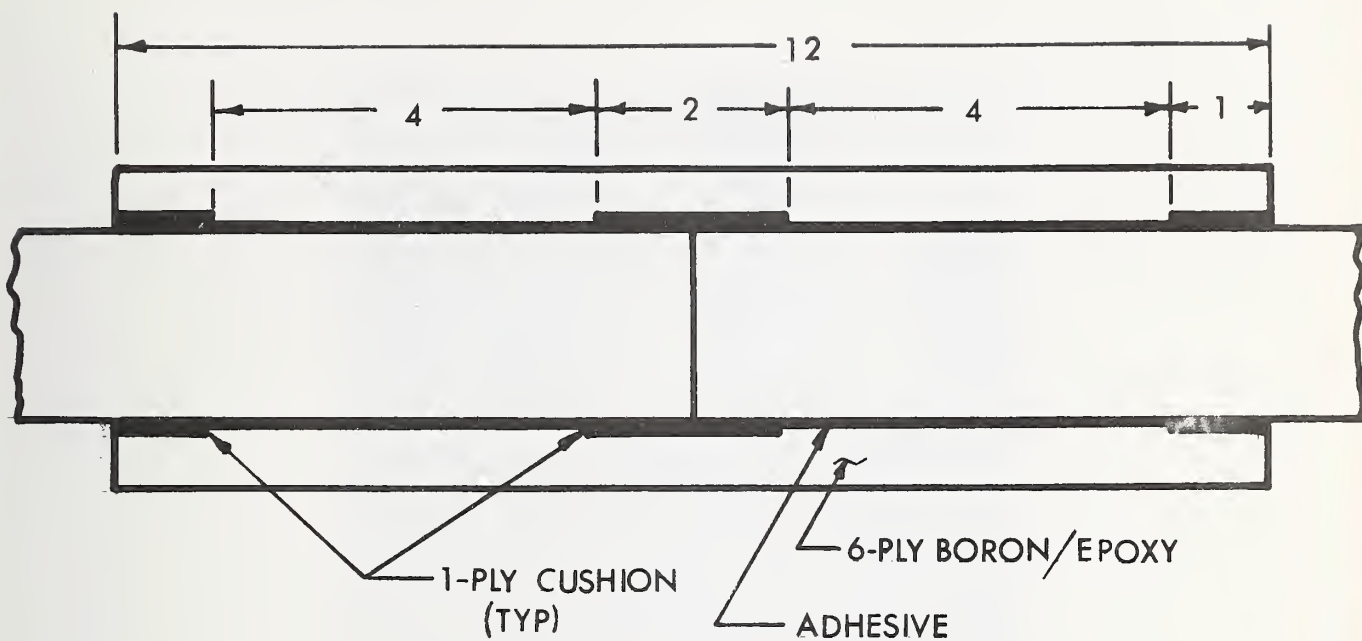


(a) PLAIN OVERLAY SPECIMENS(PA1, PB1, PB 2)

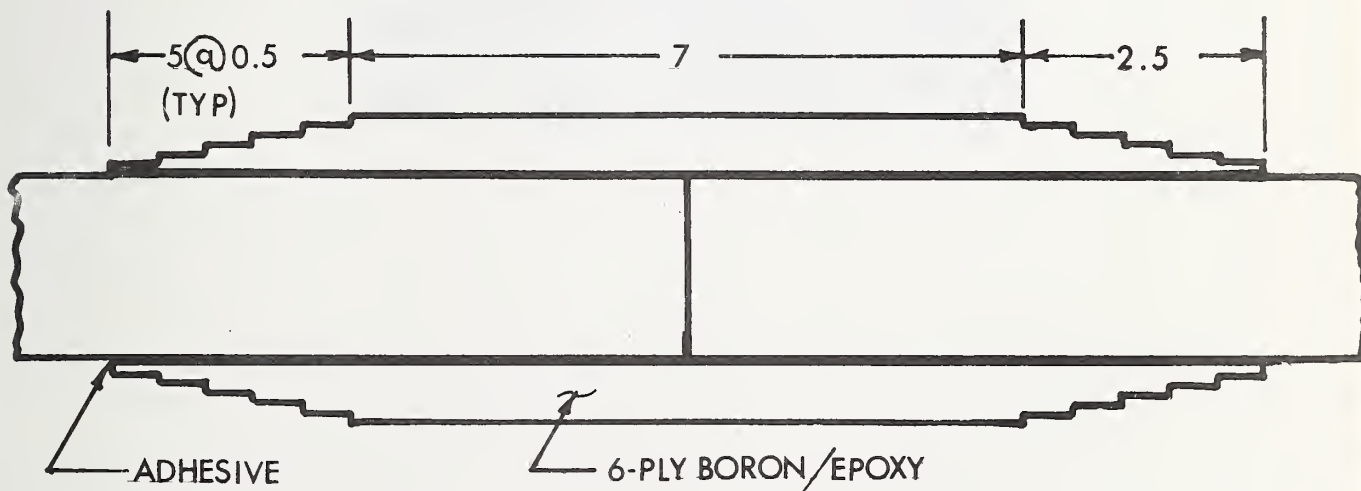


(b) PARTIALLY-BONDED OVERLAY SPECIMENS(DA1, DB1, DB 2)



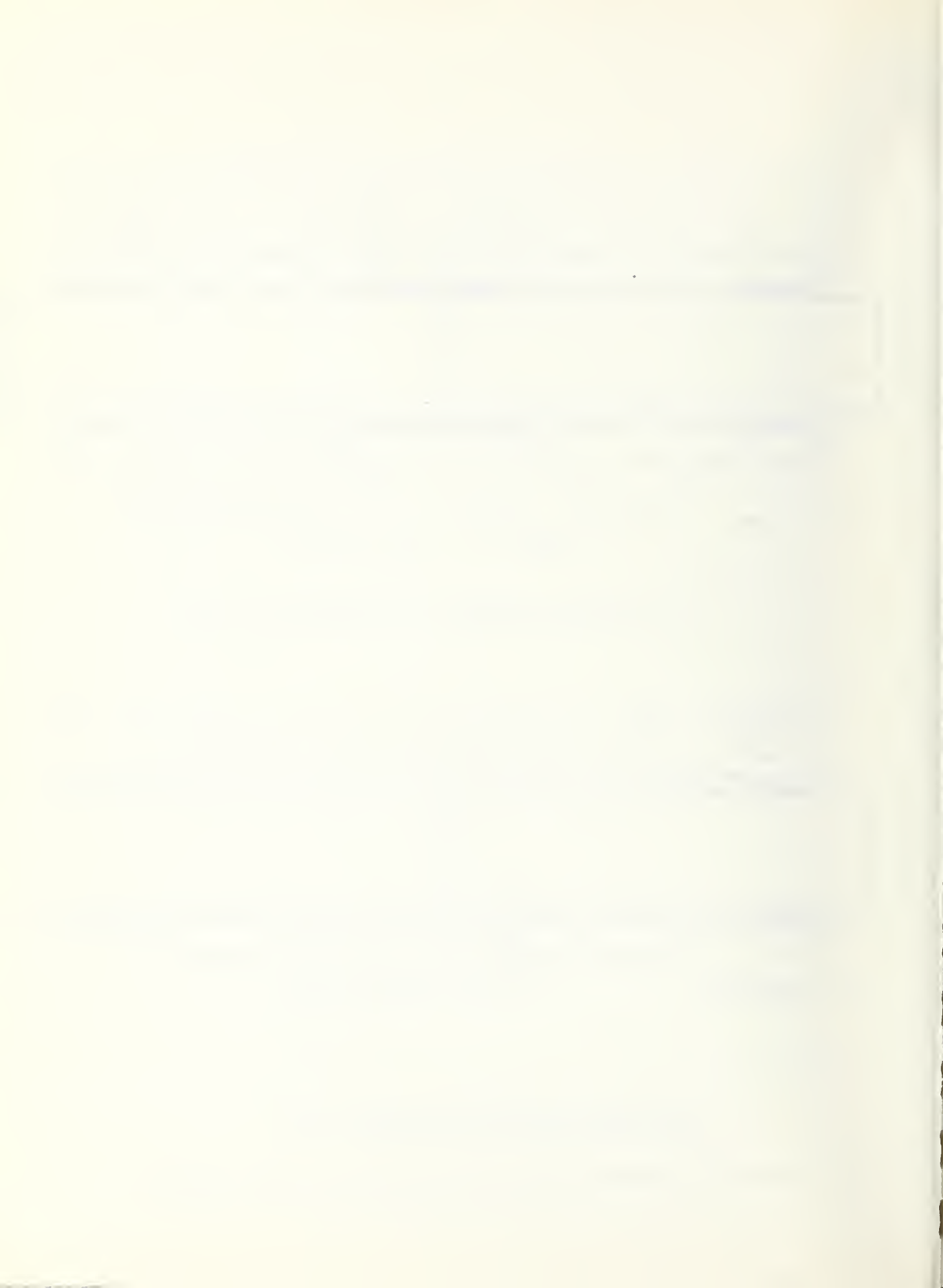


(c) CUSHIONED OVERLAY SPECIMENS (CB1, CB 2)



(d) TAPERED OVERLAY SPECIMEN (TA1)

Figure 30 - Schematic details of the double-lap-joint specimens.



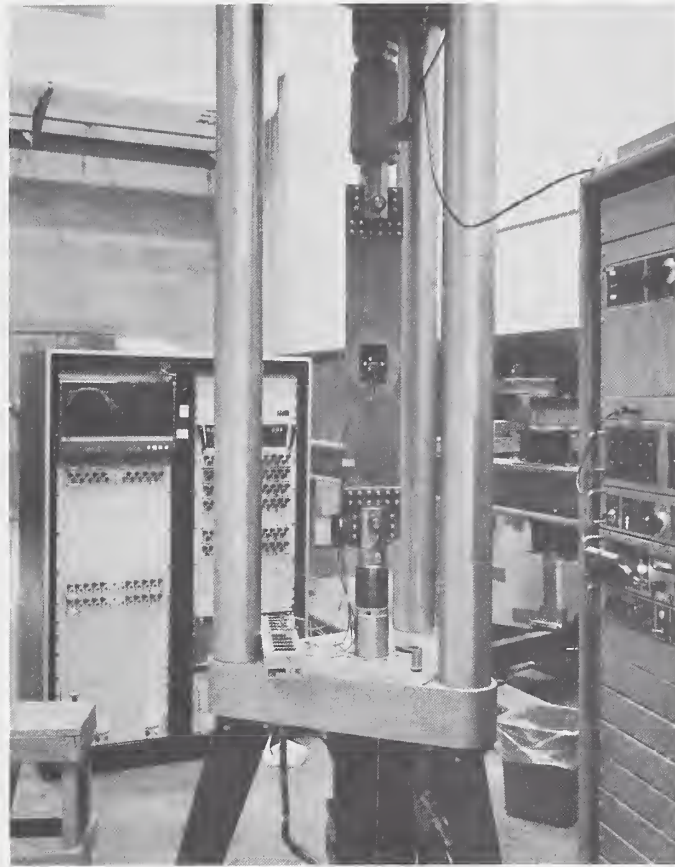


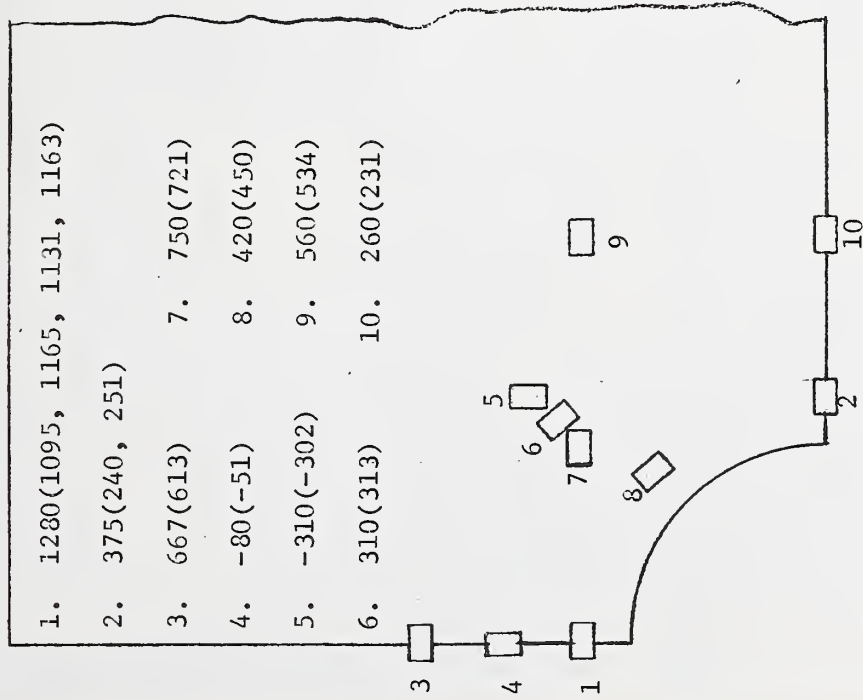
Figure 31 - Test setup using a multi-channel data acquisition system and an electrohydraulic testing machine.



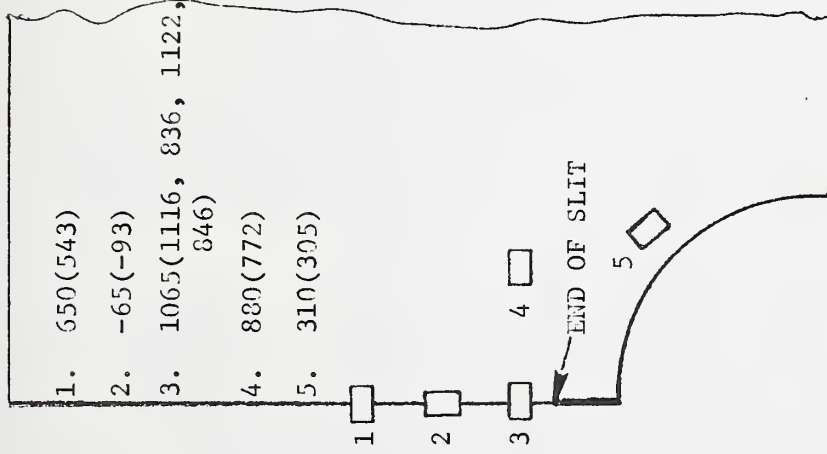


Figure 32 - Unreinforced-sheet specimens.

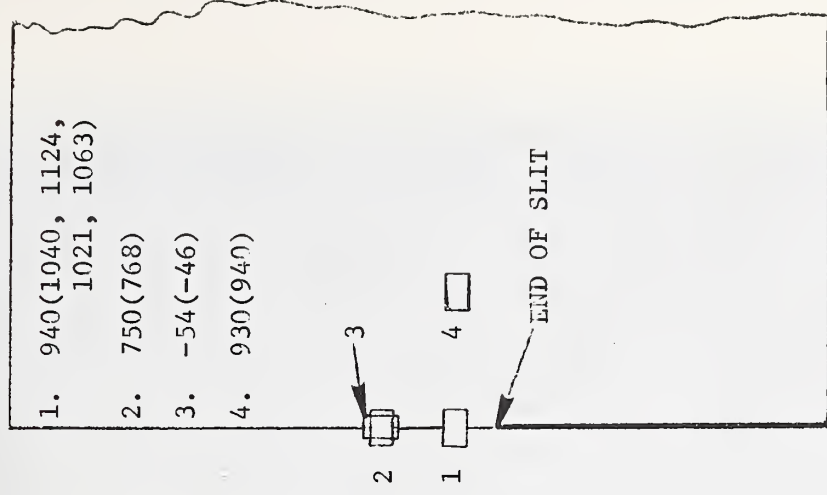




(a) UNREINFORCED CUTOUT (CUU1)

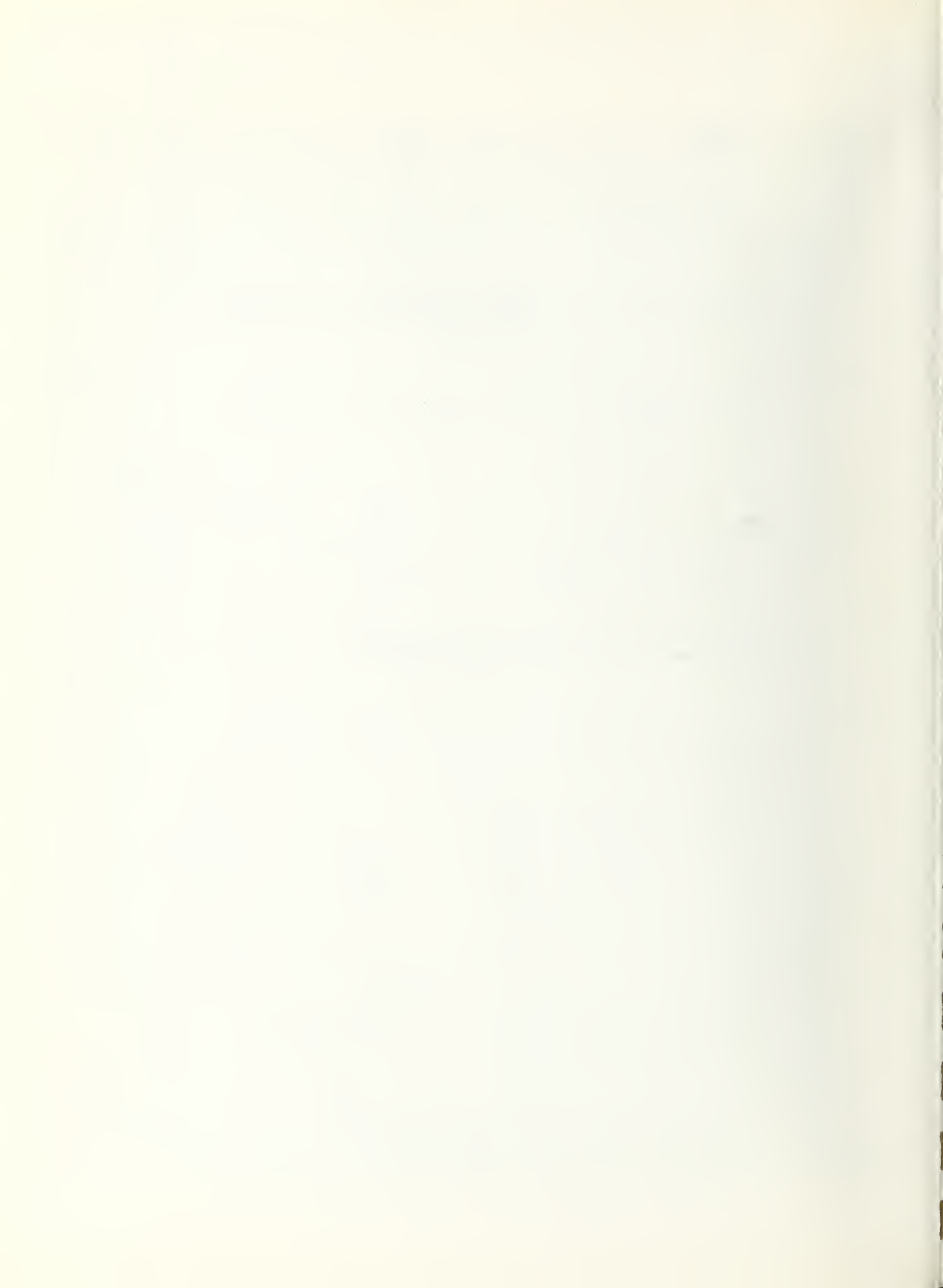


(b) UNREINFORCED CUTOUT-
WITH-SLIT (CCU1)



(c) UNREINFORCED SLIT (CRU1)

Figure 33 - Experimental microstrains (in parentheses) and analytical microstrains for the three unreinforced sheet specimens subjected to tensile loads of 4000 lbf (17800N).



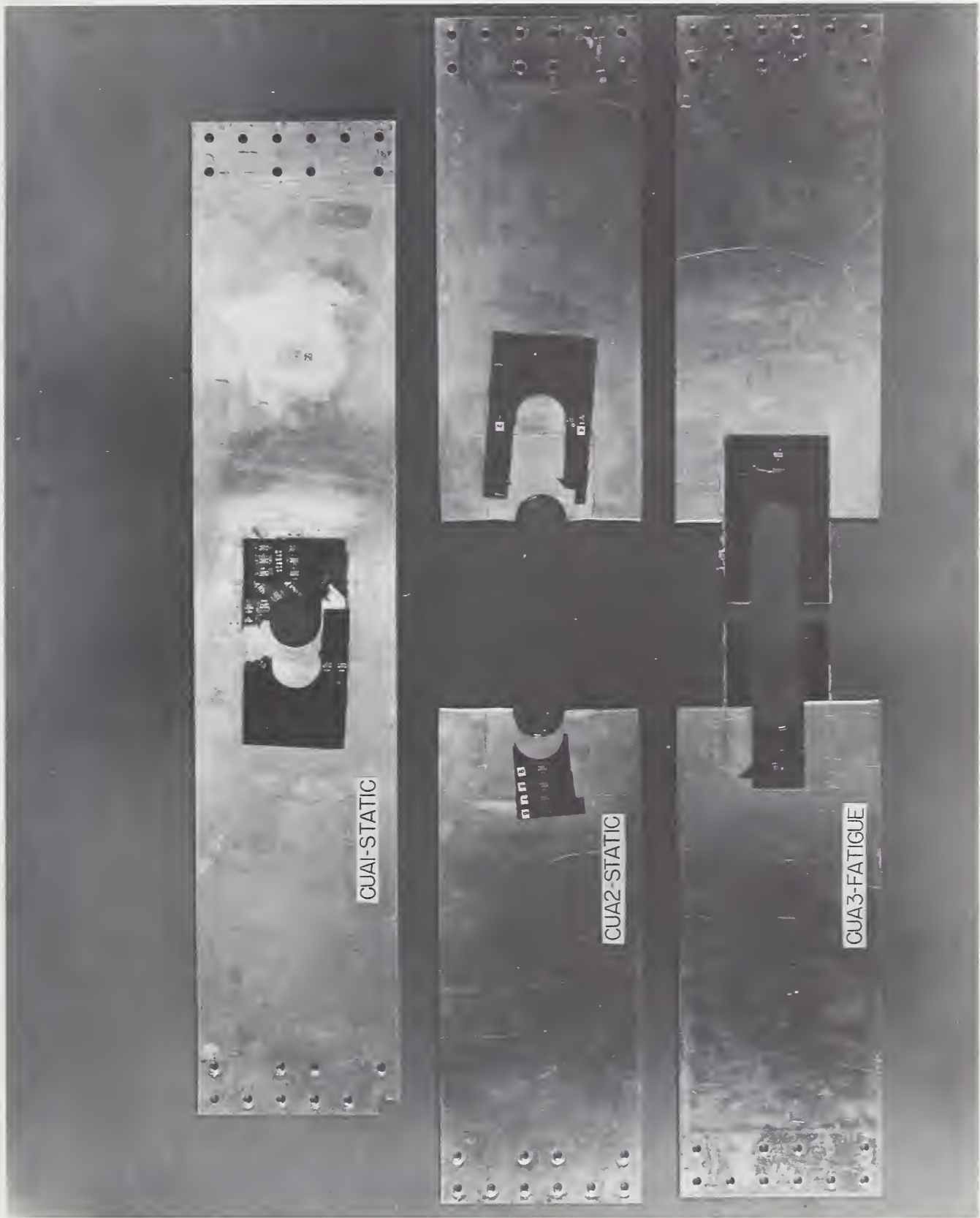


Figure 34 - Reinforced-cutout specimens (Design A, $\alpha = 45^\circ$).



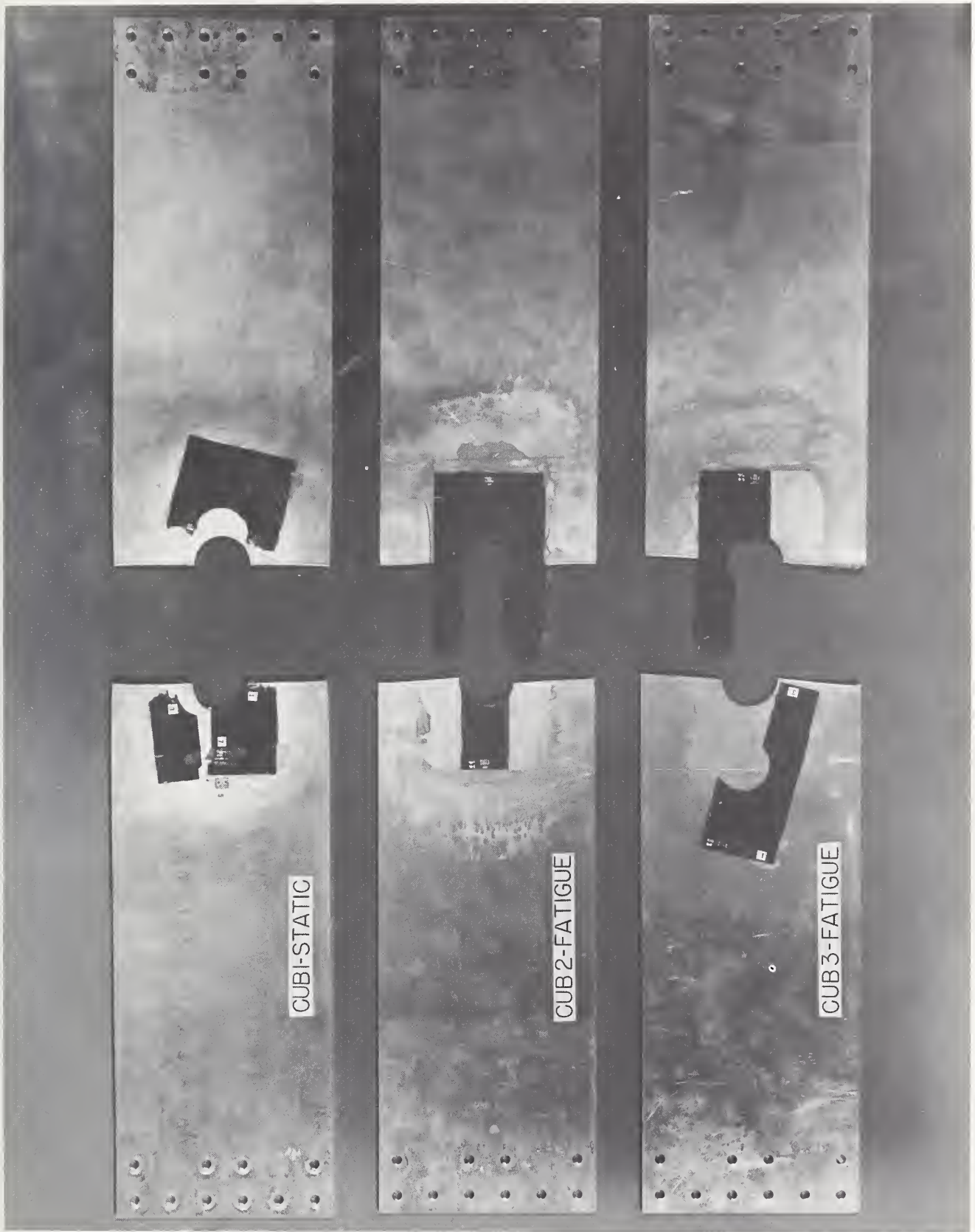


Figure 35 - Reinforced-cutout specimens (Design B, $\alpha = 30^\circ$).



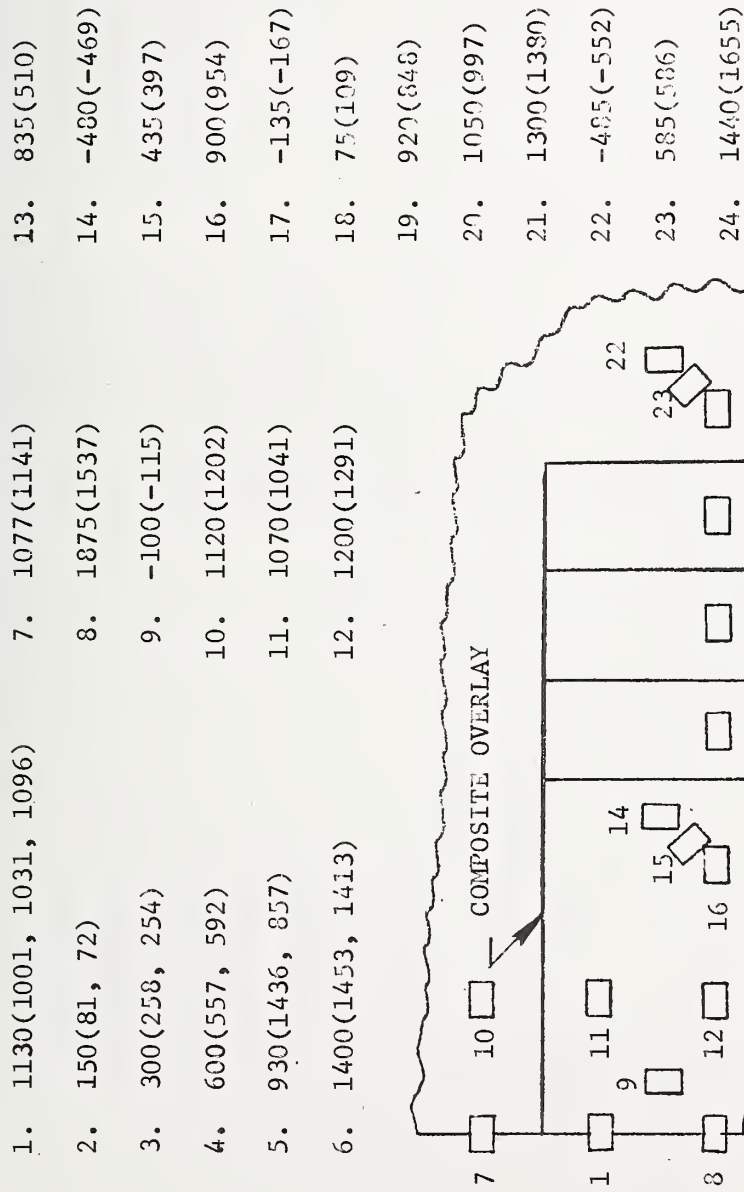


Figure 36 - Experimental microstrains (in parentheses) and analytical microstrains for one reinforced cutout specimen (CUA1) subjected to a tensile load of 11250 lbf (50040N).

- | | | |
|---------------------------------|---------------|----------------|
| 1. 1785(1495, 1101, 1495, 1480) | 7. 875(958) | 13. 290(259) |
| 2. 540(482, 569) | 8. -480(-481) | 14. 1000(982) |
| 3. 1395(1444, 1366) | 9. 420(466) | 15. 1300(1195) |
| 4. 1020(1002) | 10. 900(859) | 16. 900(788) |
| 5. 1055(1003) | 11. 95(65) | |
| 6. 1200(1238) | 12. 875(825) | |

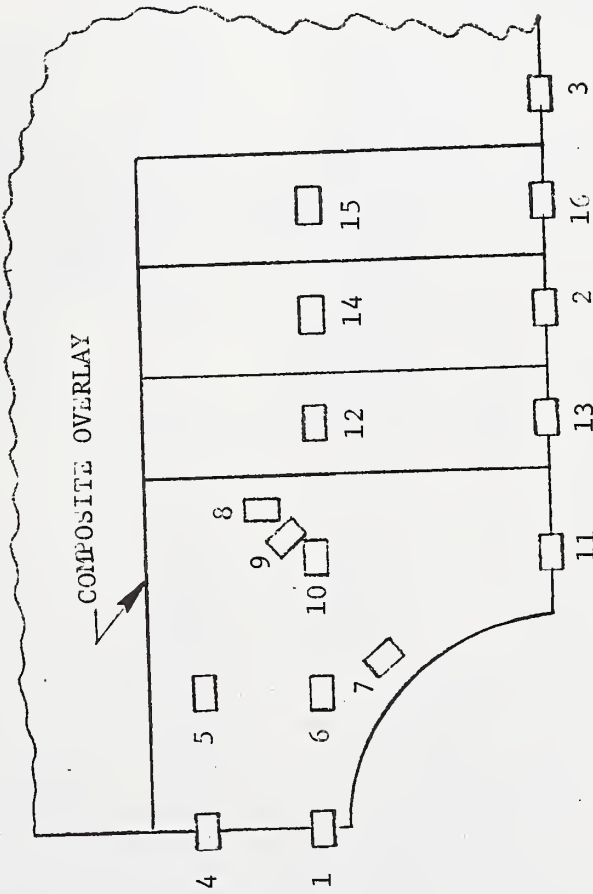
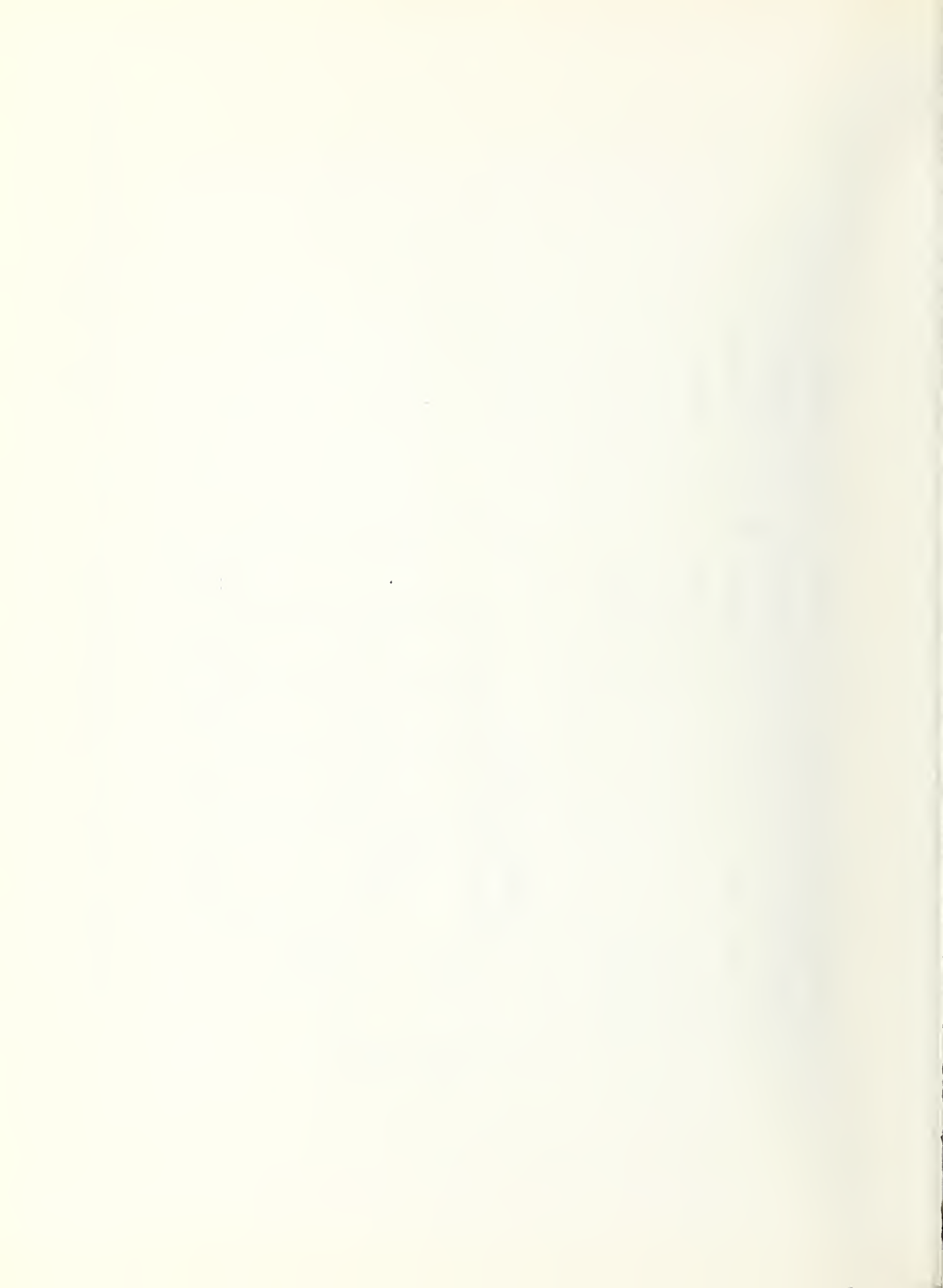


Figure 37 - Experimental microstrains (in parentheses) and analytical microstrains for one reinforced cutout specimen (CUB1) subjected to a tensile load of 11250 lbf (50040N).



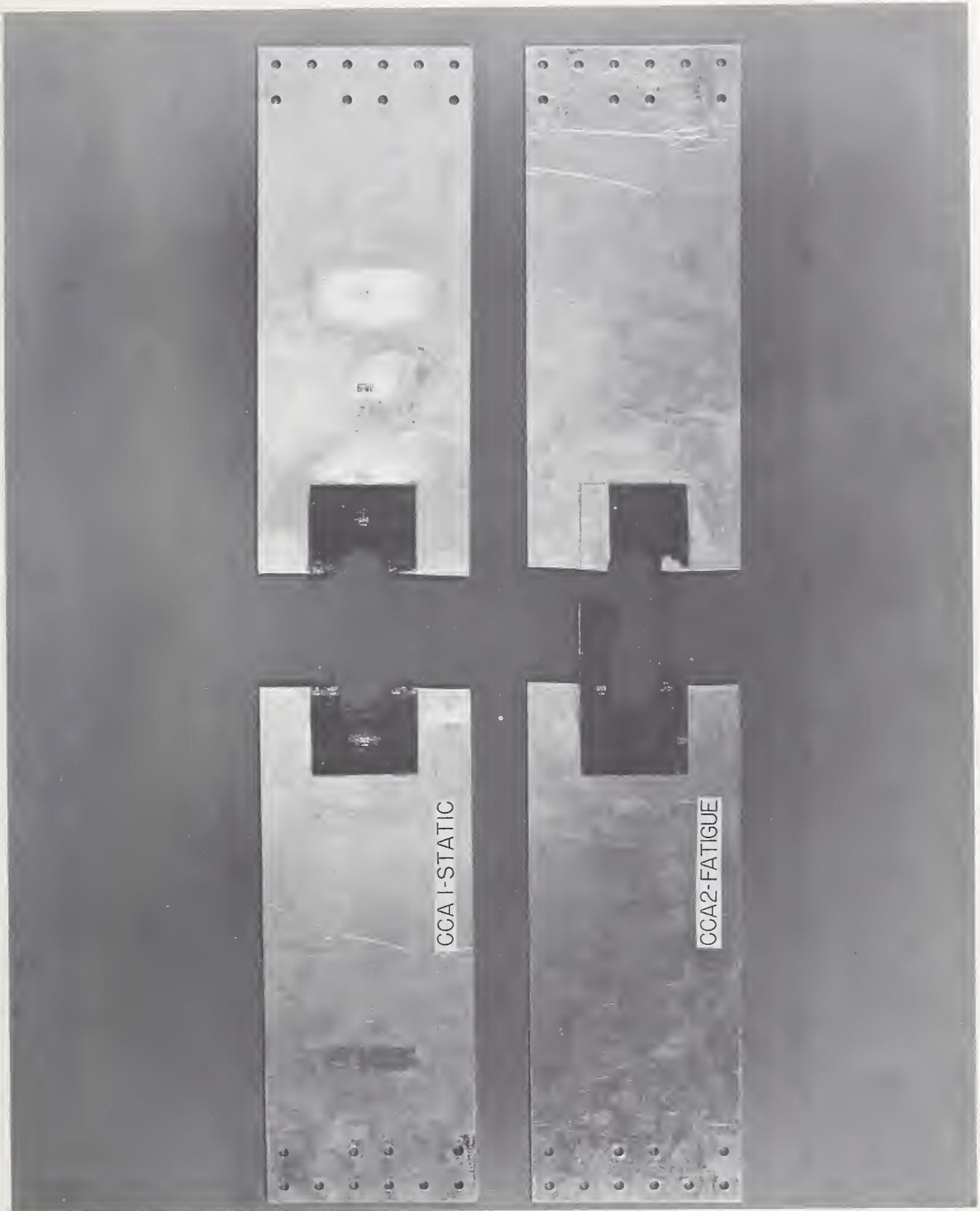


Figure 38 - Reinforced cutout-with-slit specimens (Design A, $\alpha = 45^\circ$).

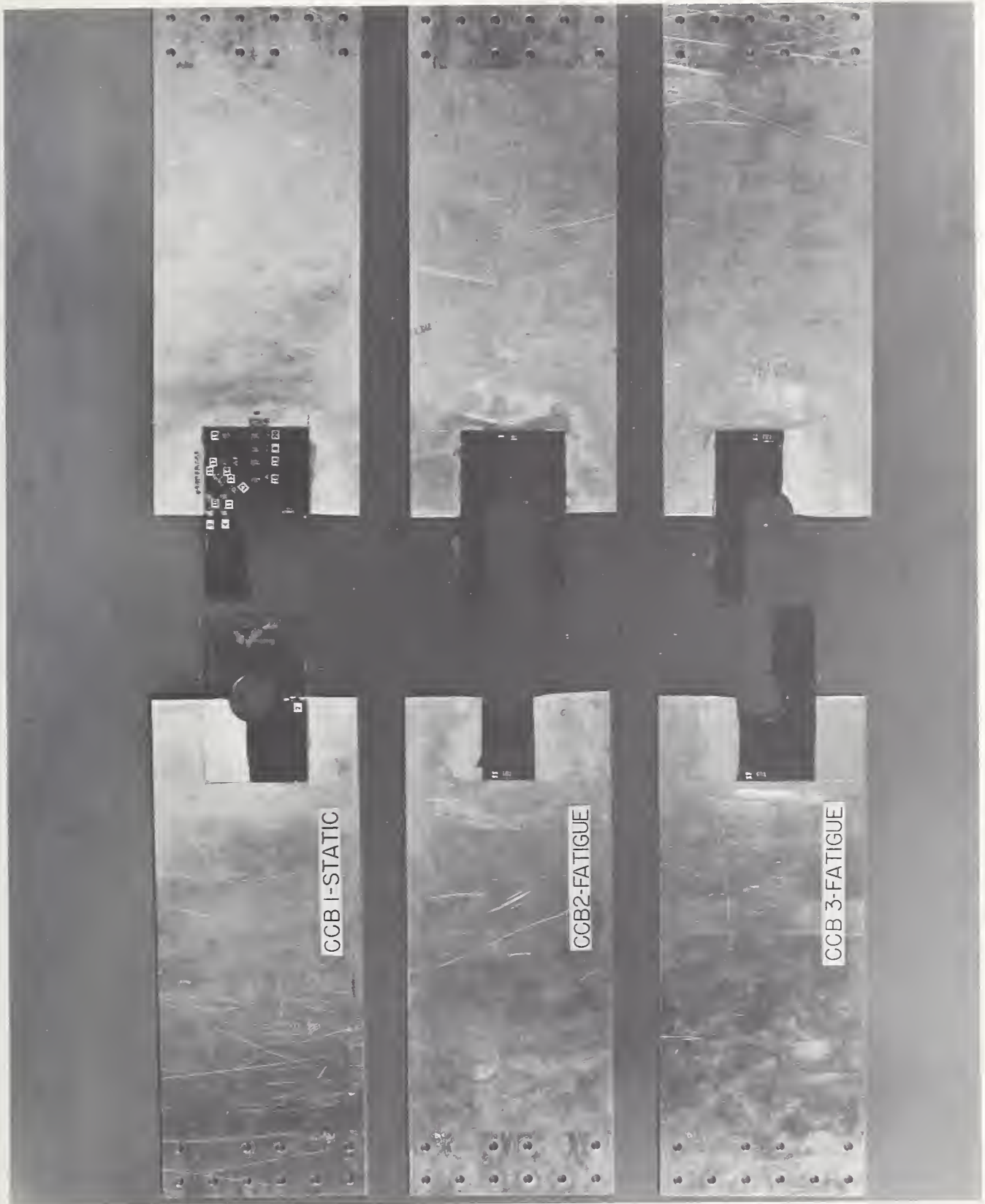


Figure 39 - Reinforced cutout-with-slit specimens (Design B, $\alpha = 30^\circ$).



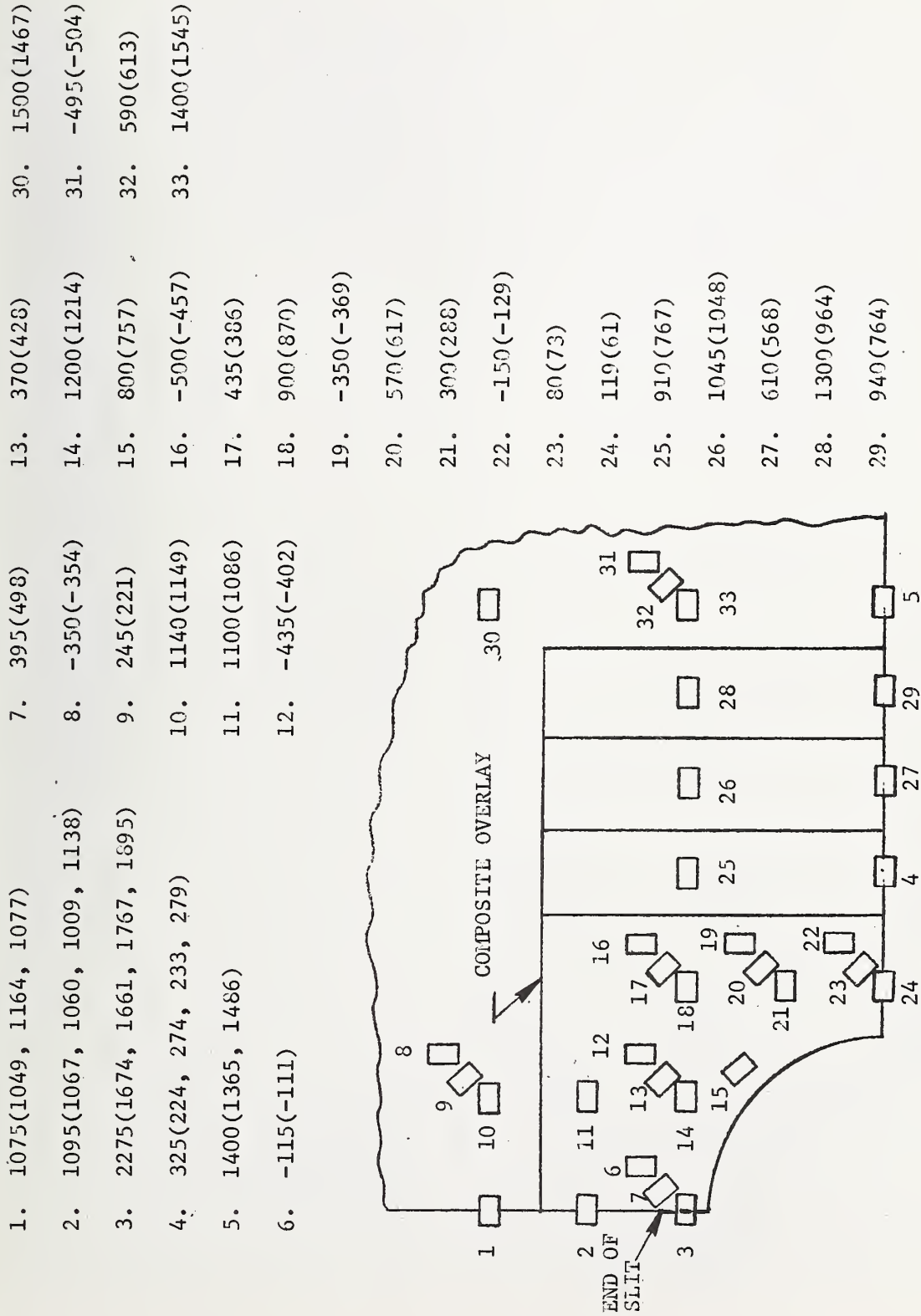


Figure 40 - Experimental microstrains (in parentheses) and analytical microstrains for one reinforced cutout-with-slit specimen (CCAI) subjected to a tensile load of 11250 lbf (50040N).



- | | | | | | |
|----|------------------------------|-----|------------|-----|------------|
| 1. | 2035(1446, 1986, 1618, 1717) | 7. | 825(956) | 13. | 309(235) |
| 2. | 555(530, 422) | 8. | -470(-503) | 14. | 1305(1362) |
| 3. | 1395(1361, 1389) | 9. | 455(339) | 15. | 900(1042) |
| 4. | 1050(976) | 10. | 865(963) | | |
| 5. | 950(1039) | 11. | 105(58) | | |
| 6. | 1140(1212) | 12. | 990(924) | | |

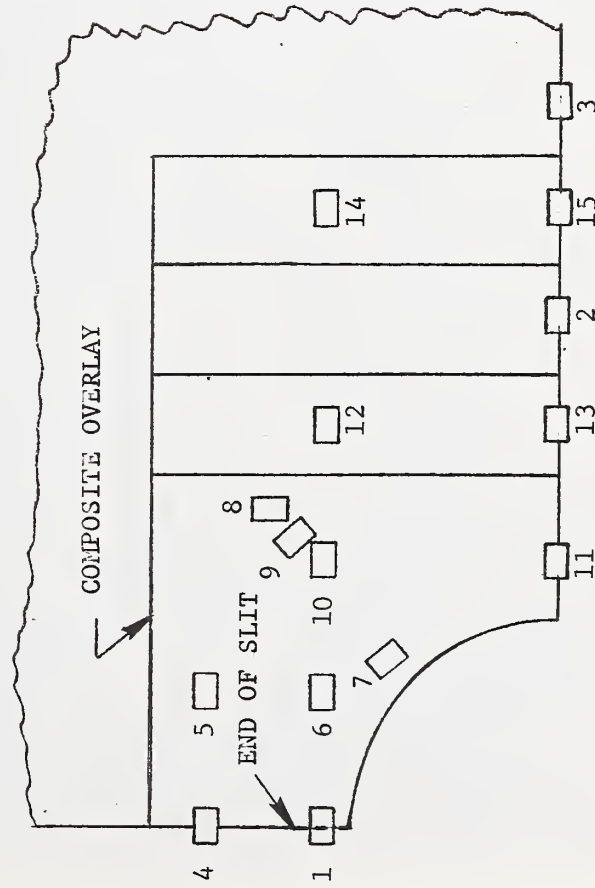


Figure 41 - Experimental microstrains (in parentheses) and analytical microstrains (CCB1) subjected to a tensile load of 11250 lbf (50040N).
cutout-with-slit specimen



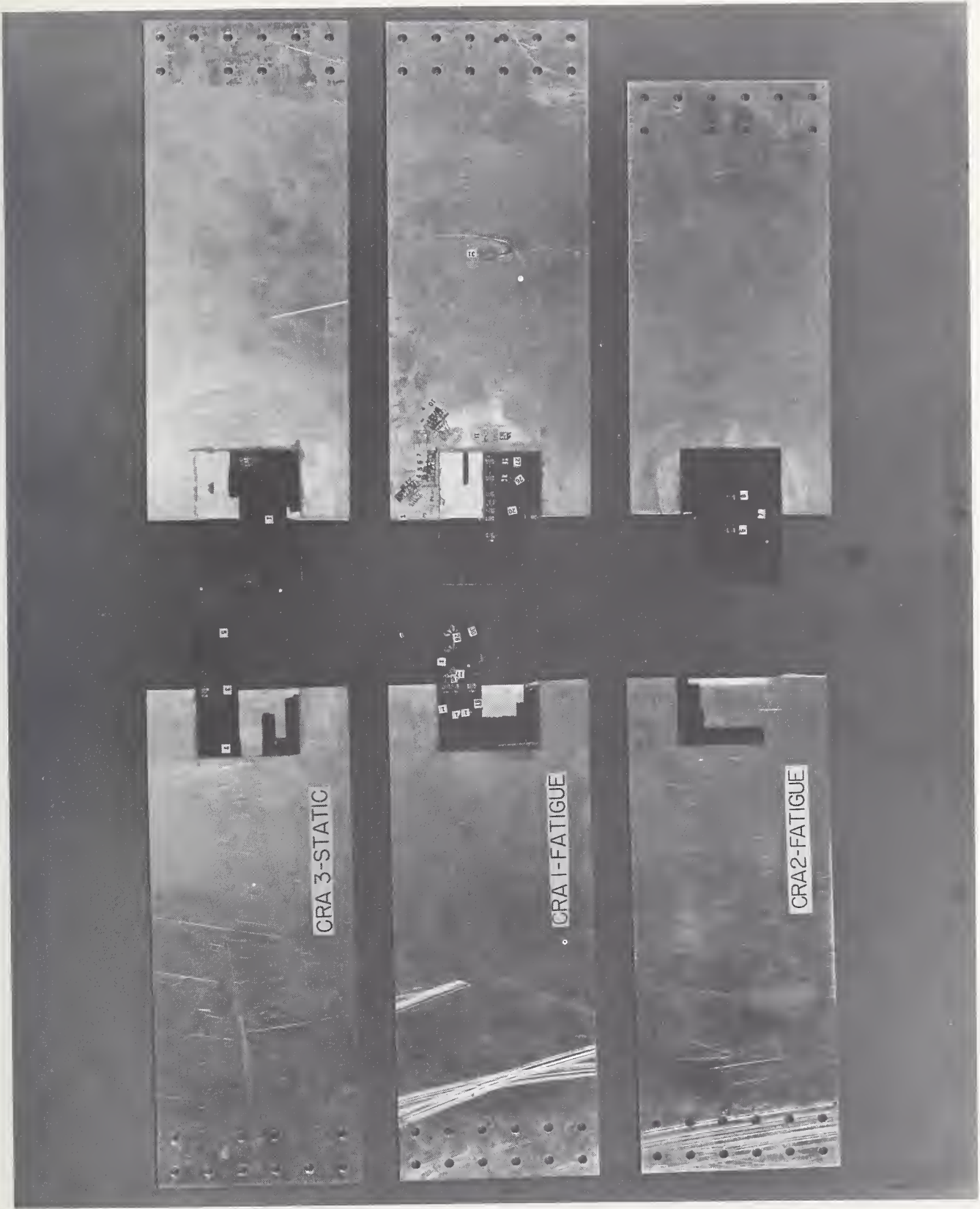


Figure 42 - Reinforced transverse-slit specimens with 4-ply unidirectional overlays.

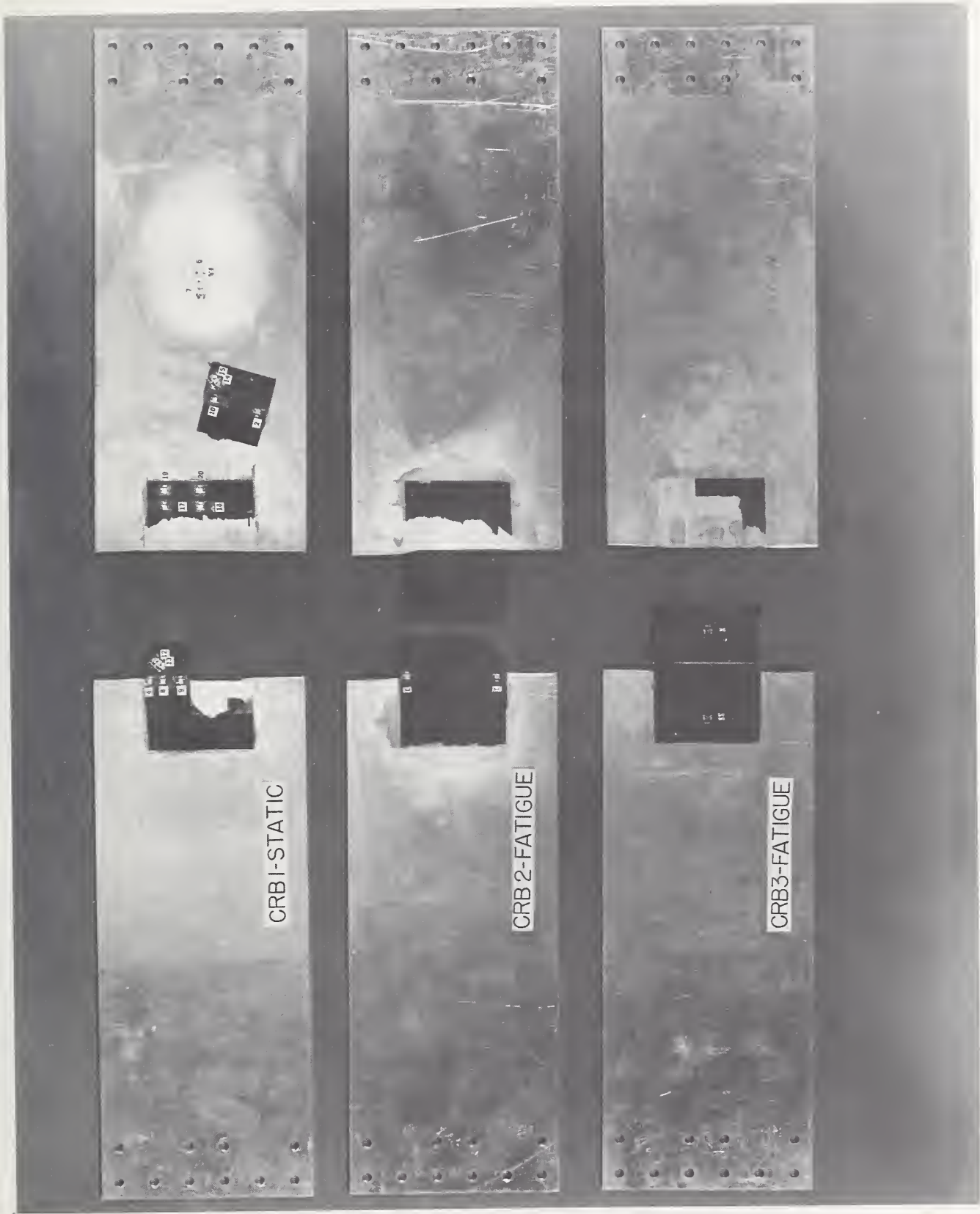


Figure 43 - Reinforced transverse-slit specimens with 6-ply overlays.

- | | | |
|---------------------------|----------------|----------------|
| 1. 1050(1086, 1099, 1034) | 7. 1250(1341) | 13. 306(326) |
| 2. 1300(1388, 1226) | 8. 925(1016) | 14. 875(844) |
| 3. 1275(1376, 1227) | 9. -400(-417) | 15. -165(-171) |
| 4. 800(825, 792, 807) | 10. 445(477) | 16. 329(369) |
| 5. 840(851, 913) | 11. 1230(1221) | 17. 770(747) |
| 6. 1300(1213, 1223) | 12. -230(-244) | 18. -270(-269) |
| | | 19. 323(350) |
| | | 20. 900(871) |
| | | 21. -360(-335) |
| | | 22. 483(547) |
| | | 23. 1330(1304) |
| | | 24. 1440(1396) |
| | | 25. -465(-474) |
| | | 26. 630(661) |
| | | 27. 1580(1568) |
| | | 28. 1585(1579) |

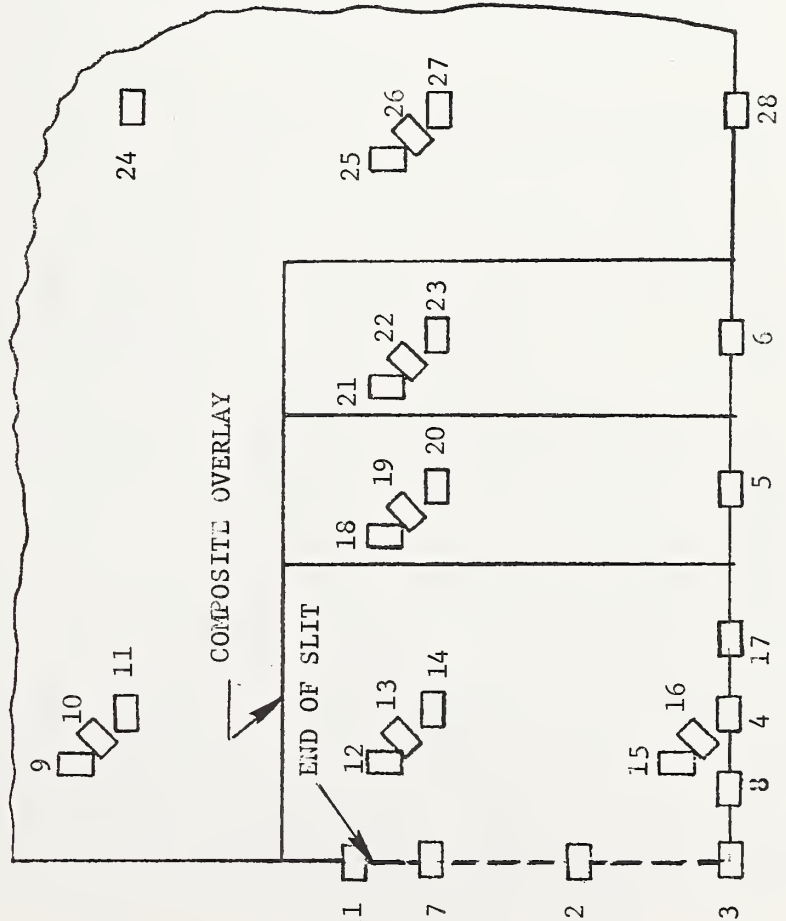


Figure 44 - Experimental microstrains (in parentheses) and analytical microstrains for one reinforced transverse-slit specimen (CRA1) subjected to a tensile load of 11250 lbf (50040N).



- 1. 1003(967, 1044, 888)
- 2. 985(704)
- 3. 1140(1039)
- 4. 1200(1171)
- 5. 1175(1061)
- 6. -300(-300)
- 7. 320(356)
- 8. 850(808)
- 9. -230(-242)
- 10. 270(299)
- 11. 800(763)
- 12. 985(947)
- 13. 1250(1172)
- 14. 1175(1201)

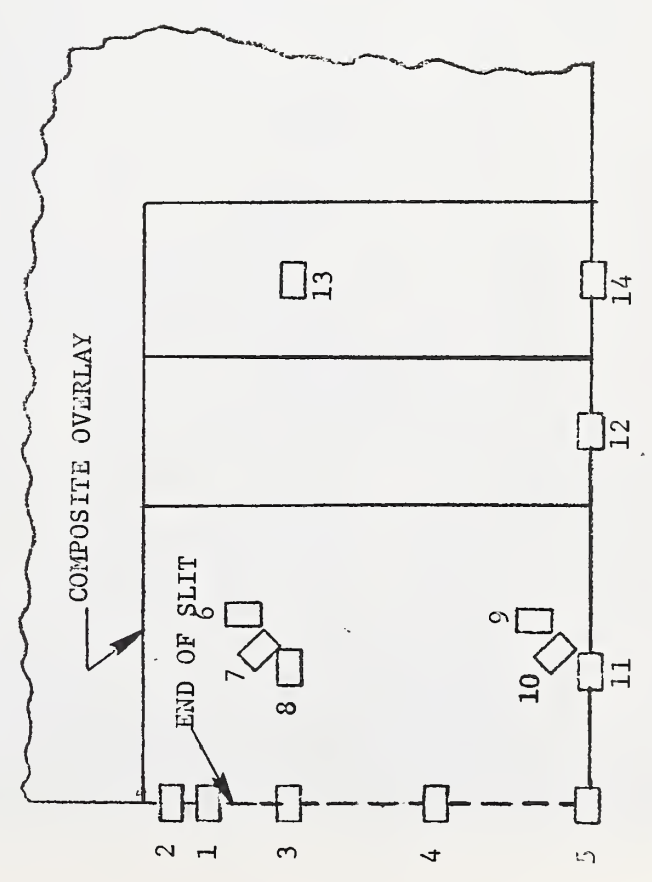


Figure 45 - Experimental microstrains (in parentheses) and analytical microstrains for one reinforced transverse-slit specimen (CRB1) subjected to a tensile load of 11250 lbf (50040N).



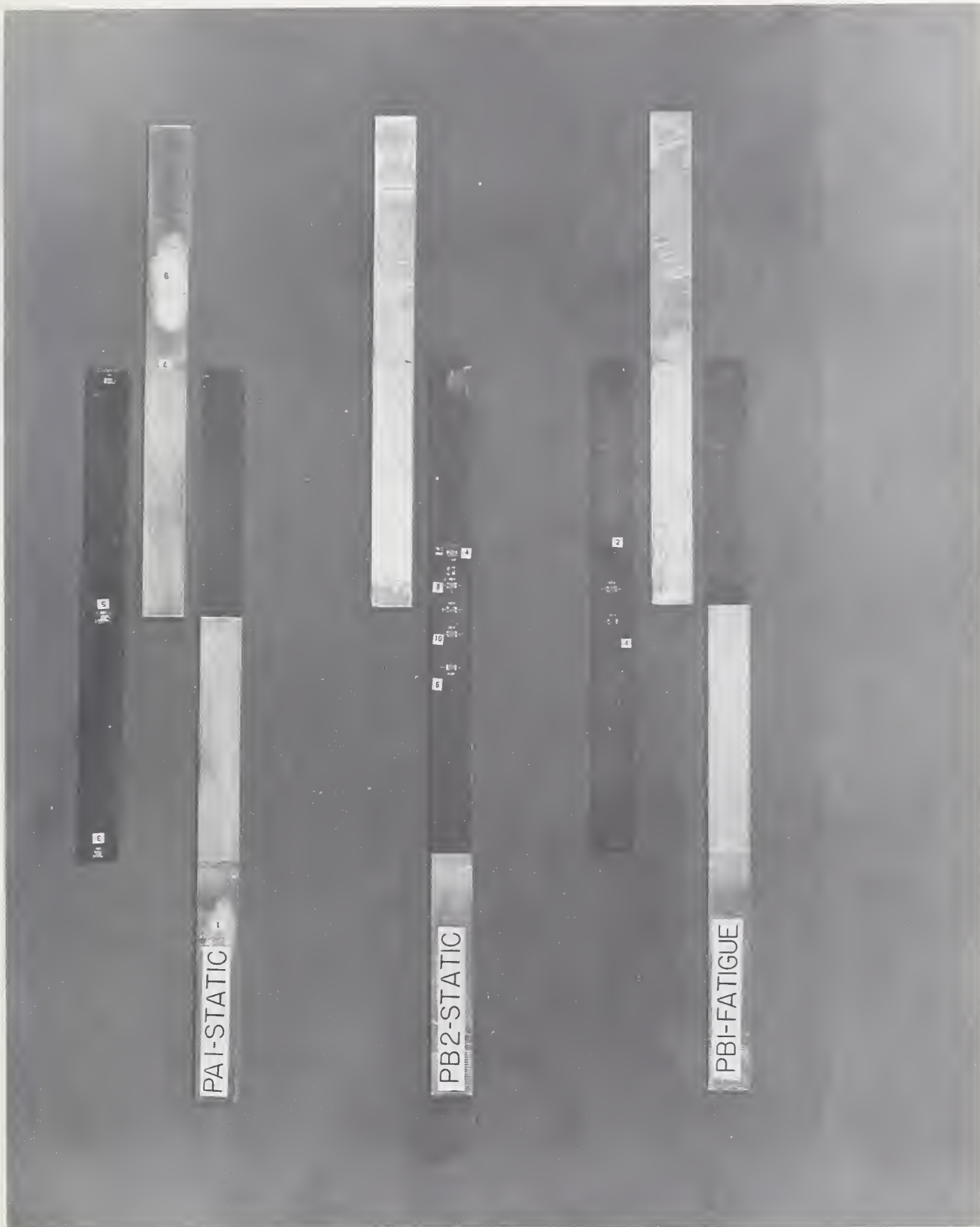


Figure 46 - Double-lap joint specimens spliced with plain, fully bonded, uniform-thickness overlays.



Figure 47 - Double-lap joint specimens spliced with plain, uniform-thickness overlays that were initially bonded over only two-thirds of their contact surface.



Figure 48 - Double-lap joint specimens spliced with fully bonded, uniform-thickness overlays having one-ply cushions at the center and at each end.

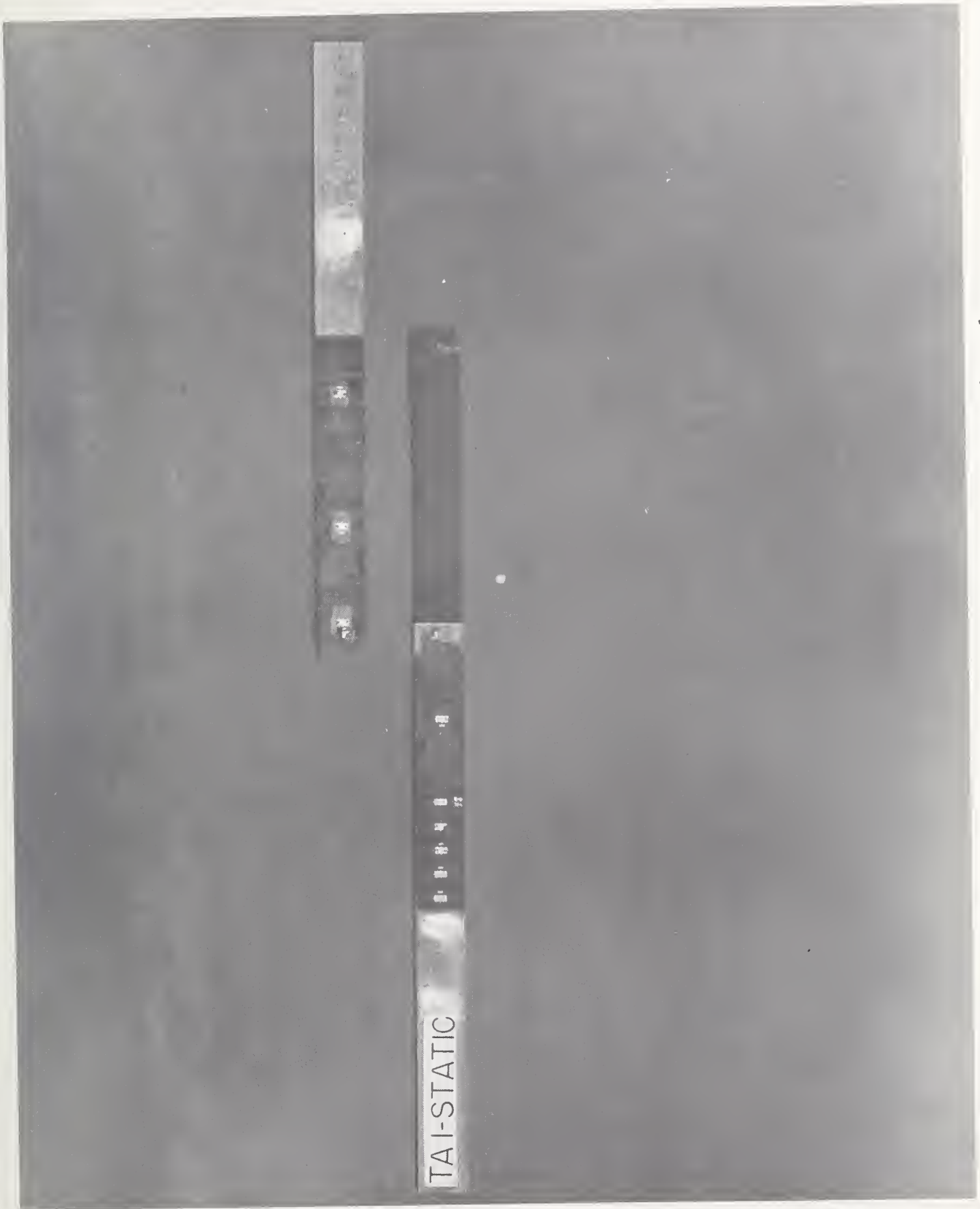


Figure 49 - Double-lap joint specimen spliced with fully bonded, step-tapered overlays.



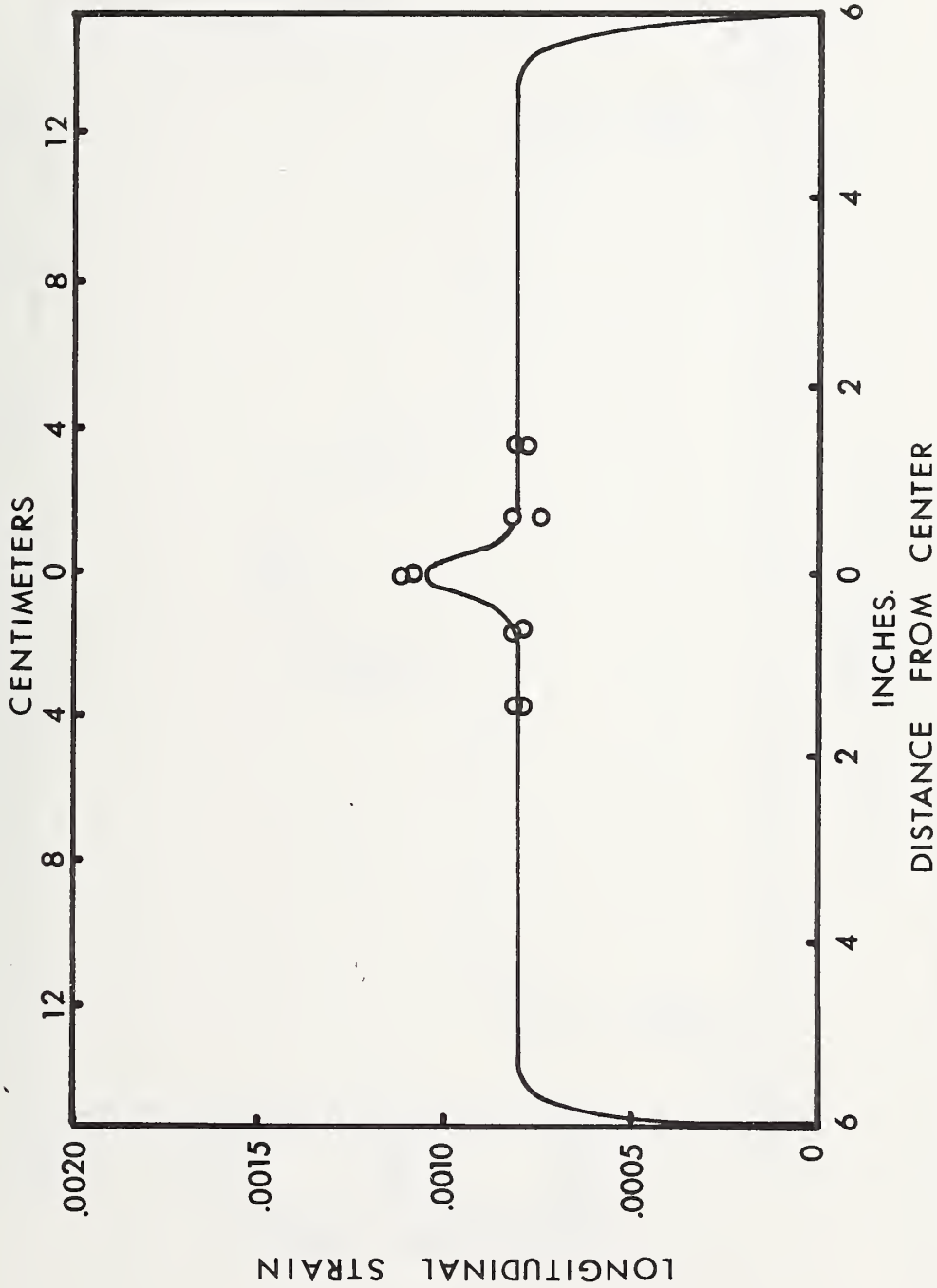


Figure 50 - Experimental strain (points) and analytical strain (curve) for a double-lap joint specimen spliced with plain, fully bonded, uniform-thickness overlays (PB2), subjected to a tensile load of 2500 lbf (11100N).



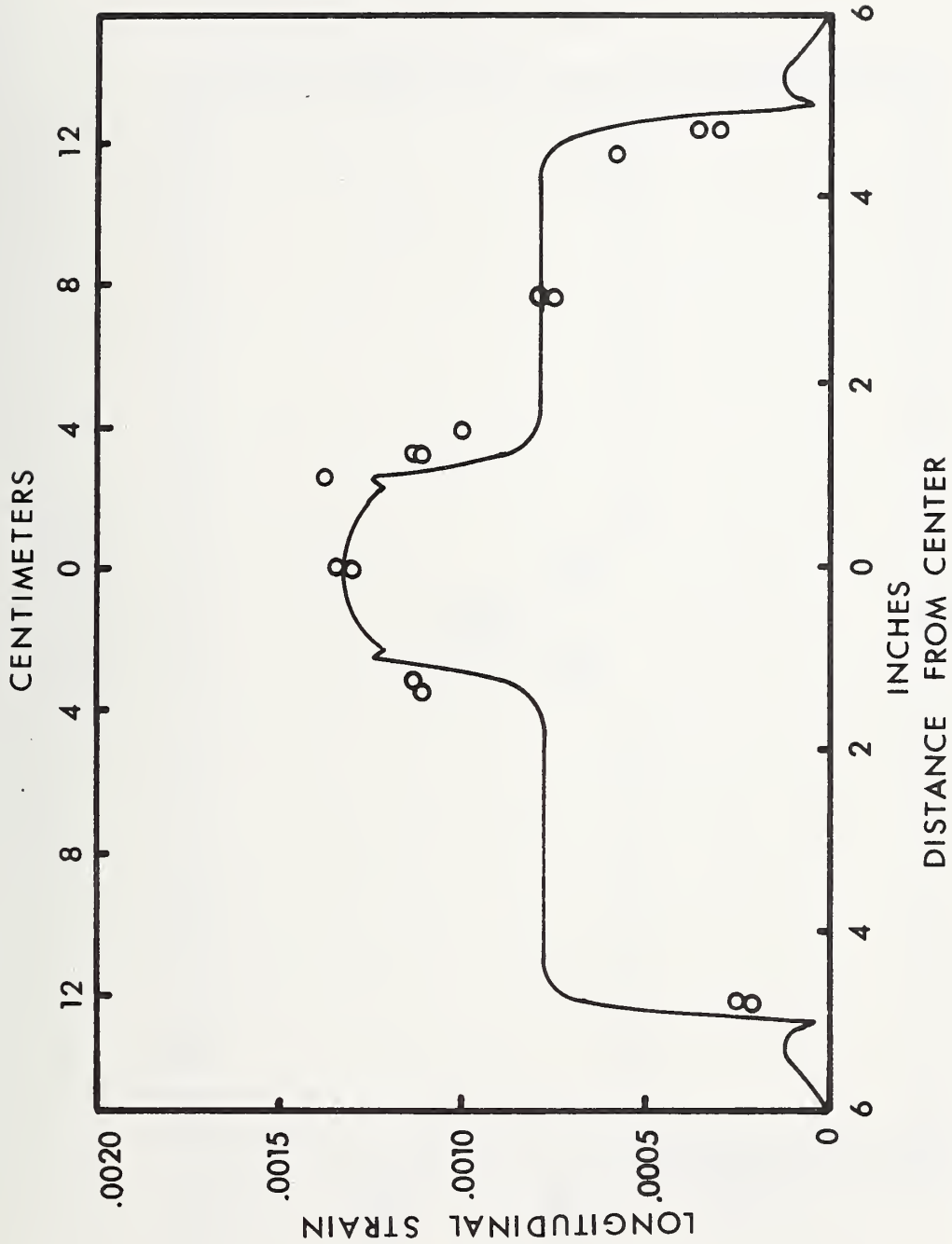


Figure 51 - Experimental strain (points) and analytical strain (curve) for a double-lap joint specimen spliced with plain, uniform-thickness overlays that were initially bonded over only two-thirds of their contact surface (DAL), subjected to a tensile load of 2500 lbf (11100N).



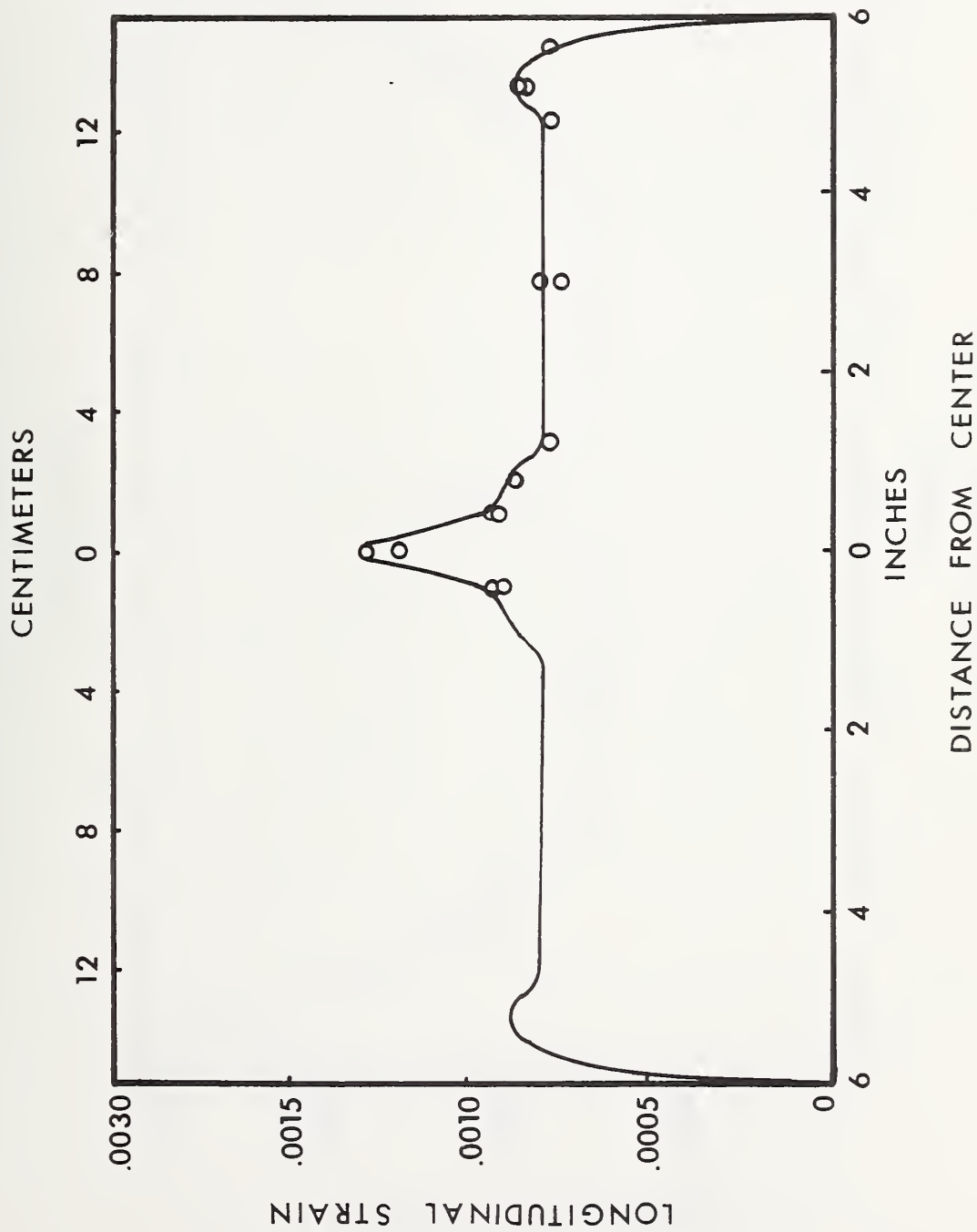


Figure 52 - Experimental strain (points) and analytical strain (curve) for a double-lap joint specimen with fully bonded, uniform-thickness overlays having one-ply cushions at the center and at each end (CB2), subjected to a tensile load of 2500 lbf (11100N).



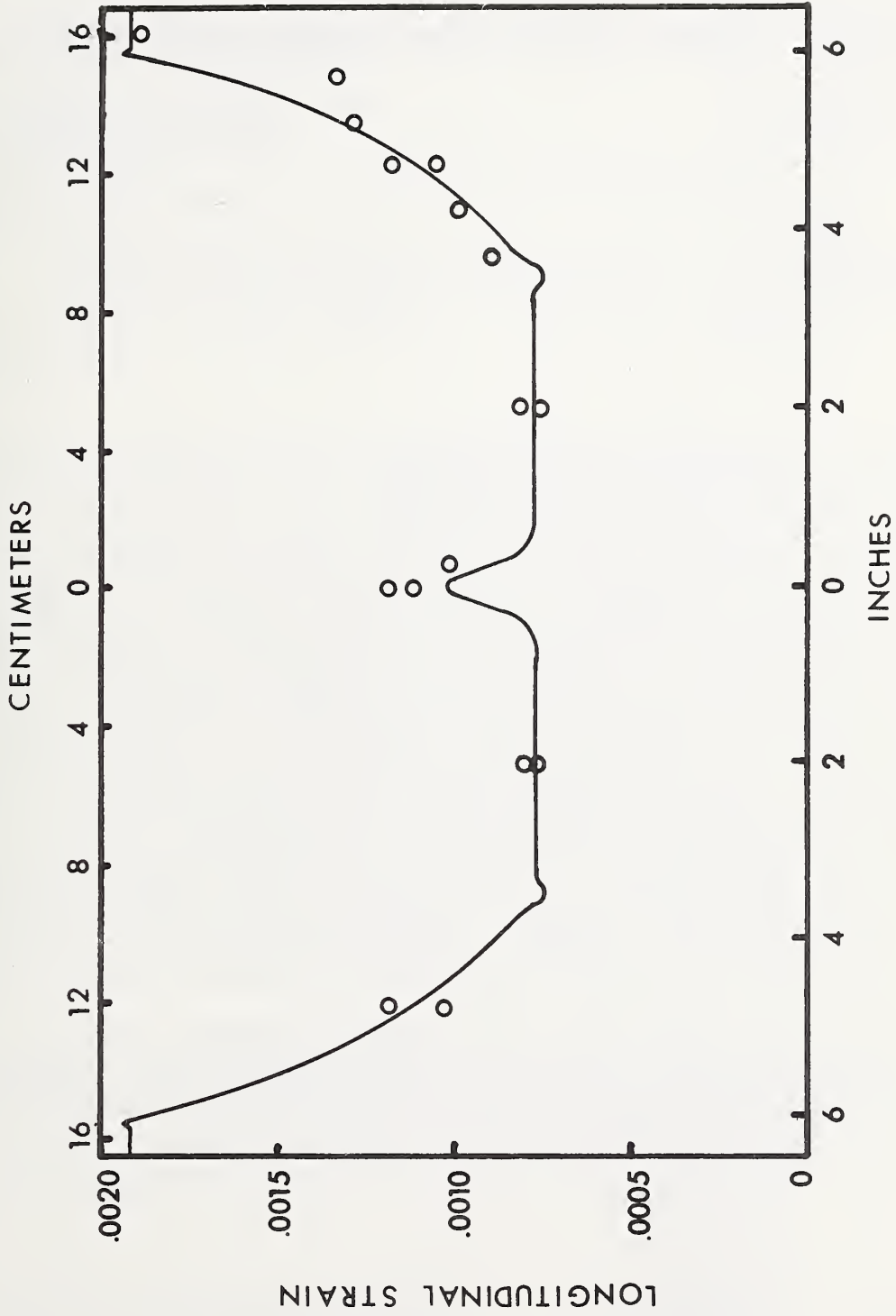


Figure 53 - Experimental strain (points) and analytical strain (curve) for a double-lap joint specimen spliced with fully bonded, step-tapered overlays (TAL), subjected to a tensile load of 2500 lbf (11100N).



U.S. DEPT. OF COMM. BIBLIOGRAPHIC DATA SHEET	1. PUBLICATION OR REPORT NO. NBSIR 73-201	2. Gov't Accession No.	3. Recipient's Accession No.
4. TITLE AND SUBTITLE Composite-Overlay Reinforcement of Cutouts and Cracks in Metal Sheet		5. Publication Date Feb. 1973	
		6. Performing Organization Code	
7. AUTHOR(S) Richard A. Mitchell, Ruth M. Woolley, Daniel J. Chwirut		8. Performing Organization NBSIR 73-201	
9. PERFORMING ORGANIZATION NAME AND ADDRESS NATIONAL BUREAU OF STANDARDS DEPARTMENT OF COMMERCE WASHINGTON, D.C. 20234		10. Project/Task/Work Unit No. 2130446	
		11. Contract/Grant No. L-48, 857	
12. Sponsoring Organization Name and Address Langley Research Center National Aeronautics and Space Administration Hampton, Virginia 23365		13. Type of Report & Period Covered Final	
		14. Sponsoring Agency Code	
15. SUPPLEMENTARY NOTES			
<p>16. ABSTRACT (A 200-word or less factual summary of most significant information. If document includes a significant bibliography or literature survey, mention it here.) Finite element computer programs were developed for the planform analysis and the longitudinal cross-section analysis of metal sheet reinforced by adhesively bonded overlays of composite material. The analyses articulate the separate responses of the metal sheet, the composite overlays, and the adhesive layers. All materials are assumed to be orthotropic and linear elastic, with the provision that nonlinear interlaminar shear deformation can be approximated by a series of stepwise-linear solutions. The computer programs were developed specifically for the study of three general configurations: (1) a sheet with a reinforced cutout; (2) a sheet with a reinforced cutout with two symmetrical transverse cracks, within the sheet, radiating away from the cutout edge; and (3) a sheet with a reinforced transverse crack. The programs are also suitable for the study of bonded lap joints. The principal output of the computer programs is a set of contour plots of stress and strain fields throughout the sheet, the overlays, and the adhesive layers. A series of laboratory tests was conducted to demonstrate the validity of the analyses. Strains measured on the surfaces of specimens representing the general configurations studied were, for the most part, in good agreement with strains predicted by the finite element analyses. Significant correlations between certain failure modes and the stresses computed by the finite element analyses were apparent. Similarities between the modes of failure under static and fatigue loading were also evident.</p> <p>Key Words: Adhesively bonded joints; composite materials; composite-overlay reinforcement; contour plotting; cracks, reinforcement of; cutouts, reinforcement of; debond analysis, progressive; finite element analysis; joints, adhesively bonded;</p>			
17. KEY WORDS (Alphabetical order, separated by semicolons) nonlinear analysis, shear; reinforcement, composite overlay; reinforcement, cutouts and cracks; shear analysis, nonlinear.			
18. AVAILABILITY STATEMENT <input checked="" type="checkbox"/> UNLIMITED. <input type="checkbox"/> FOR OFFICIAL DISTRIBUTION. DO NOT RELEASE TO NTIS.		19. SECURITY CLASS (THIS REPORT) UNCLASSIFIED	21. NO. OF PAGES
		20. SECURITY CLASS (THIS PAGE) UNCLASSIFIED	22. Price



